

NASA/TM–2016-219185



NASA Hybrid Wing Aircraft Aeroacoustic Test Documentation Report

*Stephanie L. Heath, Thomas F. Brooks, Florence V. Hutcheson,
Michael J. Doty and Christopher J. Bahr
Langley Research Center, Hampton, Virginia*

*Danny Hoad and Lawrence Becker
Northrop Grumman Corporation, Hampton, Virginia*

*William M. Humphrey and Casey L. Burley
Langley Research Center, Hampton, Virginia*

*Daniel Stead
Northrop Grumman Corporation, Hampton, Virginia*

*Dennis S. Pope
Analytical Services and Materials, Inc., Hampton, Virginia*

*Taylor B. Spalt
Langley Research Center, Hampton, Virginia*

*Dennis H. Kuchta
ROME, Hampton, Virginia*

*Gerald E. Plassman
National Institute of Aerospace, Hampton, Virginia*

*Jaye A. Moen
Langley Research Center, Hampton, Virginia*

April 2016

NASA STI Program . . . in Profile

Since its founding, NASA has been dedicated to the advancement of aeronautics and space science. The NASA scientific and technical information (STI) program plays a key part in helping NASA maintain this important role.

The NASA STI program operates under the auspices of the Agency Chief Information Officer. It collects, organizes, provides for archiving, and disseminates NASA's STI. The NASA STI program provides access to the NTRS Registered and its public interface, the NASA Technical Reports Server, thus providing one of the largest collections of aeronautical and space science STI in the world. Results are published in both non-NASA channels and by NASA in the NASA STI Report Series, which includes the following report types:

- **TECHNICAL PUBLICATION.** Reports of completed research or a major significant phase of research that present the results of NASA Programs and include extensive data or theoretical analysis. Includes compilations of significant scientific and technical data and information deemed to be of continuing reference value. NASA counter-part of peer-reviewed formal professional papers but has less stringent limitations on manuscript length and extent of graphic presentations.
- **TECHNICAL MEMORANDUM.** Scientific and technical findings that are preliminary or of specialized interest, e.g., quick release reports, working papers, and bibliographies that contain minimal annotation. Does not contain extensive analysis.
- **CONTRACTOR REPORT.** Scientific and technical findings by NASA-sponsored contractors and grantees.

- **CONFERENCE PUBLICATION.** Collected papers from scientific and technical conferences, symposia, seminars, or other meetings sponsored or co-sponsored by NASA.
- **SPECIAL PUBLICATION.** Scientific, technical, or historical information from NASA programs, projects, and missions, often concerned with subjects having substantial public interest.
- **TECHNICAL TRANSLATION.** English-language translations of foreign scientific and technical material pertinent to NASA's mission.

Specialized services also include organizing and publishing research results, distributing specialized research announcements and feeds, providing information desk and personal search support, and enabling data exchange services.

For more information about the NASA STI program, see the following:

- Access the NASA STI program home page at <http://www.sti.nasa.gov>
- E-mail your question to help@sti.nasa.gov
- Phone the NASA STI Information Desk at 757-864-9658
- Write to:
NASA STI Information Desk
Mail Stop 148
NASA Langley Research Center
Hampton, VA 23681-2199

NASA/TM-2016-219185



NASA Hybrid Wing Body Aircraft Aeroacoustic Test Documentation Report

*Stephanie L. Heath, Thomas F. Brooks, Florence V. Hutcheson,
Michael J. Doty and Christopher J. Bahr
Langley Research Center, Hampton, Virginia*

*Danny Hoad and Lawrence Becker
Northrop Grumman Corporation, Hampton, Virginia*

*William M. Humphrey and Casey L. Burley
Langley Research Center, Hampton, Virginia*

*Daniel Stead
Northrop Grumman Corporation, Hampton, Virginia*

*Dennis S. Pope
Analytical Services and Materials, Inc., Hampton, Virginia*

*Taylor B. Spalt
Langley Research Center, Hampton, Virginia*

*Dennis H. Kuchta
ROME, Hampton, Virginia*

*Gerald E. Plassman
National Institute of Aerospace, Hampton, Virginia*

*Jaye A. Moen
Langley Research Center, Hampton, Virginia*

National Aeronautics and
Space Administration

Langley Research Center
Hampton, Virginia 23681-2199

April 2016

Acknowledgments

The Hybrid Wing Body Aircraft Aeroacoustic Wind-Tunnel Test was funded by NASA's Environmentally Responsible Aviation (ERA) Program. The authors would like to acknowledge valuable contributions from many dedicated staffs at Boeing, NASA Langley Research Center (LaRC), the Massachusetts Institute of Technology (MIT), and the University of California-Irvine. The authors would like to thank Fay Collier, Hamilton Fernandez, Russ Thomas, Bob Bush, and Steve Syrett for management support, and the 14-by 22-Foot Subsonic Tunnel Staff for their outstanding test support.

The use of trademarks or names of manufacturers in this report is for accurate reporting and does not constitute an official endorsement, either expressed or implied, of such products or manufacturers by the National Aeronautics and Space Administration.

Available from:

NASA STI Program / Mail Stop 148
NASA Langley Research Center
Hampton, VA 23681-2199
Fax: 757-864-6500

Table of Contents

1	Introduction	1
1.1	Test Objectives.....	1
1.2	Overview.....	1
2	Main Personnel.....	2
3	Test Equipment.....	3
3.1	Facility Description.....	3
3.2	HWB Model.....	6
3.2.1	HWB Model Details.....	7
3.2.2	Model References	8
3.2.3	Transition Grit on Model	10
3.3	Engine Simulators	10
3.3.1	Engine Location Documentation.....	10
3.3.2	Broadband Engine Noise Simulator (BENS).....	12
3.3.3	Compact Jet Engine Simulator (CJES)	14
3.4	Model Support Systems	15
3.5	HWB Model Location and Alignment.....	15
4	Data Acquisition Systems.....	17
4.1	Tunnel Data Acquisition System	17
4.1.1	BENS Airflow Data	18
4.1.2	CJES Data	18
4.2	Acoustic Data Acquisition System.....	18
4.2.1	Acoustic DAS Hardware Description	18
4.2.2	Acoustic DAS Software Description	18
5	Instrumentation and Calibration	19
5.1	HWB Model Instrumentation.....	19
5.1.1	HWB Model Surface Pressure Data.....	19
5.1.2	Temperature Sensors.....	20
5.1.3	Angle-of-Attack Instrumentation	20
5.1.4	HWB Model Embedded Point Sources.....	20
5.2	Engine Noise Simulators Instrumentation and Control.....	22
5.2.1	BENS Instrumentation	22
5.2.2	CJES Instrumentation	23
5.3	Acoustic Instrumentation	25
5.3.1	Microphone Phased Array	25
5.3.2	Tower and Truss Microphones (Directivity Microphones).....	28

5.3.3	Photogrammetric Tracking System for Microphone Phased Array	29
6	Test Matrix	30
6.1	Broadband Turbomachinery Noise	30
6.1.1	BENS Exhaust Noise Radiation Data	30
6.1.2	BENS Inlet Noise Radiation Data.....	30
6.2	Airframe Noise.....	31
6.3	Jet Noise.....	31
6.4	Facility Acoustic Properties	31
6.4.1	Interrupted Noise Test.....	32
6.4.2	Impulse Response Test.....	32
6.5	Testing Configurations and Tunnel Parameters	33
6.5.1	HWB Model Parameters Describing Test Configurations	33
6.5.2	Angle-of-Attack Settings and Cp Matching.....	34
7	Data Processing and Reduction	35
7.1	In Situ Data Analysis	35
7.2	Post-Test CSM Construction	36
7.3	Post-Test Data Corrections	37
7.3.1	Background Subtraction.....	37
7.3.2	Shear Layer Correction	37
7.3.3	Atmospheric Attenuation	38
7.3.4	Microphone Directivity.....	38
7.4	Data Results and Analyses	38
8	Summary.....	39
9	References	40
10	Appendices	42
	Appendix A: HWB Model Flight Condition Settings.....	42
	Appendix B: Tunnel DAS Data Listing.....	42
	Appendix C: Acoustic DAS Data Listing.....	42

List of Figures

Figure 1. NASA Langley 14- by 22-Foot Subsonic Tunnel circuit. Dimensions are given in feet.	4
Figure 2. HWB test section configuration.	5
Figure 3. 14- by 22-Foot Subsonic Tunnel acoustic treatment.	6
Figure 4. General N2A-EXTE HWB test model. Flow-through and engine noise simulator nacelles are not shown.	7
Figure 5. General HWB Model arrangement drawing details – oblique and front views. Units are given in inches.	8
Figure 6. General HWB Model arrangement drawing details – side view. Units are given in inches.....	9
Figure 7. General HWB Model arrangement drawing details – top view. Units in inches unless otherwise marked.....	9
Figure 8. Engine positions and dimensions (in inches).....	11
Figure 9. Nominal engine position definition. Units are in inches.	11
Figure 10. Cross section of Broadband Engine Noise Simulator.....	12
Figure 11. BENS assembly on the acoustic model support.	13
Figure 12. BENS engine nacelles in inlet and exhaust noise radiation configurations (nacelles shown in their nominal position with respect to the model airframe).	13
Figure 13. Schematic of the Compact Jet Engine Simulator.	14
Figure 14. Baseline nozzles installed on the Compact Jet Engine Simulators.....	15
Figure 15. "F8" low-noise chevron nozzle in NASA Langley's Low Speed Aeroacoustic Wind Tunnel.	15
Figure 16. HWB Model and model support assembly within 14- by 22-Foot Subsonic Tunnel coordinates. All dimensions are in inches.	16
Figure 17. HWB Check Loading Fixture assembly drawing.	17
Figure 18. Spanwise locations (based on the model semispan dimension) of four chordwise pressure tap rows on port side of model.....	20
Figure 19. Embedded point sources and speaker cavity locations.....	21
Figure 20. Embedded speakers.	21
Figure 21. Embedded speaker cavity cover.	22
Figure 22. Kulite sensor cable and wiring diagram.	23
Figure 23. CJES pressure rakes.....	24
Figure 24. CJES temperature rakes.....	25
Figure 25. Phased Array. Irregular circular pattern of microphones is comprised of 16 arms with 6 microphones in each arm and 1 in the center of the array.....	26
Figure 26. Lateral angles of the overhead traverse truss and sideline tower microphones. View facing upstream.	28
Figure 27. Embedded speaker showing the socket in the underside of the model (facing upwards).....	32
Figure 28. a) IN test example time history, and b) IR test example time history. Traverse 203" downstream of nozzle. Top north-sideline tower microphone.	33
Figure 29. a) Blasting cap holders mounted on model test stand, and b) Sideline, and overhead, traverse stations for IR test.	33
Figure 30. Example of directivity profile generated by analysis system. Source emission angles as refracted through the open jet shear layer were incorporated into the generated plots for tunnel flow cases.	36
Figure 31. Example of UDAMAS processing output.	36

List of Tables

Table 1. Main Personnel Contact List	2
Table 2. HWB Model Details	7
Table 3. BENS DAS Parameters	22
Table 4. Kulite Channel Assignments	23
Table 5. Model Test Parameters	34
Table 6. N2A-EXTE Noise Certification Flight Conditions	35

1 Introduction

This report summarizes results of the Hybrid Wing Body (HWB) N2A-EXTE model aeroacoustic test. The N2A-EXTE model was tested in the NASA Langley 14- by 22-Foot Subsonic Tunnel (14x22 Tunnel) from September 12, 2012 until January 28, 2013 and was designated as test T598. This document contains the following main sections: Section 1 – Introduction, Section 2 – Main Personnel, Section 3 – Test Equipment, Section 4 – Data Acquisition Systems, Section 5 – Instrumentation and Calibration, Section 6 – Test Matrix, Section 7 – Data Processing , and Section 8 – Summary.

Due to the amount of material to be documented, this HWB test documentation report does not cover analysis of acquired data, which is to be presented separately by the principal investigators. Also, no attempt was made to include preliminary risk reduction tests (such as Broadband Engine Noise Simulator and Compact Jet Engine Simulator characterization tests, shielding measurement technique studies, and speaker calibration method studies), which were performed in support of this HWB test. Separate reports containing these preliminary tests are referenced where applicable.

1.1 Test Objectives

NASA’s Environmentally Responsible Aviation (ERA) Project and Langley Aeroacoustics Branch initiated this HWB aircraft aeroacoustic test in 2008 to develop high-fidelity, state-of-the-art computational tools for designing quiet, low-emission aircraft to meet the agency’s goals. The HWB aircraft is an integrated fuselage-wing configuration with twin, podded nacelles mounted on the vehicle upper surface between twin vertical tails. The low-speed experimental investigation was conducted on a 5.8-percent scale HWB model in NASA Langley’s 14x22 Tunnel.

This test was uniquely designed to demonstrate progress toward achieving NASA’s noise emission goal (which is 42 Effective Perceived Noise Level in decibels – EPNL dB cumulative noise below the Federal Aviation Administration (FAA) Federal Aviation Regulations (FAR) 36 Stage 4 certification level, (Noise Standards: Aircraft Type and Airworthiness Certification. Title 14, Chapter I, Parts 36 and 91, 2003)) as well as to develop, test, and understand new aircraft propulsion airframe aeroacoustic (PAA) interactions and technologies, such as shielding effects, diffraction around aircraft edges, and flows through and around the engines and airframe. NASA’s HWB project was first presented to the aeroacoustic community in 2009 (Collier, 2009) and further defined in Brook’s keynote address (Brooks, 2011). A more-recent summary of the test preparations, including a summary of preliminary studies and facility upgrades required to invert the HWB model and sweep an acoustic array over a large range of directivity angles for this test, is documented in paper AIAA-2013-2623 (Heath et al., 2013).

1.2 Overview

The research efforts were broken into two stages – an aerodynamic wind-tunnel test in July 2011 and an aeroacoustic test from September 2012 through January 2013. Both tests were conducted in the 14x22 Tunnel. The 14x22 Tunnel was ideal for the HWB acoustic tests because it could accommodate the large 12.35-foot wing-span model needed to obtain full-scale high frequency data of interest for acoustics. The closed-test-section, aerodynamic test evaluated low-speed aerodynamic performance, stability, and control characteristics. These aerodynamic results were then used as input to establish proper flight conditions for the aeroacoustic test. The results of the aerodynamic test are documented in paper AIAA-2012-2669 (Gatlin, Vicroy, & Carter, 2012).

Two types of engine noise simulators were used to test the effectiveness of engine shielding benefits – a Broadband Engine Noise Simulator (BENS) to represent broadband turbomachinery noise and a Compact Jet Engine Simulator (CJES) to represent the jet noise. This test involved not just shielding of the engine noise but also understanding and rearranging the noise sources to take advantage of shielding. Airframe noise and jet noise produced in this tunnel environment were intended to be scalable to that produced by full-scale HWB vehicles. The purpose of the engine noise simulation was to establish the shielding

effectiveness of nacelle positioning. Wind-tunnel test conditions matched realistic flight conditions in order to capture all propulsion aircraft acoustic influences of this unconventional HWB aircraft.

Acoustic data from phased array microphones (mounted on a traversing overhead structure) and from individual microphones (mounted on two sideline towers and on the overhead traversing truss structure) were acquired over a variety of streamwise and spanwise locations in the open-jet facility test section for a range of tunnel dynamic pressures. In order to obtain good validation of shielding effects, the model configuration and testing apparatus were optimized to identify the noise source regions, quantify their strength, and determine the directivity of the radiated noise. The phased microphone array, when coupled with the Deconvolution Approach for the Mapping of Acoustic Sources (DAMAS) method, enabled the localization and quantification of the strength of those sources (Brooks & Humphreys, 2006). The DAMAS method is able to determine the acoustic noise source distribution more accurately than with traditional beam-forming techniques, generate noise source localization maps with high spatial resolution, and determine noise sources below wind-tunnel background noise levels.

Results of this HWB test will serve as quality benchmark data for propulsion-airframe shielding effects including integrated twin broadband turbomachinery, dual-stream hot jets, and hybrid wing body airframe noise. Data and supplemental test information can be made available through any of the contacts listed in Section 2. The HWB model and the test apparatus are modular with versatile components to facilitate future studies in anticipation of continuing this research past the current HWB test. There remains much to be learned with regard to integrated aerodynamic, structural, and acoustic disciplines, as well as, specifically, their influences on free-flight shielding effects.

2 Main Personnel

Table 1. Main Personnel Contact List

Responsibility	Name	Organization	Email
Principal Investigator	Thomas Brooks	NASA LaRC Aeroacoustics Branch	Thomas.F.Brooks@NASA.gov
Co-principal Investigator – Main Contact for BENS	Florence Hutcheson	NASA LaRC Aeroacoustics Branch	Florence.V.Hutcheson@NASA.gov
Co-principal Investigator – Main Contact for CJES	Michael Doty	NASA LaRC Aeroacoustics Branch	Michael.J.Doty@NASA.gov
Co-test Preparation Lead and Test Director	Danny Hoad	Northrop Grumman	Danny.R.Hoad@NASA.gov
Co-test Preparation Lead and Test Director	Stephanie Heath	NASA LaRC Aeroacoustics Branch	Stephanie.L.Heath@NASA.gov
Data Acquisition System	Lawrence Becker	Northrop Grumman	Lawrence.E.Becker@NASA.gov
Acoustic Instrumentation and Data Management Lead	William Humphreys	NASA LaRC Advanced Sensing and Optical Measurement Branch	William.M.Humphreys@NASA.gov
Array Hardware Technician	Scott Bartram	NASA LaRC Advanced Sensing and Optical Measurement Branch	Scott.M.Bartram@NASA.gov

CJES and Fuel System Designer	Harry Haskin	NASA LaRC Aeroacoustics Branch	Henry.H.Haskin@nasa.gov
Photogrammetric System Designer and Data Analysis	Benny Lunsford	NASA LaRC Advanced Sensing and Optical Measurement Branch	Charles.B.Lunsford@nasa.gov
Research Investigator and HWB Assessment	Casey Burley	NASA LaRC Aeroacoustics Branch	Casey.L.Burley@NASA.gov
Test Data Reduction and Coordinator	Chris Bahr	NASA LaRC Aeroacoustics Branch	Christopher.J.Bahr@NASA.gov
Test Data Reduction and Analysis	Taylor Spalt	NASA LaRC Aeroacoustics Branch Coop	T.B.Spalt@NASA.gov
Instrumentation Technician , Data Acquisition, Processing and Analysis	Dan Stead	Northrop Grumman	D.J.Stead@NASA.gov
Instrumentation Technician	Dennis Kuchta	ROME Jacobs	Dennis.H.Kuchta@NASA.gov
Mechanical Technician	Jaye Moen	NASA LaRC Aeroacoustics Branch	Jaye.A.Moen@NASA.gov
Data Processing and Analysis	Stuart Pope	Analytical Services and Materials Inc.	Dennis.S.Pope@NASA.gov
Data Processing and Analysis	Jerry Plassman	NIA	Gerald.E.Plassman@NASA.gov
HWB Aerodynamic Test Coordinator	Greg Gatlin	NASA LaRC Configuration Aerodynamics Branch	Gregory.M.Gatlin@NASA.gov

3 Test Equipment

This section describes the facility and model equipment used in the HWB Test.

3.1 Facility Description

The 14- by 22-Foot Subsonic Tunnel at the NASA Langley Research Center is a closed-circuit, single return, atmospheric wind tunnel capable of producing a maximum speed of 348 feet per second (Mach 0 to 0.3) with a test section measuring 14.5' H x 21.75' W x 50' L. A sketch showing the details of the complete tunnel circuit is presented in Figure 1.

The facility can be operated in either an open or a closed test-section configuration. The open test section configuration, which has a maximum speed of approximately 270 ft/sec, is formed by raising the ceiling and walls. All results presented in this paper were obtained while operating the facility in the open test-section configuration. Further tunnel details and facility information are presented in NASA TP-3008 (Gentry, Quinto, Gatlin, & Applin, September 1990).

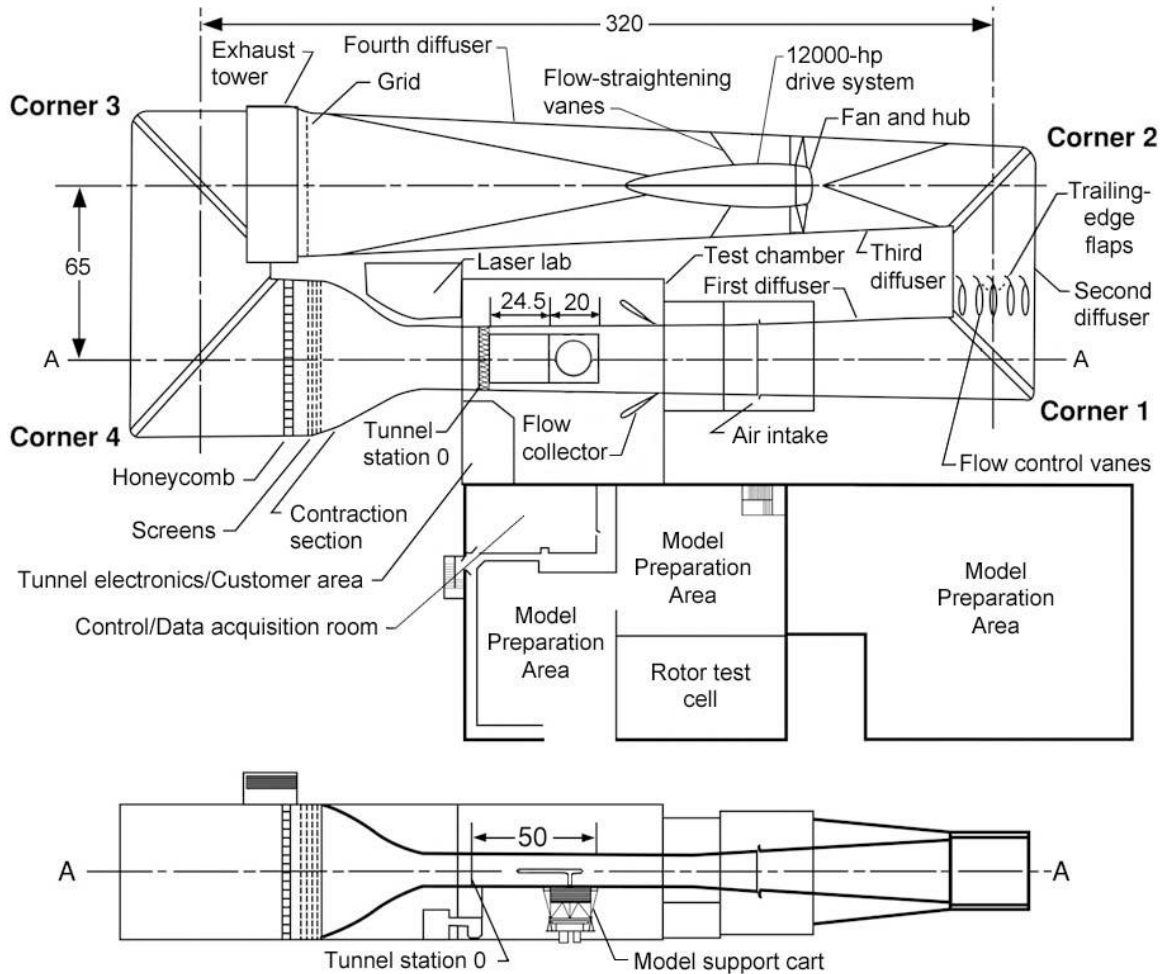


Figure 1. NASA Langley 14- by 22-Foot Subsonic Tunnel circuit. Dimensions are given in feet.

The acoustic measurements were performed in an acoustically treated, open test section with continuous tunnel flow. The model was inverted. The engine noise simulators on the model were positioned at several locations forward and just aft of the model trailing edge as defined in the test matrix (presented in Section 6). A major facility upgrade was required to accommodate the installation of the new microphone phased array in the ceiling of the tunnel. As part of the upgrade, a two-axis overhead traverse system was fabricated and installed above the facility crane rail system in the ceiling. The overhead traverse had the ability to translate along the full length and width of the test section. The traverse carriage height was adjusted to ensure that buffeting of the phased array panel was minimized across the entire speed range of the tunnel. The optimal height of the traverse carriage above the floor of the tunnel was determined in the summer of 2010 via detailed microphone rake measurements of the thickness of the upper shear layer in the open jet (Humphreys, 2010) (Brooks, 2010). A unique motorized winch system was developed to allow the array to be lowered to the floor of the test section to accommodate installation, removal, and maintenance of the microphone phased array. Intersecting serpentine cable trays were installed in the ceiling of the tunnel to route signal cables from the overhead traverse carriage to the control room and cable conduits were installed to route signal cables from the far side of the test section to the control room. Also, the tunnel area directly above the tunnel entrance nozzle was modified to provide a storage area for the traverse carriage and array panel when not in use.

In addition to the new overhead traverse, four separate 44-foot linear traversing rails were manufactured for use on the floor of the test section. Two rails were mounted on each side of the test section to support two 11-foot tall open frame sideline microphone towers, which also traverse the full length of the tunnel

(i.e., from the entrance lip of the tunnel test section to the collector at the rear of the tunnel) outside of the flow shear layer, as shown in Figure 2. Sideline tower and truss mounted microphones, in addition to the phased array on the overhead traverse, were used to obtain hemispherical characterizations of the noise directivity.

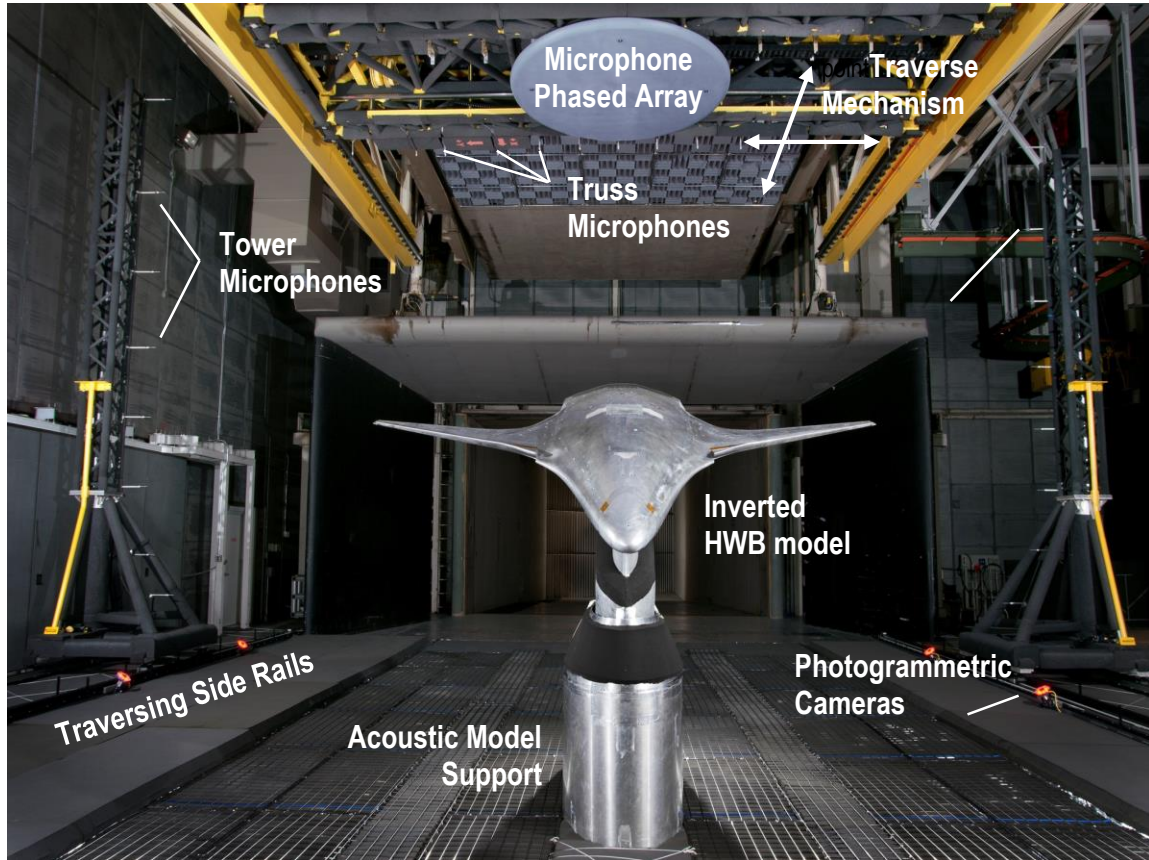


Figure 2. HWB test section configuration.

The facility was also acoustically treated, to minimize any acoustic reflections, with perforated plates that cover most of the facility, including the main tunnel walls and collector. In addition to these plates, the floor, ceiling, and blast wall were treated with foam wedges, as shown in Figure 3.

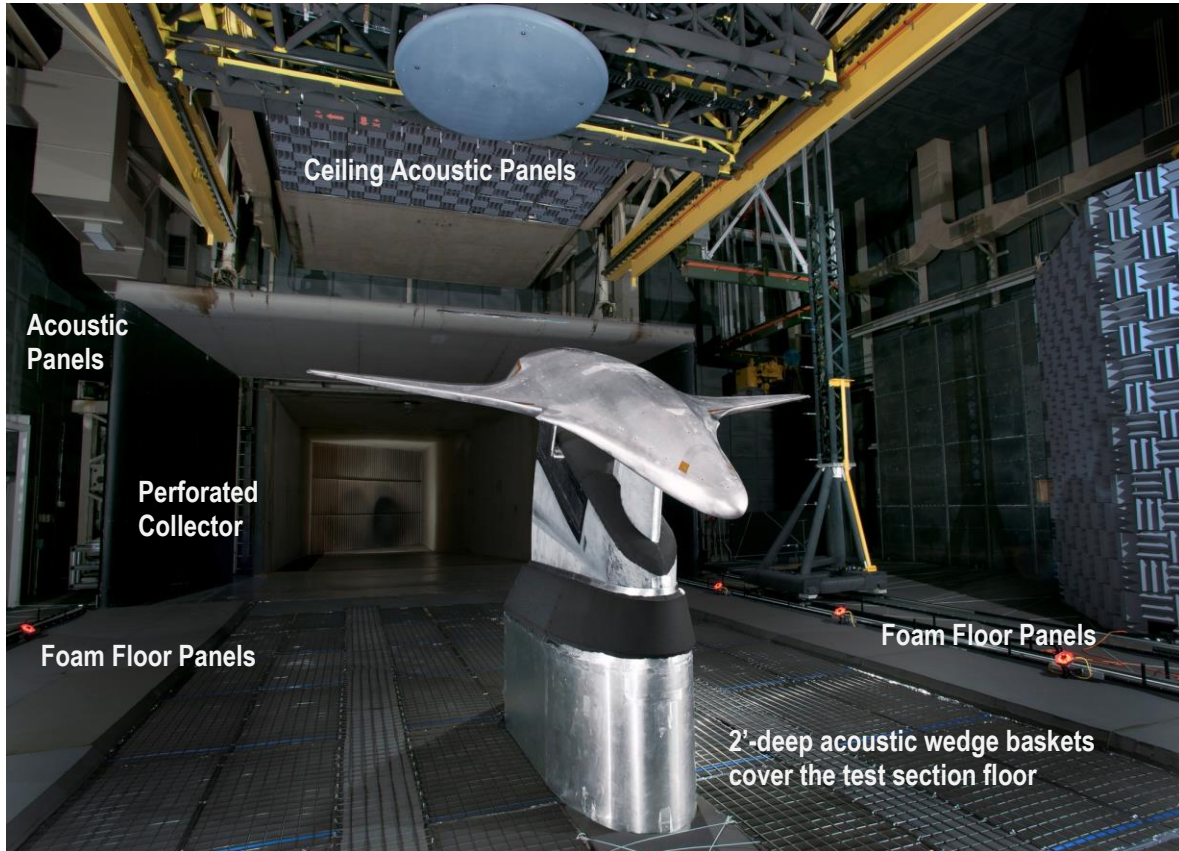


Figure 3. 14- by 22-Foot Subsonic Tunnel acoustic treatment.

During the jet noise studies of the test program, the facility supplied gaseous propane to the CJES units. The CJES propane flow was controlled by a valve pallet located under the tunnel test section. The valve pallet operations were commanded and monitored using an Allen Bradley Programmable Logic Controller (PLC) with PanelView screens. The valve pallets controlled the facility nitrogen, propane, and air operations as well as control of the engine simulator operating conditions (temperatures and pressures) by adjusting the mass flow rates. There was one valve pallet for each CJES and each pallet supplied one fuel line and two air lines (one for the fan and one for the core flow) on the CJES.

3.2 HWB Model

The HWB model was 5.8 percent of the full-scale vehicle, which allowed acoustic measurements over the full-scale equivalent range of about 230 Hz to 4.1 kHz (4 to 70 kHz at model scale). The HWB low-speed wind-tunnel model represented Boeing's Quiet R1 configuration aircraft, and was designated as N2A-EXTE (Kawai, 2011). The model was 8.583 feet long with a 12.354-foot span, and the fuselage geometric details were accurately scaled for airframe noise studies. The model is illustrated in Figure 4. The model was modular with components and control surfaces that could be deflected to match specific flight conditions. The components included drooped and cruise leading edges, trailing-edge elevons, vertical tails, landing gear, and flow-through nacelles (not shown), which were replaced during the acoustic testing with turbomachinery and jet noise simulators.

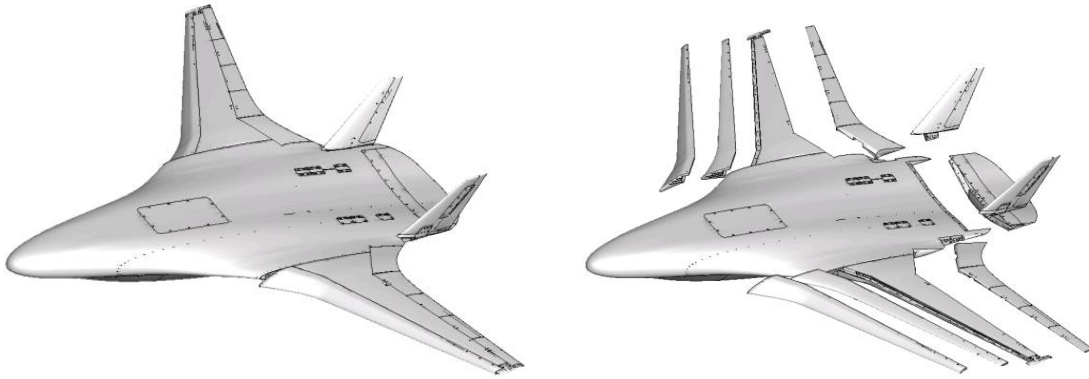


Figure 4. General N2A-EXTE HWB test model. Flow-through and engine noise simulator nacelles are not shown.

3.2.1 HWB Model Details

Table 2. HWB Model Details

Airframe Component		Details
Wings		
	Basic Shape	<ul style="list-style-type: none"> The wing had a reference chord of 60.552 inches The wing had -8.87 degrees of twist at the wingtip Sweep angle at the quarter-chord of the constant sweep, outboard portion of the wing was 24.2 degrees
	Leading Edge	<ul style="list-style-type: none"> Removable leading-edge shapes; one for cruise and one “drooped” for the approach and take-off conditions. The drooped leading-edge was deflected 20 degrees down, toward the concave side of the airfoil, between the wing spanwise location, η, of $\eta=0.311$ and $\eta=0.400$. The droop then transitions to 30 degrees down from $\eta=0.400$ to $\eta=0.445$, and to 30 degrees for the remainder of the outboard portion of the wing span. The wing span, η, is defined as the semispan distance divided by the full semispan length.
	Trailing-Edge Elevons	<ul style="list-style-type: none"> There were eleven independently deflectable elevons along the trailing edge of the vehicle (see Figure 4); a center elevon (E1) positioned between the two vertical tails; and five elevons extending across the trailing edge of each wing (E2-E6). E2 is adjacent to the center elevon and E6 is the most outboard elevon. This pattern repeats for elevons E7-E11, where E7 is adjacent to the center elevon. Wing elevon settings were at -40°, -10°, 0°, $+10^\circ$, or $+40^\circ$ deflection angles (+ indicates a deflection toward the landing gear and – indicates a deflection toward the engines) Model scale trailing-edge thickness was 0.009” to accurately represent full-scale geometry
Vertical Tails		<ul style="list-style-type: none"> Configurations include two vertical tail geometries (long span/short chords and short span/long chords) Two tail positions; a forward and a rear longitudinal position. Two cant angles (10° and 30°) for each tail geometry Vertical tails also contain variable rudders allowing three deflection angles including 0 degrees
Landing Gear		<ul style="list-style-type: none"> Removable high-fidelity landing gear included left and right main gears and a nose gear Hydraulic lines, actuators, side braces, brake system, and tire treads were accurately modeled Gear wells and partially covered wheel wells and gear doors were modeled

3.2.2 Model References

As-built part files (CATIA and STEP format) from MicroCraft, Inc. computer aided design (CAD) drawings created from the electronic files are stored on the Central Storage System (CSS). Information on the CAD model may be obtained from either Florence Hutcheson or Greg Gatlin of NASA LaRC using the contact information provided in Section 2 of this report. Figure 5 – Figure 7 show the general HWB characteristics.

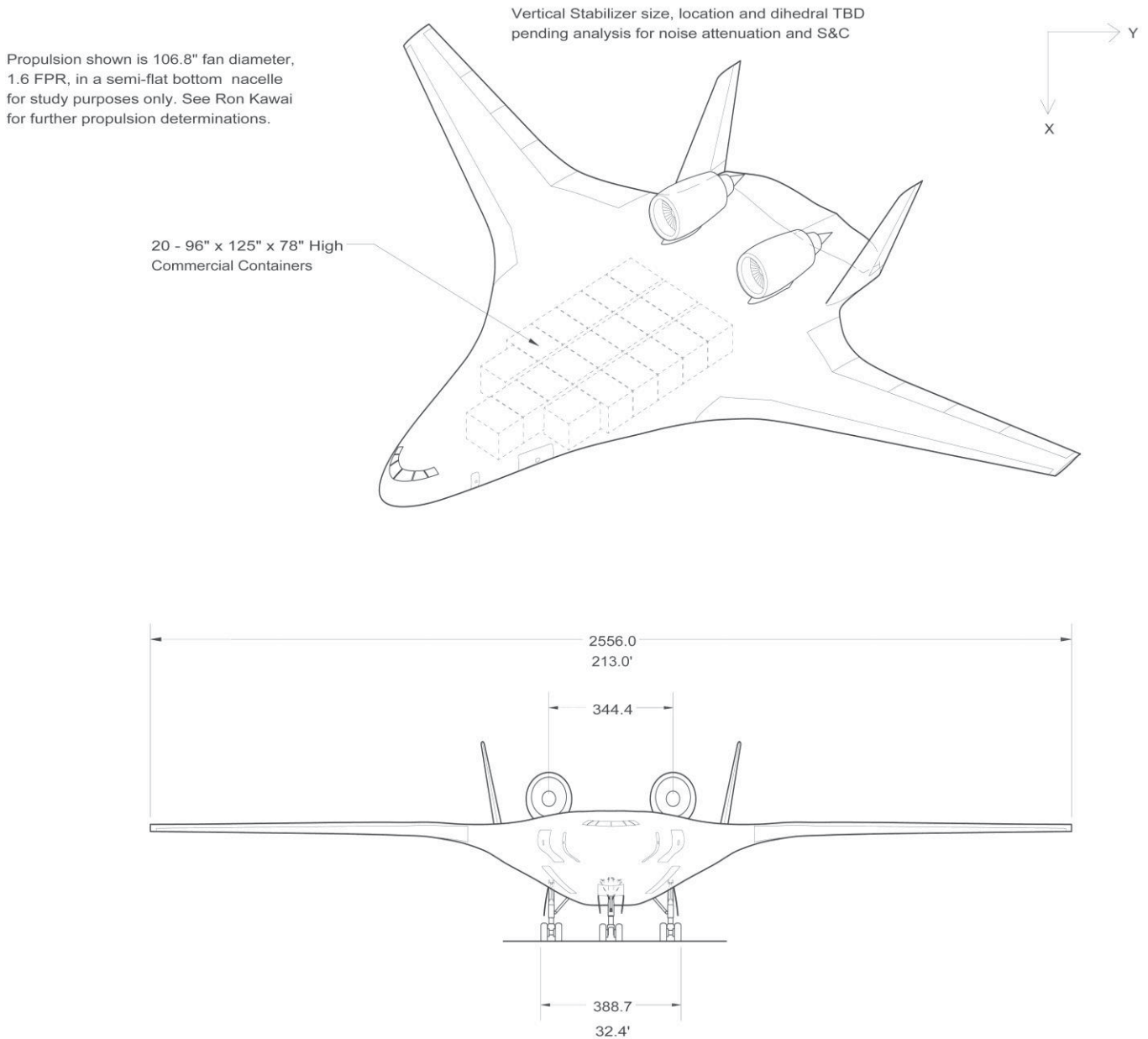


Figure 5. General HWB Model arrangement drawing details – oblique and front views. Units are given in inches.

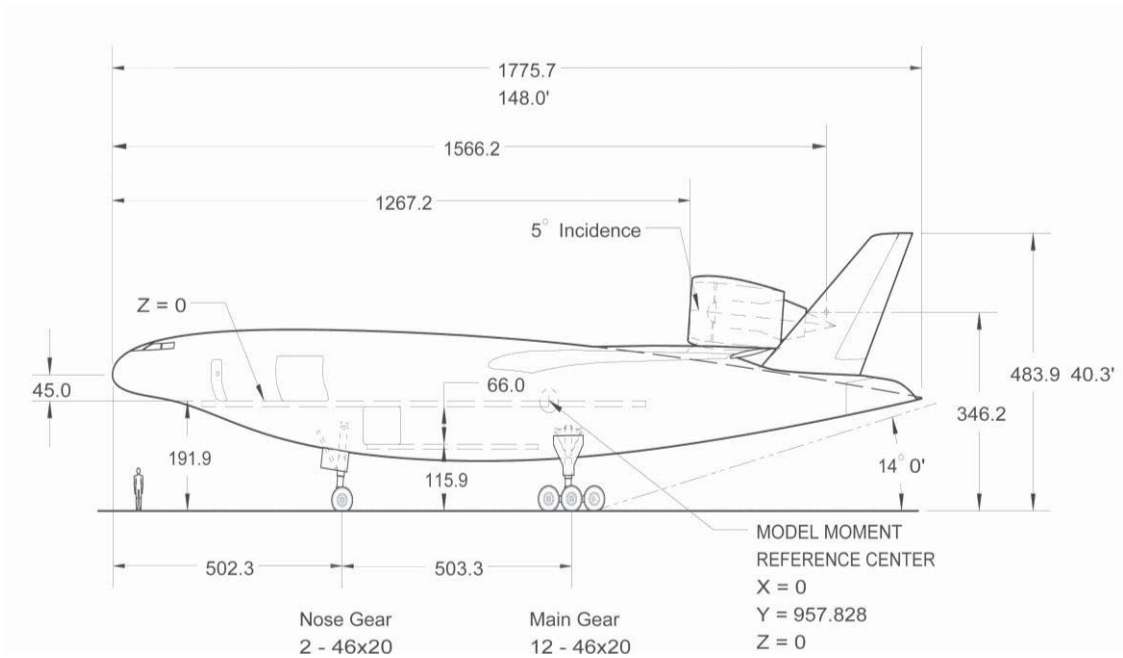


Figure 6. General HWB Model arrangement drawing details – side view. Units are given in inches.

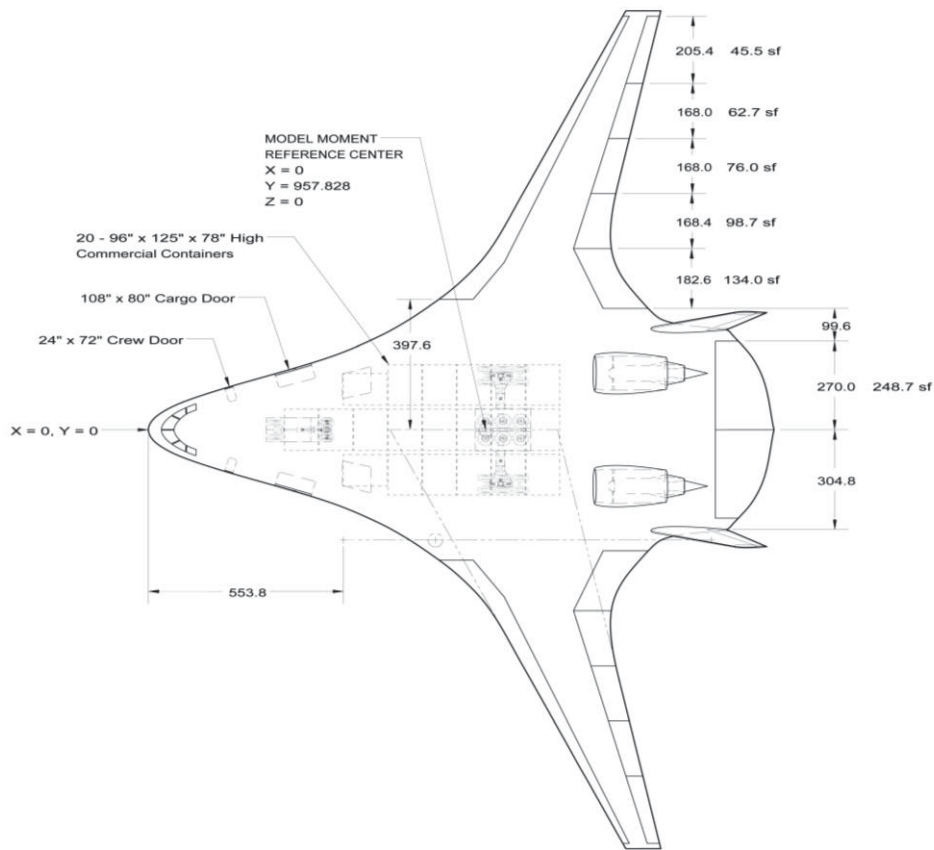


Figure 7. General HWB Model arrangement drawing details – top view. Units in inches unless otherwise marked.

3.2.3 Transition Grit on Model

Transition grit was applied to the model for all test runs to ensure that the boundary layer along the surface of the model properly transitioned to a turbulent state in a repeatable manner throughout the investigation. Transition grit was applied to several areas of the HWB model including – a ring around the nose of the model; along the length of the forebody, beginning three inches aft of the leading edge on the upper surface and two and a half inches aft of the fuselage leading edge on the lower surface; on the wings beginning 1.7 inches aft of the leading edge on both the upper and lower surfaces; and around the leading edge of the vertical tails. All distances aft of the leading edges were measured perpendicular to the leading edge and along the model surface. The grit was a silicon carbide grain with a grit number of 90, and its application was guided by common practices used in the 14- by 22-Foot Subsonic Tunnel and the methods presented in (Braslow & Knox, 1958).

3.3 Engine Simulators

Two engine simulators were developed for use with the HWB model; CJES to accurately produce hot jets with noise production and shielding that was scalable to full-scale vehicles, and BENS to evaluate shielding of the broadband component of turbomachinery noise.

Numerous preliminary risk reduction tests were completed for each of the main engine components prior to the HWB 14x22 Wind-Tunnel Test. References can be obtained from the appropriate person listed in the Main Personnel Contact List in Section 2, and are listed in following sections where applicable.

3.3.1 Engine Location Documentation

In the acoustic testing configuration, the BENS and CJES simulators were mounted on the acoustic model support pitching arm and were aligned with the aft section of HWB Model suction surface. The exit plane of all three model engines (CJES, BENS, and the HWB Model flow-through nacelle) were located in the same nominal position relative to the HWB. There were five (5) discrete axial locations, including the nominal position, defined in terms of fan nozzle exit diameters, D , upstream or downstream of the model trailing edge (TE), and measured along the engine axis. The distances from the model TE to the center of fan nozzle exit plane were; $3.0D$ (the most forward position), $2.5D$ (the nominal position), $1.5D$, $0.0D$, and of $-0.5D$ (the most aft position). The nominal engine location is offset $8.315''$ from the balance center (away from the model centerline) and $9.991''$ outboard of the model centerline; which is 2.5 engine diameter lengths (D) upstream of the model trailing edge. This corresponds to a distance of $29.801''$ downstream of the model balance center, as shown in Figure 8, and a distance of $38.188''$ downstream of the model aerodynamic center (MAC), as shown in Figure 9. For all engine locations, the engine centerline was pitched 5 degrees with respect to the model centerline.

The original full-scale fan nozzle exit diameter, D , was originally established as 5.8 percent of $107.3''$, or $6.223''$. The engine noise simulators and flow-through nacelles are defined and built based on this diameter, as shown in Figure 9. However, the fan exit diameter was changed slightly a couple of times (to $6.238''$ and $6.248''$) during the construction of the model and support hardware to meet updated engine core and fan flow requirements. Because of this, the $3.0D$, $1.5D$, $0.0D$, and $-0.5D$ engine locations have varying reference diameters. The reference diameter used for the axial position of $3.0D$ (or more specifically, the spacing forward of the nominal $2.5D$ location) was $6.238''$ (which corresponds to a spacing of $3.119''$ upstream of the nominal location). To complicate matters, the $-0.5D$, $0.0D$, and $1.5D$ locations used a reference diameter spacing of $6.248''$. These engine spacing dimensions are shown in Figure 8. These diameter variances were determined to be insignificant in the scope of this test, and no further mention is made to their axial spacing deviations, but is listed here to explain minor differences.

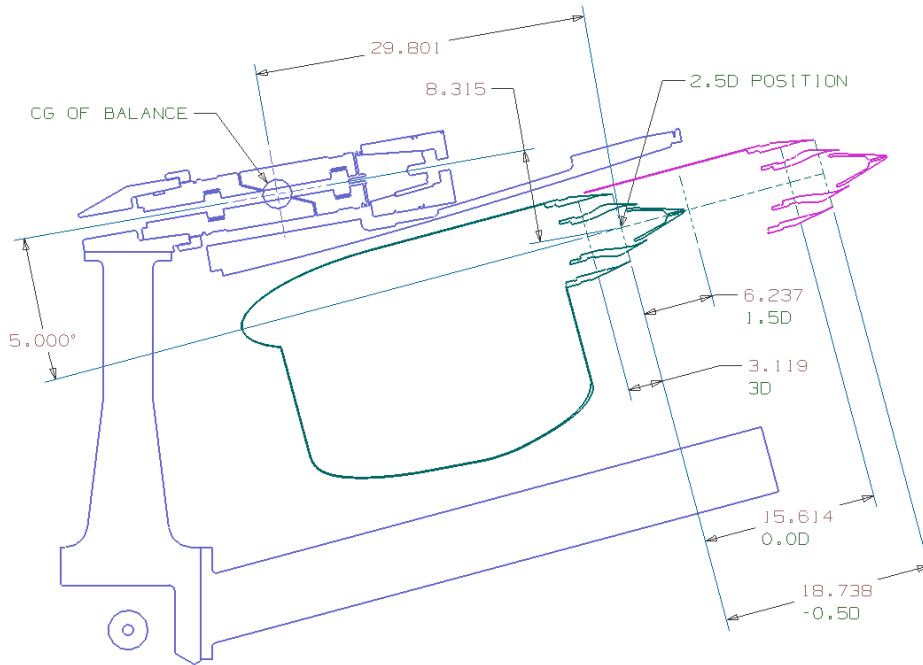
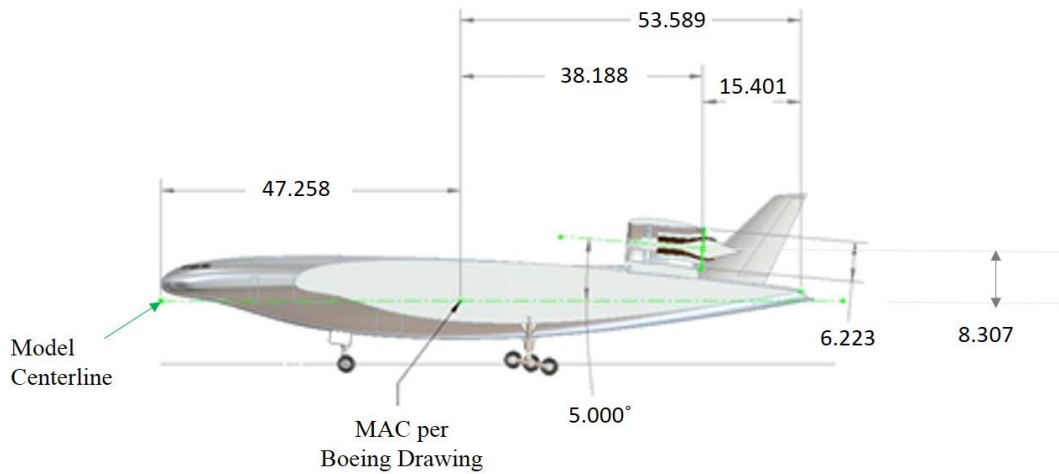


Figure 8. Engine positions and dimensions (in inches).



- N2A-EXTE HWB Model Scale is 5.8%
- Full-scale fan exit diameter of 107.3"
- Model based on a fan exit diameter of 6.223"
- Nominal engine axial position:
 - Lateral spacing between the two engines (fixed at cruise position) is 9.988" from model centerlines.
- Vertical engine dimension above Model Aerodynamic Center (MAC), when the fan nozzle exit located at the nominal position of X=15.401", is 8.307" with respect to the model centerline.
- Other engine positions are moved along a 5° angle between engine centerline and model centerline. : Distances of the fan nozzle exit forward of the TE are measured along engine centerline.

Figure 9. Nominal engine position definition. Units are in inches.

The engine simulators were mounted to a saddle block that rides along the engine support arm discussed in Section 3.4 – Model Support Systems. The engine simulators were aligned with the model using mating holes on the side of the saddle block and the engine support arm. The nominal component stack up (taken from the solid model) included a 0.150” shim between the saddle block and the BENS and CJES units. As-built tolerances allowed for a 0.070” shim on the BENS assembly and a 0.093” shim on the CJES assembly. However, to provide more clearance between the engine simulators and the surface of the HWB model, these shims were not used in the engine assemblies during this test.

3.3.2 Broadband Engine Noise Simulator (BENS)

The BENS simulators were used to determine insertion loss due to shielding of the broadband component of turbomachinery inlet and exhaust noise by the HWB airframe. The BENS nacelle was approximately 6” in diameter and 12” long with removable (and aerodynamically shaped) inlet and outlet caps. Shielding of inlet and exhaust radiation was examined separately by alternately capping the nacelle inlet and exhaust to isolate noise radiation from either the inlet or outlet of the nacelles.

Each BENS consisted of an internally-open nacelle with a representative core structure and three interchangeable rings of impinging air jets with isolated plenums (shown in Figure 10). Each impinging jet noise source was formed by four coplanar tubes arranged in a cruciform planform. Air was supplied at 120 psia to each plenum through 0.5” lines. The BENS inlet and exhaust were instrumented with unsteady surface pressure sensors to monitor the noise output. Figure 11 and Figure 12 show the BENS assembled on the acoustic model support.

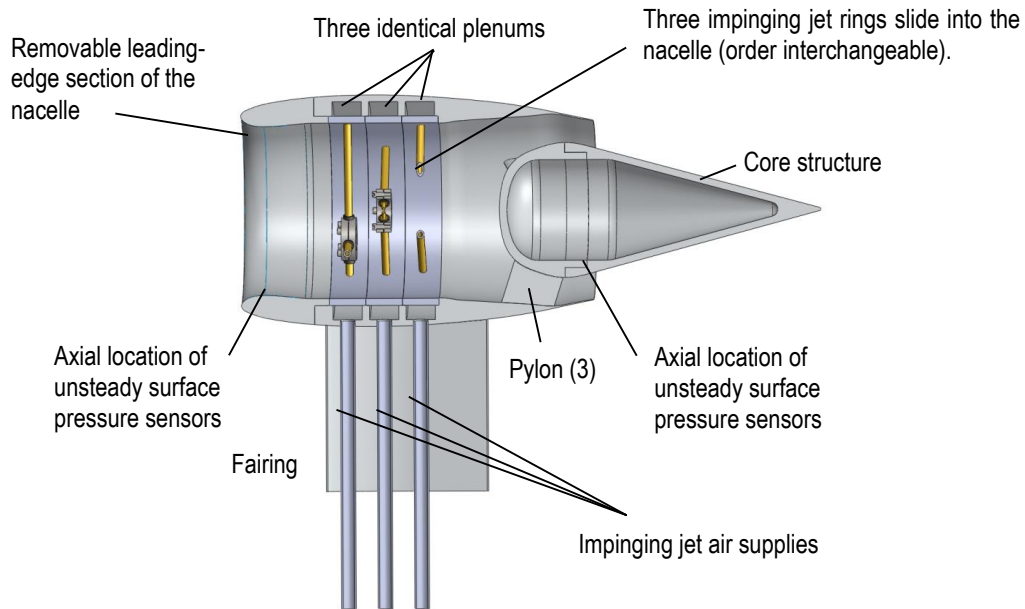


Figure 10. Cross section of Broadband Engine Noise Simulator.

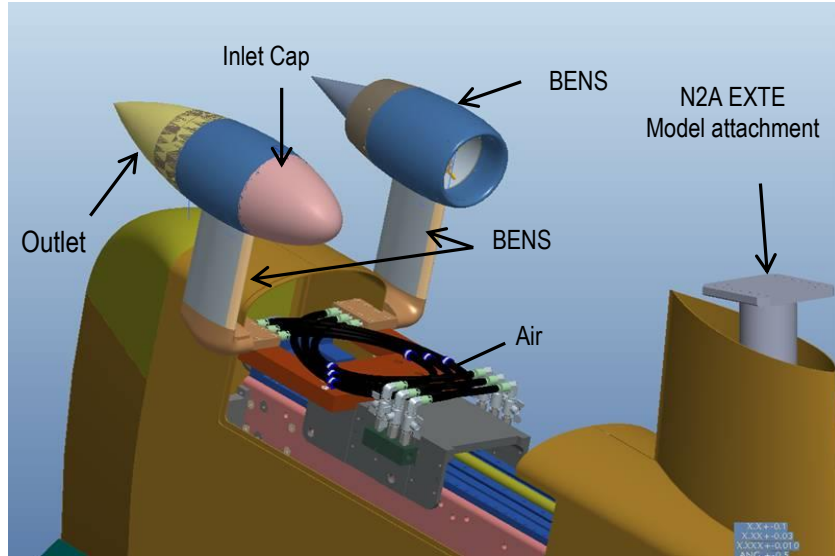


Figure 11. BENS assembly on the acoustic model support.



Figure 12. BENS engine nacelles in inlet and exhaust noise radiation configurations (nacelles shown in their nominal position with respect to the model airframe).

3.3.3 Compact Jet Engine Simulator (CJES)

The jet noise source was produced by two dual stream jet engine simulators consisting of an interior heated core flow and outer fan flow. A facility fuel system supplied gaseous propane to a combustor in the core flow. The air and fuel flows for each engine simulator were independently controlled by two valve pallets, one per each engine simulator.

The combustor used a unique compact annular propane burner to heat the core flow. The propane was burned in the annular combustion chamber followed by a flow straightening core vane assembly. A schematic of the jet engine simulator is shown below in Figure 13. The combustor injected fuel radially into a swirl cavity at six locations. Swirl air was injected on either side of the fuel jets, which were angled at 45 degrees to the radial direction to promote mixing of the fuel and air that allowed a shorter combustor length and a more efficient combustor.

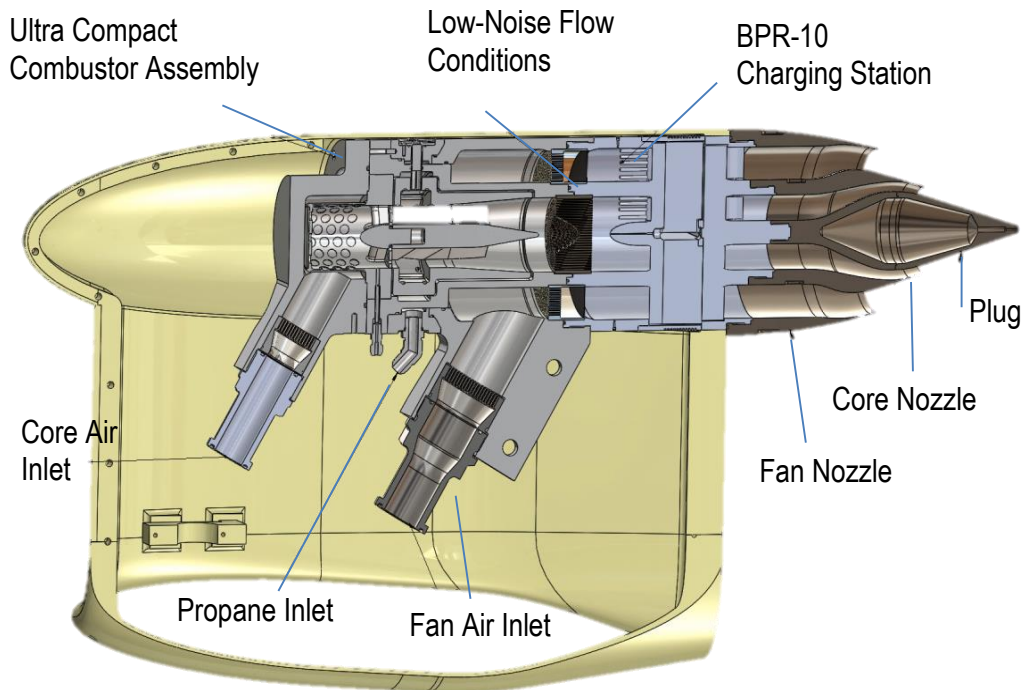


Figure 13. Schematic of the Compact Jet Engine Simulator.

The CJES simulated a BPR 10 engine with a bypass nozzle exit area of 4470 in² (15.12 in² model scale). Engine nozzle design and corresponding cycle parameters (Mach number-M#, Nozzle Pressure Ratio-NPR, and Nozzle Temperature Ratio-NTR) were predicted based upon engine state tables provided by Numerical Propulsion System Simulation (NPSS) analysis for relevant HWB flight speeds, altitudes, and throttle settings. Reference (Berton, Envia, & Burley, 2009) and (Lytle, 2000) for further details.

Two 5.8-percent scale nozzles were used with the CJES. The first nozzle was a standard baseline model that was circumferentially uniform, as shown in Figure 14. The second nozzle was a “low-noise” chevron nozzle that included a T-fan chevron array oriented with the longer chevrons in an asymmetrical pattern, as shown in Figure 15.

The HWB test consisted of installed (jet with airframe) configurations. CJES assembly information and aeroacoustic characteristics including flow conditioner effects are described in these two papers, (Doty & Haskin, 2013) and (Doty, Brooks, Burley, Bahr, & Pope, 2014).

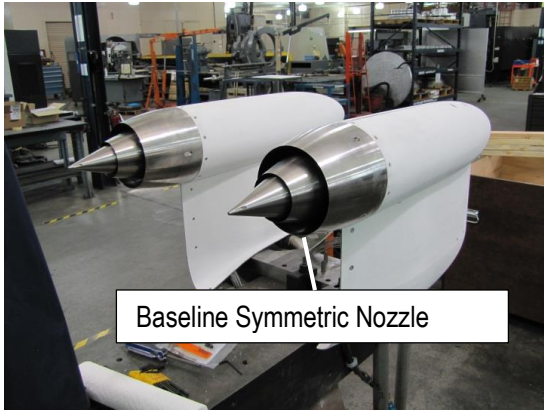


Figure 14. Baseline nozzles installed on the Compact Jet Engine Simulators.



Figure 15. "F8" low-noise chevron nozzle in NASA Langley's Low Speed Aeroacoustic Wind Tunnel.

3.4 Model Support Systems

The HWB model was mounted in an inverted orientation on facility cart #1 in the front bay during the acoustic portion of the test. The fully assembled configuration is shown in Figure 16. The model support strut allowed for independent pitching and rolling mechanisms on the strut. The top of the strut connected the model to the pitch mechanism and also supported an attachment arm to mount the engine simulators. The lower portion connected the pitch to the roll joint, located below the pitch mechanism, and allowed the model to be manually rolled and locked at -30° , 0° , and $+30^\circ$. The roll knuckle was located below the pitch mechanism so that the model angle of attack could be set while the model was rolled without inducing a yaw angle. The model was rolled to permit noise directivity measurements from an overhead phased microphone array over a broader range of angles.

Variation in angle of attack (AOA) was accomplished by an independent pitch mechanism and was controlled by the facility's control and data acquisition systems. With the model at 10° angle of attack, the pitch mechanism was at the center of its permissible angle range and the post was vertical. The required range in this configuration was $+25^\circ$ to -5° with a resolution of 0.01° , as shown in Figure 16.

3.5 HWB Model Location and Alignment

The alignment of the model within the tunnel is described in this section. The dimensions for the model placement within the tunnel are shown in Figure 16. A check-loading fixture was built to help align the model. The fixture has two perpendicular reference surfaces that are both aligned with the model centerline, as shown in Figure 17. The check-loading fixture was used to align the model in both the upright and inverted model positions on their respective model support strut in the tunnel.

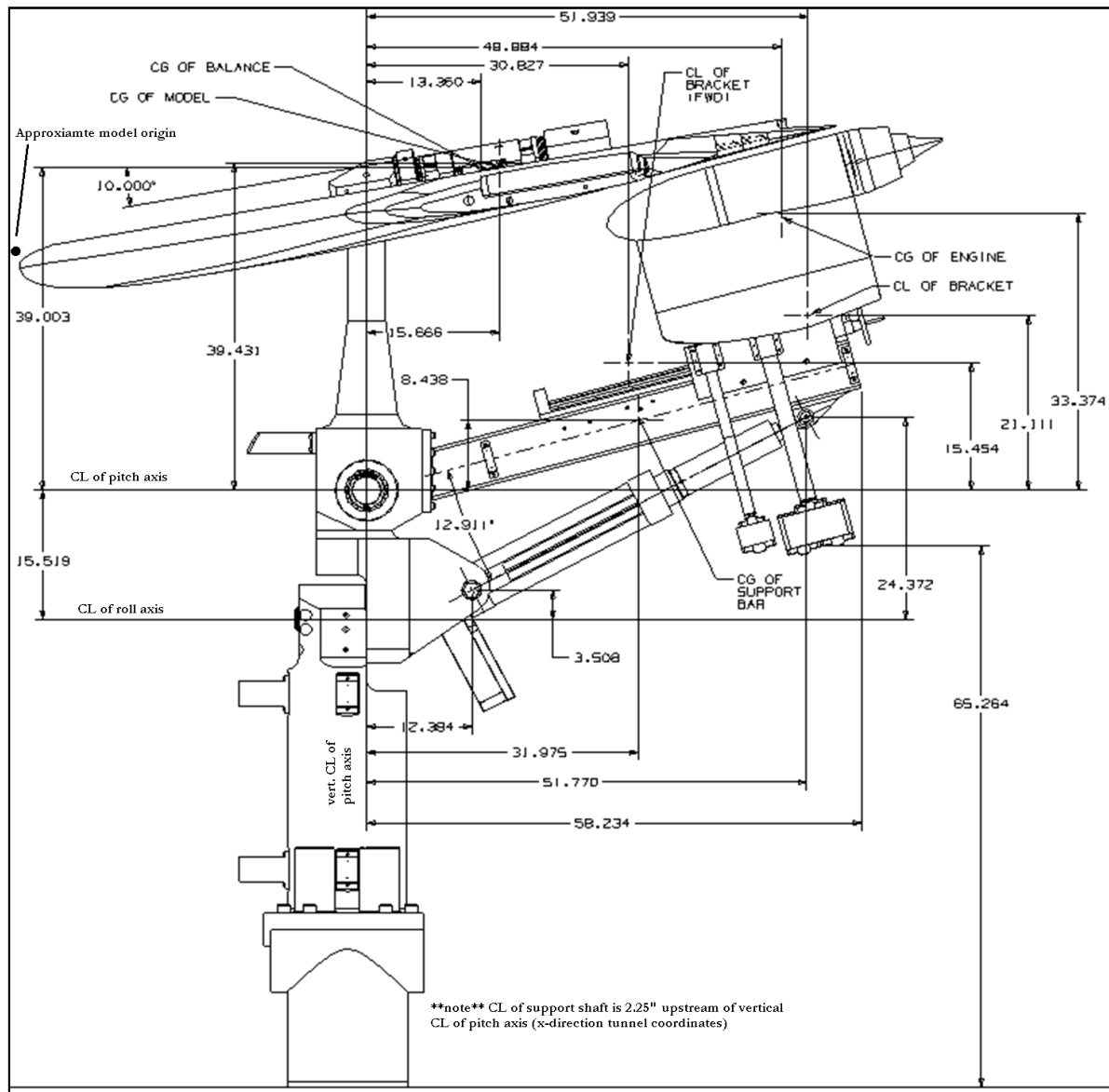


Figure 16. HWB Model and model support assembly within 14- by 22-Foot Subsonic Tunnel coordinates. All dimensions are in inches.

The following are Figure 16 drawing notes:

- Floor (wedges) to roll axis = 32.05" (z-direction, tunnel coord.)
- Floor (wedges) to pitch axis = 47.57" (z-direction, tunnel coord.)
- Nozzle exit to center of support shaft = 210.5" (x-direction in tunnel coord.)
- Center of support shaft to vertical CL of pitch axis = +2.25" (x-dir. tunnel coord.)
- Array face from floor = 246.5"
- Array face from point source 1 at 0° pitch/0° roll = 157.34" (z-direction, tunnel coord.)
- Center of Gravity (CG) Model in model coord. = (0.00, 57.90, 0.48) in.
- Center of Gravity (CG) Model from floor (wedges) = 87" (z-dir. tunnel coord.)
- Tunnel Coordinates for CG Balance at 0° pitch/0° roll: (235.18, 0.00, 83.66) in.
- Tunnel Coordinates for CG Balance at 10° pitch/0° roll: (228.61, 0.00, 86.57) in.
- Tunnel Coordinates for CG Model at 10° pitch/0° roll: (230.92, 0.00, 86.99) in.

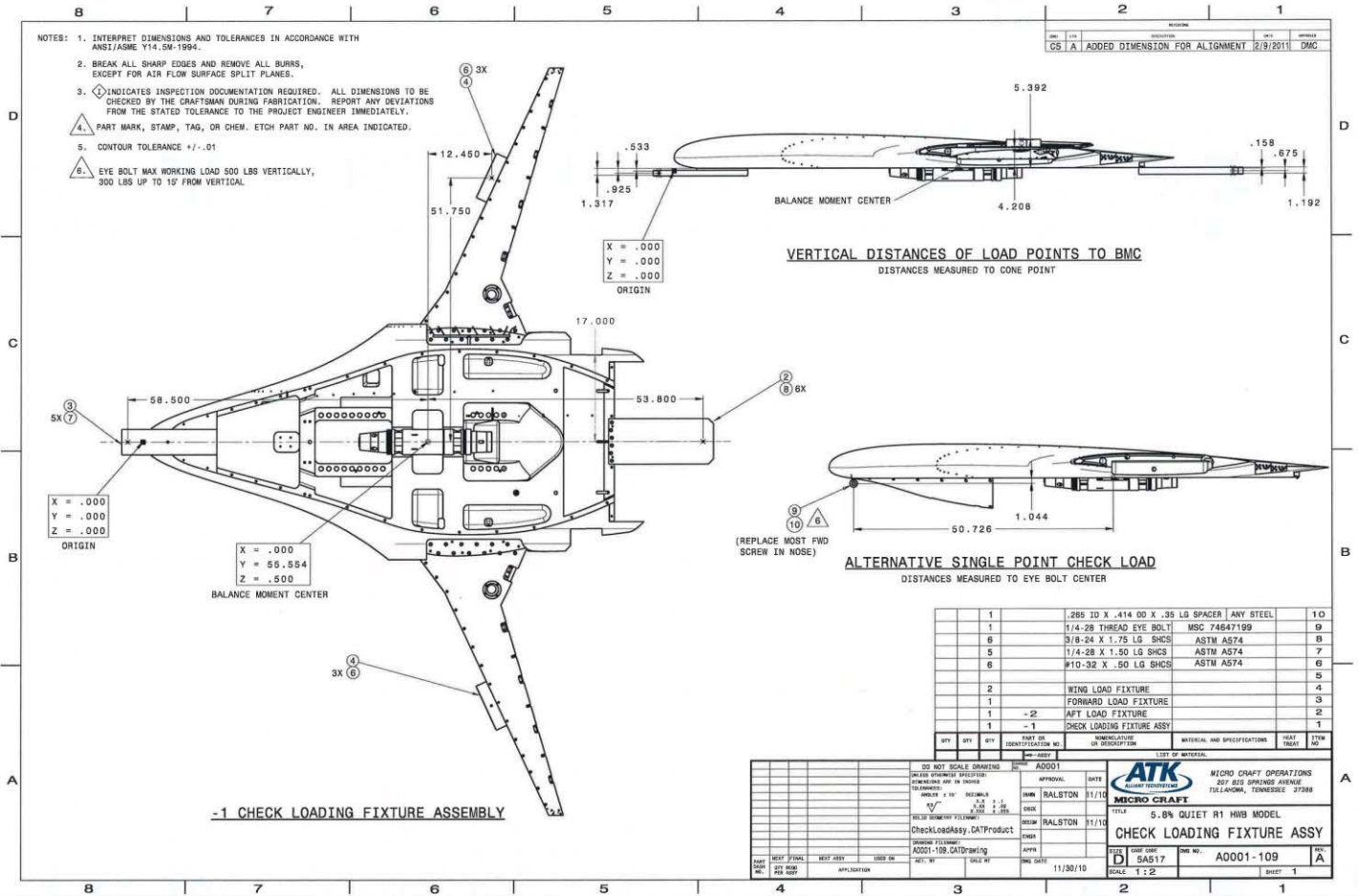


Figure 17. HWB Check Loading Fixture assembly drawing.

4 Data Acquisition Systems

Two data acquisition systems (DAS) were used during the HWB test – the tunnel DAS and the acoustic DAS. Both are described in detail below. All data taken by the tunnel DAS were tracked and integrated with the acoustic DAS for use in data reduction.

4.1 Tunnel Data Acquisition System

Flow-related measurements on the HWB were made solely from the model's pressure taps and were stored on the tunnel DAS. All wind-tunnel data, including model angle of attack (inclinator data), were gathered by the tunnel data acquisition system and integrated with the acoustic data. The tunnel was equipped with an on-line static data reduction system that displayed computed average aerodynamic coefficients with interactions and wall interference corrections in real time and other critical required test data. The DAS data collected included – Tunnel Parameter Calculations, Model Temperatures, Model Rotations, BENS Parameters (with the exception of the Kulites, which were acquired by the Acoustic DAS), CJES Parameters, the data available from the raw Tunnel DAS, and HWB Model Pressure Tap data. A complete listing of the data parameters is included in Appendix B: Tunnel DAS Data Listing. The tunnel DAS was calibrated daily in accordance with tunnel procedures.

4.1.1 BENS Airflow Data

With the exception of unsteady surface pressure signals acquired for the BENS, all air flow and other operating parameters were stored and controlled through the tunnel DAS. The parameters gathered for the BENS are listed and explained in section 5.2.1. The unsteady surface pressure signals were obtained using the acoustic DAS.

4.1.2 CJES Data

The CJES had special data requirements including temperatures, air flow and fuel flow parameters which were controlled by the valve pallet programmable logic controllers. The data and PLC information were integrated and recorded by the tunnel DAS, as described in section 5.2.2.

4.2 Acoustic Data Acquisition System

A new aeroacoustic measurement capability was developed for use in the open-jet testing environment required for the HWB test. The suite of instruments utilized for the test included: (1) a streamwise traversing ensemble of individual microphones for model noise source directivity measurements along both flyover and sideline axes, and (2) a two-dimensional traversable microphone phased array for identification of noise source (locations and strengths) on the model. A customized data acquisition system was developed for the instrumentation suite that allowed for command and control of all aspects of the array and microphone hardware, and it was coupled with a comprehensive data reduction system to generate test result information in near real time. This information included such items as time histories and spectral data for individual microphones and groups of microphones, contour presentations of noise source locations and strengths, and hemispherical directivity data. The two data acquisition systems communicated to allow the integration of real-time facility parameters with the acoustic data. The acoustic data acquisition system variables are contained in Appendix C: Acoustic DAS Data Listing, and details of the various subsystem interfaces are described subsequently in this section.

4.2.1 Acoustic DAS Hardware Description

A highly distributed data acquisition system was assembled using commercially available hardware for the instrumentation suite developed for the HWB test. The data acquisition system had a total capacity of 192 channels and was constructed around National Instruments PXI-6120 high-speed, synchronous sampling digitizers. The digitizers were housed in three separate chassis, each containing an embedded client computer with local disk storage. Signal conditioning of all microphone channels was achieved using a Precision Filters, Inc., Model 28000 system populated with PF-28608 cards (8 channels per card with an approximate roll off of 28 dB/octave per channel). The entire system was controlled by a master computer that communicated with the various digitizer clients using high-speed Ethernet communication configured in a 5-subnet LAN. The process controller also provided tightly synched clock and trigger functions to each client via a PXI-1033 chassis using PXI-6653 master timing modules. An IRIG-B time code signal was acquired on one acquisition channel in each embedded client as a sanity check to ensure synchronization of the system was maintained.

4.2.2 Acoustic DAS Software Description

A National Instruments Labview program was used for command and control of all of the hardware components of the data system, the facility overhead traverse system, and the Aerotech linear rail system. The acquisition program also interfaced with the wind-tunnel data system and array inclinometers to capture relevant tunnel, model, and array orientation parameters during an acquisition cycle. Acquired microphone time history data were stored on high capacity network-attached storage (NAS) devices as a series of individual raw binary data files (one file per acquisition channel). The nominal acquisition window length was 30 seconds with adjustments during the test as needed. Simultaneous sampling rates were set to 250 kHz for all acquisition channels. Verification of these settings can be found in the CSV sensor listing accompanying the HWB test data. The acquisition software allowed for full control of the Precision Filter

signal conditioners, with all signals band pass filtered from 400 Hz to 100 kHz. The 400 Hz high-pass filtering was used to eliminate low-frequency tunnel noise, thereby preventing it from reducing the dynamic range of the noise data acquisitions. The roll-off characteristics were established for the filters used and offset effects were removed in processing.

5 Instrumentation and Calibration

5.1 HWB Model Instrumentation

The HWB model was instrumented with pressure taps, temperature sensors, and typical AOA sensing devices. A complete listing of the data parameters is contained in Appendix B: Tunnel DAS Data Listing.

5.1.1 HWB Model Surface Pressure Data

Two hundred and forty eight (248) static surface pressure probes were connected to the onboard electronically scanned pressure modules. The pressure tap numbering scheme is shown in Appendix A: HWB Model Flight Condition Settings and the pressure sensors distributed as follows:

- Three rows of pressure taps located on the left hand side (port side) wing of the model,
- One row of pressure taps on the port side body,
- Pressure taps on the right hand (starboard side) wing,
- Four internal static pressure orifices inside the starboard flow-through nacelle,
- Two balance cavity pressures,
- Pressure taps located on the elevons and removable leading-edge parts.

The pressure tap rows, as shown in Figure 18, were located on the left (port) side of the model at, respectively, 13.4, 30.5, 51.0, and 90.6 percent of the semispan distance. Similar pressure taps were located on the starboard wing at 51.0 and 90.6 percent of the semispan distance. The 13.4-percent location was aligned with the center of the nacelle and terminated just upstream of the nacelle pylon. The 30.5-percent location was just inboard of the part line where the wing leading-edge droop begins and it runs aft crossing over the inboard edge of elevon number 2. The 51.0-percent location incorporated pressure taps on both the cruise and drooped leading edges and extended aft over the center of elevon number 3. The 90.6-percent location also incorporated pressure taps on both the cruise and drooped leading edges, while it extended aft over the center of elevon number 6.

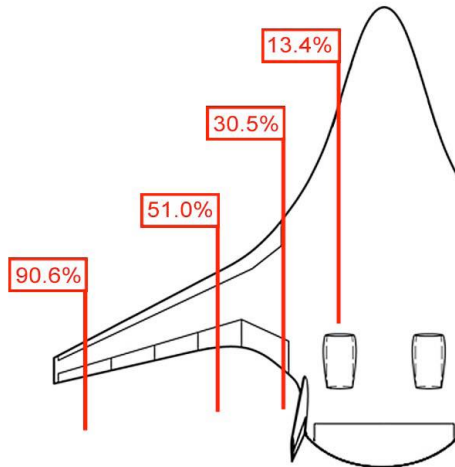


Figure 18. Spanwise locations (based on the model semispan dimension) of four chordwise pressure tap rows on port side of model.

5.1.2 Temperature Sensors

There were four temperature sensors on the fuselage upper surface, just aft of the nacelles, to monitor the fuselage temperature when the NASA Compact Jet Engine Simulators were in use.

5.1.3 Angle-of-Attack Instrumentation

Two angle-of-attack instruments were available for the HWB model – the usual AOA system used by the 14x22 Subsonic Tunnel DAS, and a duplicate AOA inclinometer package located in the nose/body cavity of the model. Data were available from both the tunnel DAS and the model-mounted AOA system. The HWB model was attached to a very stiff strut, not a balance, in the acoustic testing configuration, and while the model deflections are minimal, the actual angle of attack did vary slightly for the wind-on cases and was set for each test point accordingly. An important effect with regard to angle-of-attack setting is whether the wind tunnel is operated in the open or closed tunnel configuration. Also, the acoustic model support structure is more intrusive to the flow than the aerodynamic support. In light of these concerns, the acoustic test pitch was adjusted to match the pressure loading conditions from the aerodynamic test, as discussed in section 6.5.2 and in Appendix A: HWB Model Flight Condition Settings. It should also be noted that the recorded data from the inclinometer, located in the nose cavity, reflected skewed angles while the model was rolled through the +/- 30-degree positions. The tunnel DAS was used to accurately measure the pitch readings in the rolled cases.

5.1.4 HWB Model Embedded Point Sources

The HWB model was equipped with six small compression speaker drivers, four positioned in the center portion of the model and two in the wings (see Figure 19). The drivers were embedded into the model. Data from each embedded speaker were acquired with the phased microphone array for each array measurement location associated with a specific model configuration. The speakers were activated one at a time. These measurements were repeated for each change in angle of attack, roll, and flow speed. These data sets were used to correct for the effects of shear layer refraction and scattering, to fine-tune the pointing accuracy of the array, and to verify phased array data processing methodologies.

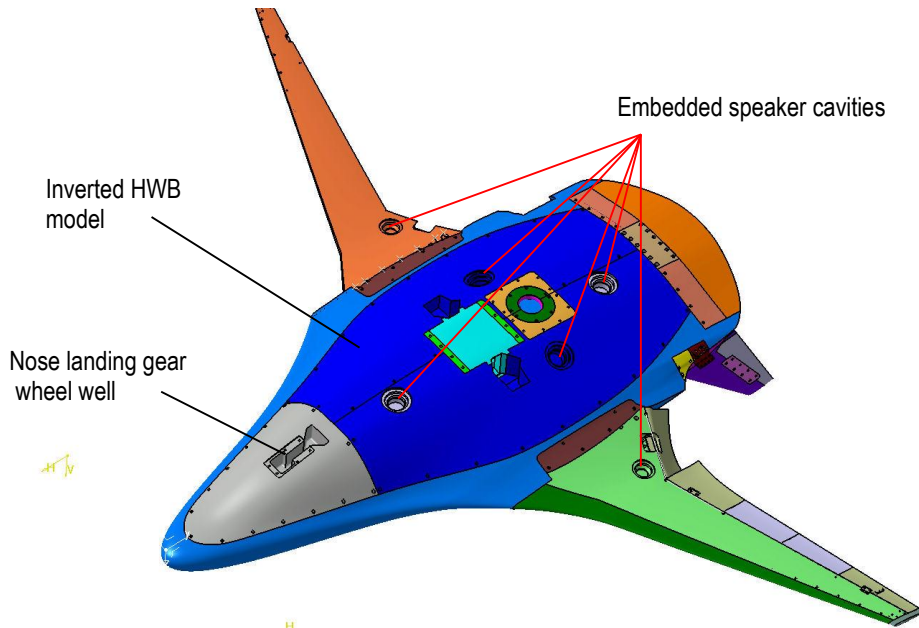


Figure 19. Embedded point sources and speaker cavity locations.

One-inch Pyle-Pro PDS222 Neodymium horn drivers were used in the center portion of the fuselage, and 1/2-inch B&C DE5 Mylar compression drivers were used in the two most outboard wing cavities (see Figure 20). These speakers were selected for their broad frequency range and suitable sound level. The cover plate of each speaker cavity followed the HWB model surface contour. Each cover plate had a 1-inch diameter hole covered with a 15 Rayl fiber metal mesh screen (Figure 21) that was acoustically “transparent” while sufficiently smooth and sturdy to not disturb the HWB model surface flow. The casings for the drivers were pressure sealed to minimize flow circulation through the screens due to pressure differential. These integration and installation measures minimized the risk of disturbing the fuselage Cp distributions.



1-inch PDS222 driver



1/2-inch B&C DE5 driver

Figure 20. Embedded speakers.

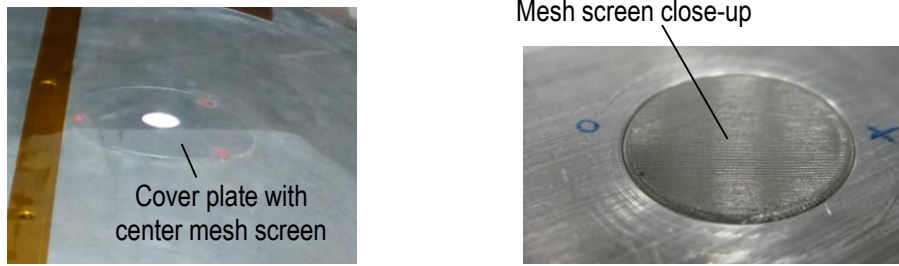


Figure 21. Embedded speaker cavity cover.

5.2 Engine Noise Simulators Instrumentation and Control

The instrumentation for the BENS and the CJES were different from one another. The BENS simulators were equipped with unsteady surface pressure sensors to monitor the noise output from the BENS nacelles for a given air input. Since the BENS operation does not involve heated flow, the BENS nacelles were not instrumented with thermocouples. The CJES operating parameters for the heated jet were more complex, which required the operating parameters to be balanced using a PLC control system to monitor fuel flow, air flow, and temperatures.

5.2.1 BENS Instrumentation

Each BENS was instrumented with 20 unsteady surface pressure sensors (10 sensors distributed around the nacelle inlet and 10 sensors distributed around the core structure in the nacelle outlet plane). The BENS air hoses were connected to the facility's 150 psi air supply. The air pressure supplied to the BENS simulators was maintained at 120 psia. The unsteady surface pressure sensor data were monitored and collected with the acoustic DAS. The supplied air pressure and mass flow rate were recorded with the tunnel DAS, as shown in Table 3.

5.2.1.1 BENS DAS

Table 3. BENS DAS Parameters

BENS 1 PARAMETERS (Port BENS)		
B1FLOHZ	Hz	BENS 1 FLOW METER FREQUENCY
B1FLOPS	psi	BENS 1 FLOW METER STATIC PRESSURE
B1FLOTT	degF	BENS 1 FLOW METER TEMPERATURE
B1DEN	lb/cuft	BENS 1 FLOW DENSITY
B1FLO	lb/sec	BENS 1 MASS FLOW
BENS 2 PARAMETERS (Starboard BENS)		
B2FLOHZ	Hz	BENS 2 FLOW METER FREQUENCY
B2FLOPS	psi	BENS 2 FLOW METER STATIC PRESSURE
B2FLOTT	degF	BENS 2 FLOW METER TEMPERATURE
B2DEN	lb/cuft	BENS 2 FLOW DENSITY
B2FLO	lb/sec	BENS 2 MASS FLOW

5.2.1.2 BENS Unsteady Surface Pressure Sensors

Kulite sensor model LQ-13-062-SSG was selected as the unsteady surface pressure sensor to be used in the BENS. The functionality and frequency response function of each sensor were determined and verified prior to installation in the BENS nacelles.

The BENS Kulite sensors were connected to two HP power supplies (set to 24 V DC) through a power distribution panel. Modified BNC cables (see Figure 22) were used to connect the sensors to the power distribution panel and to a Precision Filter box (model 28000). Finally, forty-five 50' BNC cables (includes 5 spare cables) were used to connect the filter box to the Acoustic Data Acquisition System located in the control room. The filter box, the power distribution panel, and the two power supplies were installed on the cart frame below the test section floor. The BNC cables between the filter box and the control room DAS were routed from below to above the cart, then under the foam baskets and onto the test section floor, and finally into the control room through an air-sealed opening in the control room side wall.

During the BENS portion of the wind-tunnel test, the settings on the Precision Filter box, placed below the cart to drive the Kulite sensors, were 2V for range and 8x for gain. No additional gain was added with or through the control room acoustic DAS. The BENS channels are 129–168, as assigned in Table 4.

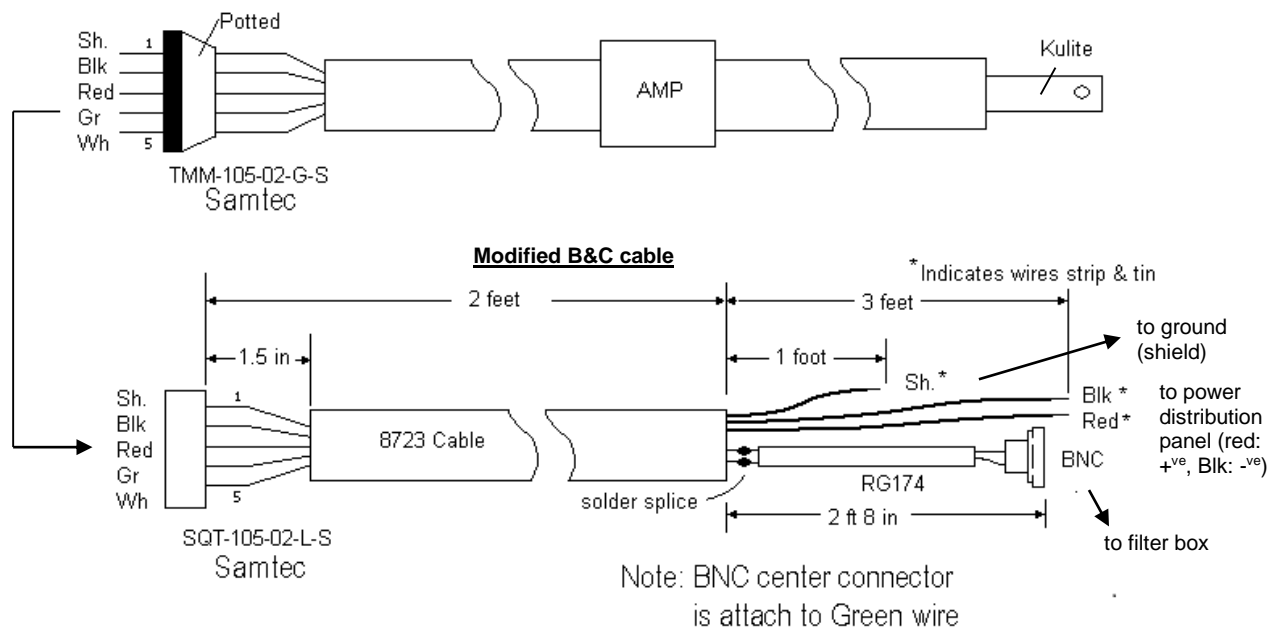


Figure 22. Kulite sensor cable and wiring diagram.

5.2.1.3 Kulite Channels

Table 4. Kulite Channel Assignments

DAS #	Kulite Sensor
129 – 138	1 – 10 (Starboard BENS, inlet sensors)
139 – 148	11 – 20 (Starboard BENS, outlet sensors)
149 – 158	21 – 30 (Port BENS, inlet sensors)
159 – 168	31 – 40 (Port BENS, outlet sensors)

5.2.2 CJES Instrumentation

The CJES charging station was equipped with both pressure and temperature instrumentation. As shown in Figure 23, two total pressure rakes of four ports each for the core stream and five ports each for the fan

stream were included, with an additional port at the tip of the charging station center body. Likewise, two temperature rakes of four thermocouples each for the core stream and five thermocouples each for the fan stream can be seen in Figure 24. In total, 19 total pressure ports and 18 total temperature probes were contained in the CJES charging station, as well as 2 static pressure ports in each of the core and fan streams and 1 pressure measurement in the core plenum main cavity just upstream of the combustor ring. The outputs of the charging station total probes were analyzed individually to verify ignition and assess flow uniformity. Furthermore, the total quantities were averaged together for use in determining Nozzle Pressure Ratio (NPR) and Nozzle Temperature Ratio (NTR). It was possible to control the CJES either manually or automatically by a valve Pallet PLC. The PLC controlled and monitored core and fan stream pressures, core and fan stream temperatures, propane mass flow, and the pressures across the core and fan stream flow conditioners (PBNR and FANCUP, respectively). Once the mass flows were set to the correct range, fine control adjustments were based on temperature (NTR) and pressure (NPR) ratios.

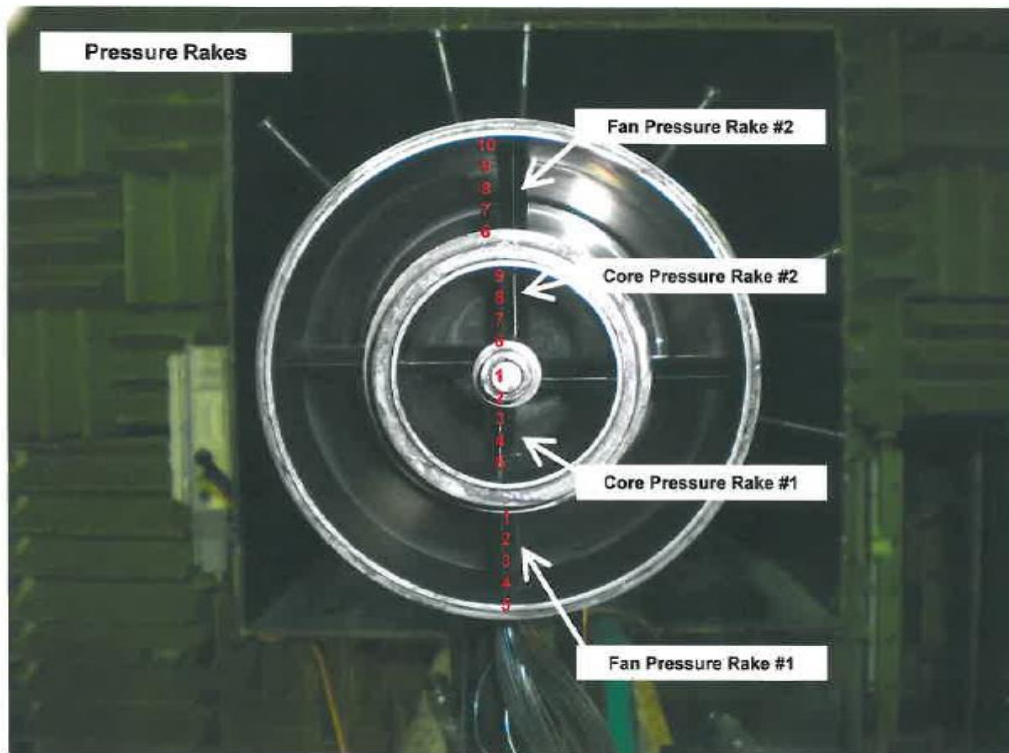


Figure 23. CJES pressure rakes.

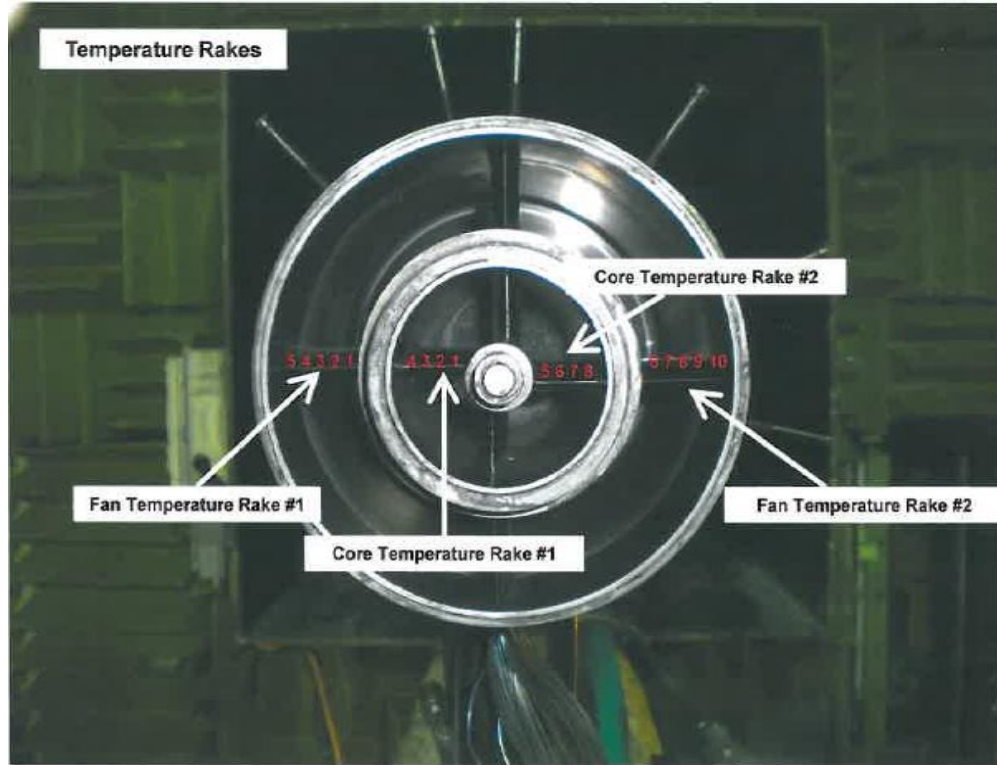


Figure 24. CJES temperature rakes.

5.2.2.1 CJES DAS Parameters and Mapping

The CJES DAS parameters, including the station port numbers, are listed in a table in Appendix B: Tunnel DAS Data Listing.

5.2.2.2 Pressure Sensor Calibration (CJES)

The charging station pressure ports were attached to Electronically Scanned Pressure (ESP) modules within the 14x22 Subsonic Tunnel facility. In situ ESP calibrations were performed each morning and at midday.

5.2.2.3 Thermocouple Verification (CJES)

A functional verification of all thermocouples was performed in which the thermocouple reader was connected to each sensor and a temperature rise was noted when heat was applied to the sensor tip. All thermocouple channels were routed through an Allen Bradley PLC module that included internal cold junction compensation.

5.3 Acoustic Instrumentation

5.3.1 Microphone Phased Array

A new microphone phased array design was constructed for the HWB test. The array consisted of 97 B&K Model 4938 1/4-inch pressure microphones attached to Model 2670 1/4-inch preamplifiers. The microphones were flush mounted (gap free) in a flat fiberglass honeycomb plate with total diameter of 8.05 feet. The array was designed for an operational frequency range of approximately 1.5 kHz to 80 kHz. This was achieved by using an irregular circular pattern of microphones comprised of 16 array arms with 6 microphones in each arm (see Figure 25). One microphone was positioned in the center of the array. The

maximum array aperture size (maximum distance between microphones) was 78.6 inches, yielding a solid collection angle of 29.4 degrees at a working distance of 12.5 feet (from the array face to the centerline of the tunnel). In the present test, the array face was about 13 feet from the HWB waterline at the overhead position. This solid collection angle was considered acceptable given the anticipated scale of the HWB model and its location in the facility.

A customized integral accelerometer and inclinometer system was designed as part of the array panel construction for monitoring panel tilt and vibration during tunnel operation. The accelerometers/inclinometers were Analog Devices ADIS16209 MEMS sensors, controlled via an on-board microcontroller system on the rear of the microphone array panel. The microcontroller digitized the inclinometer data for transmission to the data acquisition system via a standard Ethernet connection. The analog accelerometer data were transmitted to the data acquisition system via RG-174 coaxial cables.

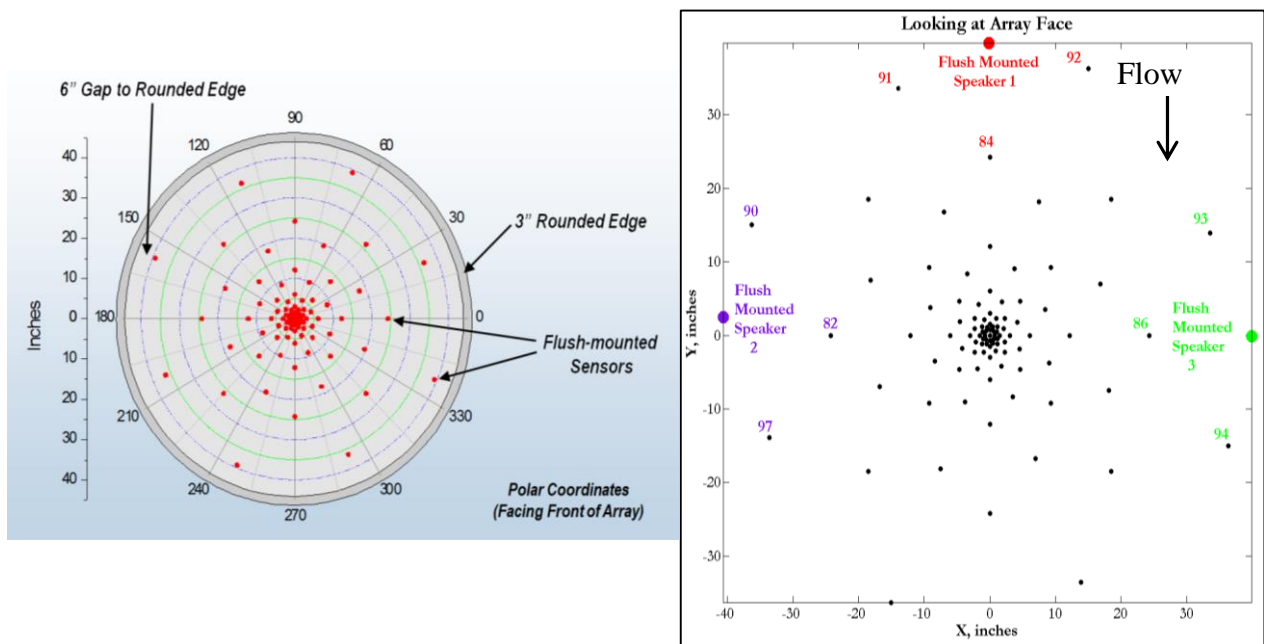


Figure 25. Phased Array. Irregular circular pattern of microphones is comprised of 16 arms with 6 microphones in each arm and 1 in the center of the array.

Microphone signals were transmitted to the data acquisition system using B&K LEMO microphone cables. The microphones were powered by two different sets of B&K power supplies – the inner 48 channels using Model 5935L dual-channel conditioning supplies with the remaining microphones using Model 2829 unity-gain, 4-channel supplies.

5.3.1.1 Phased Array Injection Calibration and Gain Settings

Array calibration methods and sensitivity studies were investigated prior to entry into the wind tunnel. These studies examined the use of noise source drivers positioned both external to the array panel and embedded on the panel to assess the best method for performing an in situ calibration of the array. These sources acted with near monopole omnidirectional character at the frequency ranges used during the test.

From these studies, it was determined that use of embedded sources on the panel was feasible and, as a result, three sources were mounted in the panel for this purpose. The speakers were flush mounted in the array at approximately 90-degree intervals referenced to the array center with an average radius of 3.34 feet. They were located as far as possible from the array microphones without getting too close to the edge of the array in order to avoid possible edge reflections. During the test, calibrations were performed where the three embedded sources were individually activated to track any drift in microphone sensitivities. Further calibration details are recorded in array microphone calibration procedures (Spalt et al., 2014). Injection calibrations were also used to track the microphone sensitivities. The injection calibrations were performed by applying a broadband white noise signal with known RMS voltage to each preamplifier and recording the output signal on the data acquisition system.

Initial pistonphone calibration files for each microphone were completed by both the manufacturer and in-house personnel prior to installing the microphones into the array and onto the towers and truss. Gain levels during test were adjusted as needed for quality data as stated previously. The precision filter gains were changed as needed and recorded in the test log.

The following procedure was developed to identify microphone failures (at some point in the acquisition chain) and/or stray signals from baseline levels on individual microphones. The combination of the test procedure and processing methodology represents a novel way to routinely calibrate the full data chain of phased array microphones using Flush-Mounted-Array-Speakers. This is an advantage because the array microphones were not readily accessible during the test.

In situ calibration procedure:

1. A 250-Hz, 124-dB pistonphone calibration was initially conducted on all microphones with necessary sensitivity adjustments made to equalize all of the channels to the same effective sensitivity.
2. The array was positioned at a designated location in the tunnel, chosen to avoid close reflecting objects. Each of the embedded sources was driven in turn using a defined level of input white noise (1 volt peak) over the target frequency band (1-5 kHz). This procedure was repeated when averages were desired.
3. For each microphone/source combination, the pressure squared values (which had external gains and sensitivities already accounted for) were summed over a frequency band of 1.5 to 4.9 kHz and a sound pressure level (SPL) calculated in dB referenced to $(2 \times 10^{-5} \text{ Pascals})^2$. This equation defines the baseline value for each mic and speaker.

$$\text{dB}_{\text{SPL, baseline (spkr,mic)}} = 10 \times \log_{10} \left(\frac{\sum_{1.5 \text{ kHz}}^{4.9 \text{ kHz}} \text{Pa}_{(\text{spkr,mic})}^2}{4 \times 10^{-10} \text{ Pa}^2} \right) \quad \text{spkr}=1 \rightarrow 3, \text{ mic}=1 \rightarrow 97 \quad (1)$$

4. At defined intervals, when repeat calibrations were performed, each source was driven according to Step 2. For each source, the procedure in Step 3 applied with one difference - absolute output changes across the array due to atmospheric conditions and/or speaker changes were allowed. Thus, for each source and microphone combination, the current calibration ΔdB values had a reference ΔdB subtracted from them. This reference ΔdB was obtained by taking the difference of the medians of the inner 49 sensors of the current and baseline acquisitions:

$$\Delta\text{dB}_{\text{SPL (spkr,mic)}} = [\text{dB}_{\text{SPL (spkr,mic)}} - \text{dB}_{\text{SPL, baseline (spkr,mic)}}] - [\text{median}(\text{dB}_{\text{SPL (spkr,mics 1-49)}}) - \text{median}(\text{dB}_{\text{SPL, baseline (spkr,mics 1-49)}})] \quad (2)$$

The inner 49 array microphones were located within an approximately 9" diameter circle. Justifications for Eq. (2) were threefold: (1) taking the median avoids outliers, (2) using the

microphones in the center of the panel minimizes any possible edge effects, and (3) using the central microphones allows any directivity bias to be cancelled out between the three sources.

5. For each acquisition, a Δ dB was generated for each source/microphone combination. The three Δ dBs were averaged to produce a single metric for each channel.
6. Each subsequent calibration produced a Δ dB by subtracting the baseline levels from the current calibration. A running history of the Δ dB levels was maintained to observe trends and to correct SPLs during post-processing.

5.3.1.2 Location of the Phased Array Microphones

The array location was controlled and monitored as a subsystem on the overhead traverse. The center of the phased array and overhead traversing system were located using lasers to properly align the components with respect to the tunnel coordinates and were controlled using encoder mechanisms.

5.3.2 Tower and Truss Microphones (Directivity Microphones)

Individual microphones were mounted on the two traversing towers, described in Section 3.1 – Facility Description, and used to assess the HWB noise characteristics for various model configurations. A series of 29 individual microphones were mounted around the facility test section on the sideline towers and overhead traverse truss for use in hemispherical characterizations of noise directivity, as shown in Figure 26. The sensors were comprised of B&K Model 4138 1/8-inch pressure field microphones attached to Model 2670 1/4-inch preamplifiers using 1/4-inch to 1/8-inch adapters. The microphones were powered by B&K Model 5135L dual-channel conditioning power supplies and their signals were transmitted to the data acquisition system using LEMO microphone cables.

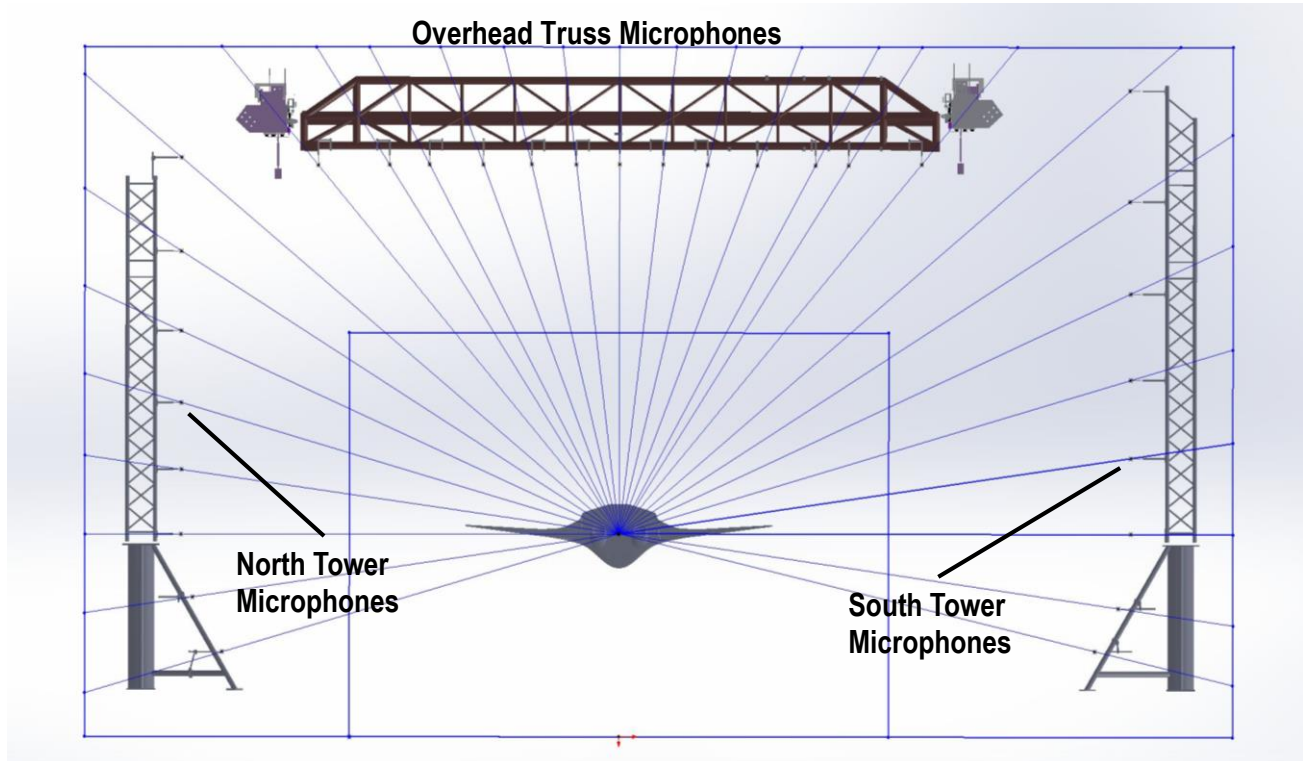


Figure 26. Lateral angles of the overhead traverse truss and sideline tower microphones. View facing upstream.

5.3.2.1 Location of Tower and Truss Directivity Microphones

The 29 tower and truss mounted microphones were arranged radially about the model center of gravity (spaced nominally at 7.5-degree increments, with a couple of exceptions due to the physical limitations). The microphones and preamplifiers were held in place by 12- to 14-inch horizontal non-conductive support tubes extending from the tower and truss structures in a direction perpendicular to the flow, as shown in Figure 26.

The two eleven-foot tall open truss vertical sideline towers were mounted on top of two sets of forty-foot floor mounted linear traversing rails, which were installed on either side of the test section outside of the tunnel shear layer, as shown in Figure 2. Thirteen of the twenty-nine microphones were distributed along the span of the truss in the same horizontal plane as the microphone phased array, and offset approximately 62 inches in the downstream direction from the center of the phased array. The two sideline rail systems were synchronized with the overhead traverse supporting the truss microphones such that all microphones were traversed together to predefined streamwise locations.

The exact location of each of the tower and truss microphones was verified by means of theodolite (laser) measurements of targets, and the results are stored with the test data. The targets, which consisted of round collars with 1/2" reflector balls, were placed over the 1/8" microphones to allow the laser instrumentation to record the locations with respect to the tunnel reference points. Based on the microphone locations, the tower and encoders were offset to an averaged microphone location within the tunnel coordinates.

The towers and overhead traverse were commanded to various tunnel locations during the test via the validated encoder positions. These positions were accurate and repeatable throughout the test. However, in addition to the positioning encoder mechanisms, a backup photogrammetric system (described below) was used to monitor the location of the phased array. This was to guard against any unforeseen position variances that could have occurred in the encoder.

5.3.2.2 Tower and Truss Microphone Calibration

Initial pistonphone calibrations were performed on tower and truss microphones and were compared to the manufacture's calibrations prior to installation. Pistonphone calibrations were also performed regularly throughout the test.

5.3.3 Photogrammetric Tracking System for Microphone Phased Array

A photogrammetric tracking system provided a backup measurement and sanity check of the array location in the facility during tunnel runs. The photogrammetric system verified that the positions reported by the overhead traverse encoders were correct and reliable.

Reflective targets on the phased array panel were illuminated using LED ring lights from eight cameras mounted on the floor of the wind tunnel. The system captured the target images from the phased array and produced a six-degrees-of-freedom (6 DOF) solution, which located it in 3D space with respect to the tunnel coordinate system by using intersections and an automatic correspondence algorithm to identify matching images for each of the eight cameras. The 3D transformation was computed using a least squares estimate solution that used the redundant data from the multiple targets to ensure a robust and accurate solution. Typical precisions (one sigma) of the location and orientation angles of the model were ± 1 mm and ± 0.05 degrees, respectively.

The photogrammetric system used commercial off-the-shelf hardware and custom software (Vision Measurement System Capture by Geometric Software) to handle image capture and processing. The video capture component of the system was comprised of eight IDS uEye GigE cameras fitted with 5mm lenses. The cameras had a five megapixel CMOS sensor with a resolution of 2560 by 1920 pixels, resulting in a field of view of approximately 90 degrees, and a maximum 14 frames per second capture rate. The cameras were operated in a synchronized mode using a separate set of trigger cables connected to a LabSmith programmable controller. Video data were transmitted to the computer over standard Cat6 Ethernet cables via a network switch. The network switch provided Power over Ethernet to power the cameras. The captured image sets were written to log files.

6 Test Matrix

The test was composed of four main parts. The first part focused on the shielding of the broadband component of turbomachinery noise (HWB model with BENS), the second part focused on airframe noise (HWB model alone), the third part focused on the examination and shielding of jet noise (HWB model with CJES), and the last part focused on the acoustics properties of the test section.

Noise measurements were performed for four flight simulation configurations – A1 (Low-noise approach configuration #1), A2 (Conventional approach configuration #2), TO (Take-Off), and CB (Cut-Back). These configurations were defined as follows:

- A1 – All Elevons (elevons 1–6) set at 0° , drooped leading edge, AOA= 13° , and $M=.19$
- A2 – Elevons 1–4 set at -10° , elevons 5–6 are set at 0° , drooped leading edge, AOA= 15.5° , and $M=.21$
- TO & CB – Elevon 1 set at -10° , elevons 2–6 set at 0° , drooped leading edge, AOA= 13.2° (TO), AOA= 14.5° (CB), and $M=.23$.
- For all configurations, $M=.17$ was tested as a reference condition

Note that the HWB aircraft elevons, tails, and drooped leading edges are described in Table 2.

6.1 Broadband Turbomachinery Noise

The following cases for exhaust and inlet broadband turbomachinery noise were tested.

6.1.1 BENS Exhaust Noise Radiation Data

Shielding of the noise radiating from the BENS exhaust was examined for:

- All four flight-simulation conditions (free-stream flow on and off), namely, A1, A2, and TO (same as CB for the BENS set up).
- A1 flight condition with alternate vertical tail configurations (free-stream flow on and off)
 - Two tail geometries – baseline (narrow chord) and alternate (wide chord)
 - Two cant angles – 10° (baseline) and 30° (alternate)
 - Two streamwise placements – aft (baseline) and forward (alternate)
- A1 flight condition with alternate BENS nacelle streamwise positions (free-stream flow on and off)
 - $X/D = 2.5$ (baseline configuration),
 - $X/D = 1.5$,
 - $X/D = 0$, and
 - $X/D = -0.5$ (unshielded noise configuration),

where X is the streamwise distance between the BENS exhaust plane and the HWB Trailing Edge (TE), and D is the BENS fan nozzle diameter.

6.1.2 BENS Inlet Noise Radiation Data

For these test cases, only the effect that the HWB Leading-Edge (LE) configuration had on the shielding of the noise radiating from the BENS inlet was examined:

- A1 flight condition with two Leading-Edge (LE) configurations (free-stream flow off):
 - Drooped LE (baseline) and
 - Un-drooped LE (cruise)

6.2 Airframe Noise

Noise measurements were acquired for A1 and A2 at $M=0.19$ and $M=0.21$, respectively, as well as at several reference cases at $M=0.17$. Cases also included airframe component variations of:

- Nose and main landing gear on and off
- Elevons deflected and un-deflected
- Leading-edge drooped and un-drooped
- Verticals on and off
- Verticals placement variation (aft and forward)

6.3 Jet Noise

Noise measurements and shielding of the noise radiating from the CJES exhaust were examined for:

- Three flight-simulation conditions – A2, CB, and TO. All test runs were completed with drooped leading edges and a center elevon deflection of -10 degrees.
- Alternate vertical tail configurations – no tails, baseline vertical tails in their forward location and baseline vertical tails in their aft location with CJES located at $x/D=2.5$ (baseline condition).
- Starboard, port, and both CJES engine combinations.
- CB, TO, and A2 flight condition with low-noise chevron nozzle engines at X/D position of 2.5 (baseline vertical tail configuration).
- Various Mach numbers and angles of attack at CB conditions for the low-noise chevron nozzle.
- Alternate CJES engine source streamwise positions with both the axisymmetric and chevron nozzles are:
 - $X/D = 2.5$ (baseline configuration),
 - $X/D = 1.5$ (chevron nozzle only), and
 - $X/D = -0.5$ (unshielded noise configuration),

where X is the streamwise distance between the CJES exhaust plane and the HWB TE, and D is the CJES fan nozzle diameter.

6.4 Facility Acoustic Properties

In order to evaluate the room-acoustic properties of the tunnel under static conditions, two common testing techniques were used. For both techniques, four general conditions were desired: 1) the sound source used mimicked steady-state conditions, 2) it was placed at the approximate position of the test article, 3) its directionality mimicked that of the test article, and 4) its output was (high) above the static sound level in the tunnel over the frequency range of interest for the test article. The end goal was to extract information at measurement locations used during the actual test campaign and use it to relate the direct sound emitted by source to that which was reflected and reverberated within the test section. This, in turn, gave an estimation of the bias in the direct sound measurement due to the reflection/reverberation which existed.

The first testing technique, referred to as the interrupted noise (IN) method, employed speakers embedded in the underside of the model driven with filtered white noise. The second, an impulse response (IR) method, ignited a blasting cap at the general position of the HWB model (Fig. 1) in order to create an impulse in the tunnel distributing energy over wide frequency bands. The outputs of each were analyzed using unique processing to provide ratios between the direct signal and that due to reflections and reverberation, local/distant reflection strength/proximity, and the reverberation time(s) of the tunnel at different measurement locations. The combination of the processing technique with the separation of the direct sound from the reflections/reverberation it generated is described below (Spalt et al., 2014).

6.4.1 Interrupted Noise Test

Three speakers embedded in the underside of the model (facing upwards, Figure 27) were driven separately with a filtered-white-noise input over the frequency range 0.87–89.81 kHz (driven separately in 7 bands – 0.87–11.27, 11.09–22.49, 22.23–35.29, 35.59–44.93, 44.50–56.15, 53.41–67.37, and 71.23–89.81 kHz). Once steady-state was reached, data acquisition commenced. At approximately 3 seconds into the 15-second long acquisition, the signal to the speakers was turned off and the remaining acquisition captured the sound decay and reverberant characteristics of the tunnel. This was repeated for streamwise locations of 139”, 173”, 203”, 231”, 259”, 289”, 323”, 365”, 421”, and 507” downstream of the nozzle exit plane.



Figure 27. Embedded speaker showing the socket in the underside of the model (facing upwards).

Frequency information was extracted from each microphone channel’s pressure-time history using a fixed-width processing block and user-defined step size. A block of 2048 samples and a step size of 512 samples were chosen. Starting at the beginning of the time series, a properly-scaled block of pressure-time data was Fourier transformed (FFT) to produce an auto spectrum (bin-width 122.07 Hz). The resulting frequency data was stored for that “time point” (designated as the time at which the first point in the block occurred) and the block was advanced by the defined step size. This process was repeated for the entire time series and resulted in Pa² levels as a function of time for narrowband frequencies. The usable bandwidth was limited by the output of the speakers.

Figure 28 gives a visual example of how the sliding-block FFT procedure works. In Figure 28a, a sample time history from the IN test is given, zoomed-in on the time when the signal driving the speakers is turned off. The resulting SPLs at the beginning of the time history will give an estimate of the total (i.e., direct signal from the speakers, early reflections to the microphones, and reverberation) signal present on the channel. After the beginning of the block passes the point in time when the speaker was turned off, only the reflections and reverberation will remain. As the block continues, a point will be reached when early reflections have subsided and only the reverberant energy is present.

6.4.2 Impulse Response Test

The IR test used Ensign-Bickford, 0.3-gram, explosive-mixture blasting caps mounted in a custom aluminum plate, which was mounted to the model test stand (Figure 29a). The plate was covered in ~1”-thick foam to reduce reflections. The ~1” long caps were mounted in their ~3” long holders such that half of the cap stuck out above the top of the holder. At ~1.5 seconds into the 12-second long acquisition, a cap was ignited (remotely). The remaining acquisition captured the direct pressure wave from the blast, any reflections to the microphones, and the reverberant characteristics of the tunnel. Data were acquired at streamwise positions of 97”, 139”, 203”, 259”, 323”, 421”, and 506” downstream of the nozzle (Figure 29b). The sampling rate was 500 kHz and no high-pass filter was used.

The processing technique described for the IN test was used for the IR test. However, in order to estimate the total signal level, the block length needed to be long enough to encompass the initial impulse, early reflections, and significant reverberation (Figure 28b). A block size of 2¹⁹ and step size of 1024 samples were chosen. In order to obtain a higher dynamic range, background subtraction was used. The first block of data (before the blast occurred) was used as an estimate of the static conditions during the acquisition. All results computed from the IR data were background subtracted unless otherwise noted.

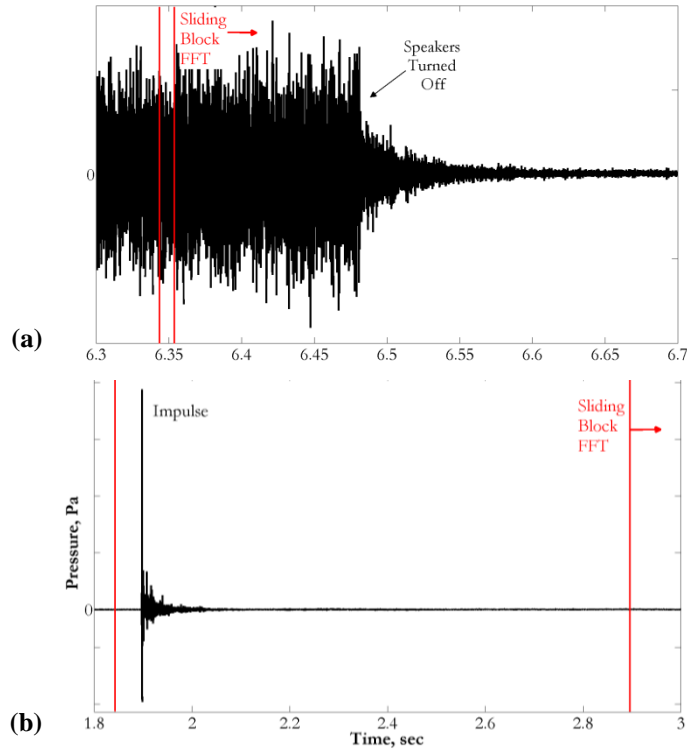


Figure 28. a) IN test example time history, and b) IR test example time history. Traverse 203" downstream of nozzle. Top north-sideline tower microphone.

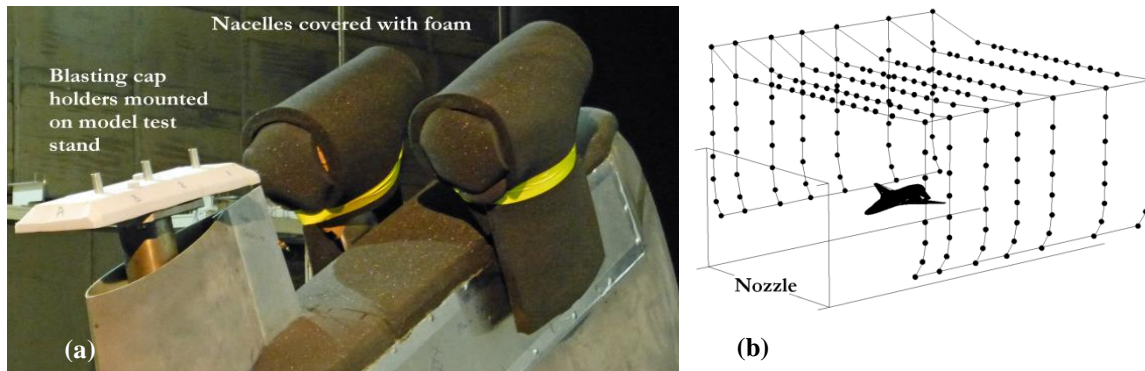


Figure 29. a) Blasting cap holders mounted on model test stand, and b) Sideline, and overhead, traverse stations for IR test.

6.5 Testing Configurations and Tunnel Parameters

The full list of all tunnel DAS parameters used during the test are listed in Appendix B: Tunnel DAS Data Listing with a brief overview given in this section.

6.5.1 HWB Model Parameters Describing Test Configurations

Throughout the HWB test, the baseline configuration was defined to include the drooped leading edge, the nacelles in the mid location ($x=2.5D$), the longer span vertical tails mounted with a 10-degree cant angle in the aft location, all elevons and rudders undeflected, and the landing gear and doors off with the landing

gear wells closed. Table 5 (below) shows the parameter name, the engineering measurements defining the parameter, and the description of the parameter.

Table 5. Model Test Parameters

Name	Unit	Description
ELEVON1	deg	Main Elevon Deflection Angle
LEVELON2	deg	Left Wing Elevon 2 Deflection Angle
LEVELON3	deg	Left Wing Elevon 3 Deflection Angle
LEVELON4	deg	Left Wing Elevon 4 Deflection Angle
LELEVON5	deg	Left Wing Elevon 5 Deflection Angle
LELEVON6	deg	Left Wing Elevon 6 Deflection Angle
RELEVON2	deg	Right Wing Elevon 2 Deflection Angle
RELEVON3	deg	Right Wing Elevon 3 Deflection Angle
RELEVON4	deg	Right Wing Elevon 4 Deflection Angle
RELEVON5	deg	Right Wing Elevon 5 Deflection Angle
RELEVON6	deg	Right Wing Elevon 6 Deflection Angle
LECOND		Leading Edge Condition: 1=Cruise, 2=Drooped
ENGCODE		Engine Code: 1=CJES, 2=BENS, 0=None
ENGLOC		Engine Location, X.X = L/D Position
NOZZLE		For CJES: 1=Baseline, 2=Chevron For BENS: 1=Baseline, 2=Inlet Capped, 3=Nozzle Capped, 4=Both Capped
VTCODE		Vertical Tail Code, 0=Not Installed, 1=Baseline, 2=Low AR
VTLOC		Vertical Tail Location, 0=Not Installed, 1=Aft(Baseline), 2=Fwd
VTDIHDL		Vertical tail Dihedral Angle: 0=off, 10, 30
LDGEAR		Landing Gear, Code=000: From left: Nose Gear, Port Gear, Starboard Gear: 0=Off, 1=On
PITCH-DES	Deg	Desired pitch angle: -5, 0, 4, 13.2, 14.5, 15.5, 18, and 25
MACH#-DES		Desired Mach#: 0, .11, .17, .23
AIRCRAFT		Desired aircraft flight condition: 0=Not specified, 1=Take-off, 2=Cut-back, 3=Landing
ROLLANGLE	Deg	Mechanical Roll Angle: -30, 0, 30

6.5.2 Angle-of-Attack Settings and Cp Matching

The HWB acoustic test and vehicle configurations were established based on the lift, drag, and moment coefficients required to meet proper flight conditions during the HWB aerodynamic wind-tunnel test. The acoustic test setup did not include a balance so the desired lift, drag, and moment coefficients were established by matching the model pressure data obtained during the corresponding aerodynamic test, which did include a balance. To ensure that the acoustic setup was properly defined for each flight condition tested, the angle of attack of the acoustic model (for a given flow velocity) was adjusted until the measured HWB chordwise pressure distributions matched those measured during the aerodynamic test at corresponding trim conditions. Details of the process for determining the chordwise pressure distributions, and for matching flight and model lift coefficients used are discussed in Appendix A: HWB Model Flight Condition Settings.

The key test conditions were developed and defined based on the flight conditions required for the HWB aircraft design to meet FAR 36, Stage 4 of the noise certification requirements (Noise Standards: Aircraft Type and Airworthiness Certification. Title 14, Chapter I, Parts 36 and 91., 2003), and 25-percent reduction in fuel burn relative to B737/767 technology. The certification flight profiles were developed using the Flight Optimization System (FLOPS) (McCullers, 2008) with measured low-speed aerodynamic

characteristics for lift, drag, and moment from the aerodynamic testing of the N2A-EXTE. Corresponding engine performance data were obtained from researchers at NASA Glenn Research Center (GRC) using Numerical Propulsion System Simulation (NPSS) (Lytle, 2000). Four main flight conditions (A1, A2, TO, CB) were identified from the FLOPS predicted flight profiles for the basis of the aeroacoustic testing of the N2A-EXTE. The key flight condition parameters for each of these conditions are provided in Table 6. The angle of attack is given for the vehicle flight condition along with the equivalent geometric angle settings, in parentheses, used during the wind-tunnel test. The equivalent geometric angle setting is different than the vehicle flight angle of attack due to the effect of tunnel wall interference. The geometric angle of attack for each condition was determined by matching the full-scale vehicle lift coefficient determined by FLOPS to the lift coefficient and its associated angle of attack determined during the aerodynamic test entry for the same configuration of leading-edge deployment and trailing-edge elevon setting.

Table 6. N2A-EXTE Noise Certification Flight Conditions

	APPROACH A1	APPROACH A2	TO	CB
Weight (lbs)	343462	343462	470632	470257
Altitude (ft)	394	394	982	2392
Speed (kts)	125.4	139.9	156.2	156.2
Est. Mach # (a=1120ft/s)	0.19	0.21	0.23	0.23
AOA (deg)	12.1 (13.1)	13.9 (15.5)	11.9 (13.25)	12.7 (14.5)
Climb Angle (deg)	-3.0	-3.0	9.2	5.1
Thrust (lbs)	10950	14842	107670	75770
% max Thrust	10.2	13.8	100.0	70.4

7 Data Processing and Reduction

This section describes the data obtained and the several processing steps performed on the data for various purposes. All data that were acquired are also kept in their as-obtained form. The following processing and correction details given below are carried out to make the data ready for most planned applications.

7.1 In Situ Data Analysis

Data were streamed from the acoustic DAS to disk in a custom 16-bit integer format. In situ, these data files were converted to the NetCDF file format, and stored with metadata, including data acquisition settings and tunnel/model parameters. A streamlined process utilizing Matlab and GPU computing was assembled to allow near-time viewing of preprocessed data in the facility. This process generated Cross Spectral Matrices or CSMSs, which contained the most common information of interest – power spectra and cross-spectra of the microphone channels. Examples of these preprocessed data are shown in Figure 30. Sample noise map results, created using DAMAS processing (Brooks & Humphreys, 2006) of the phased array data, were also available for next day viewing, as shown in Figure 31.

**Port-Side BENS at Unshielded ($x/D=-.5$) position
No tunnel flow, $M=0$**

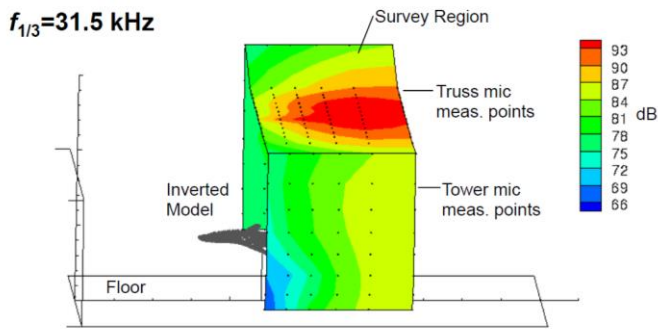


Figure 30. Example of directivity profile generated by analysis system. Source emission angles as refracted through the open jet shear layer were incorporated into the generated plots for tunnel flow cases.

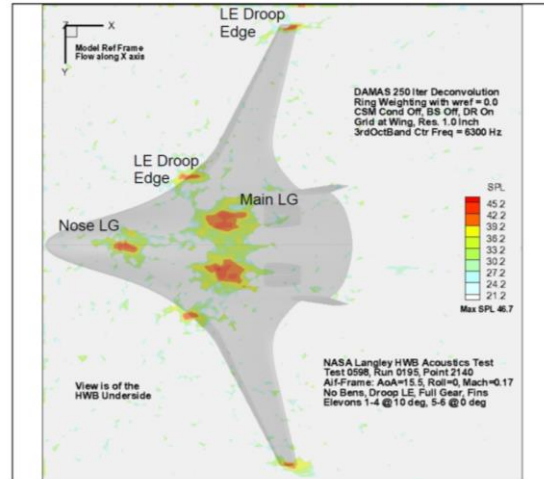


Figure 31. Example of UDAMAS processing output.

The workflow for generating the CSMs is summarized here. The workflow follows the theoretical procedure for generating a CSM. In practice, many of these steps can be combined or conducted out of order for more rapid analysis. A companion publication (Bahr, Brooks, Humphreys, Spalt, & Stead, 2014) contains additional details.

1. Load the 16-bit integer time series data.
2. Convert the data to single-precision floating-point format.
3. Use the DAS range information to scale the data from integer counts to volts, as observed at the DAS terminals.
4. Use the automatic and manual amplifier gain settings to scale the data from volts, as observed by the DAS, to volts output from the transducer.
5. Use the transducer sensitivity database to scale the time series data from volts to Pascals.
6. Check the transducer type. If it is a microphone flush-mounted in the array plate, divide the pressure signal by two to account for pressure doubling on the array plate face.
7. Split the data into blocks of 8192 points. Subtract the block mean, apply a Hamming window, and Fourier transform the data.
8. Apply the appropriate broadband level correction for the window function and correct for the transducer frequency response function to obtain a best estimate of the spectral level for every sensor and every block of data.
9. Compute one-sided auto- and cross-spectra through the traditional RMS averaging procedure (Bendat & Piersol, 2000).

For most acquisitions, the system sampling rate was set to 250 kHz, and approximately 30 seconds (920 blocks) of data were acquired. The resultant CSMs had a bin width of 30.5 Hz.

7.2 Post-Test CSM Construction

After the test, the CSMs were re-built from the time series data using a modified procedure. The Precision Filter frequency response function corrections were incorporated into the process at the same stage where transducer frequency response functions were applied. Additionally, the time series data were

analyzed for transient signals prior to CSM construction. This was demonstrated as necessary since, under certain configurations at higher flow speeds, hydrodynamic gusts were observed to contaminate the microphone signals with bursts lasting up to several seconds.

Details of the transient signal analysis and rejection procedure are presented elsewhere (Bahr, Brooks, Humphreys, Spalt, & Stead, 2014). In brief, the variances of the individual data blocks were analyzed. It was assumed that data blocks with only acoustic information will have lower variance than data blocks contaminated with hydrodynamic gusts. The data block variances were modeled to follow a Gamma distribution. The distribution had two parameters. The first was determined by an estimate of the signal bandwidth. The second was determined either from the mean of the block variances, or from the median. The median provides a statistical measure, which is less sensitive to extreme values than the mean. A Gamma distribution constructed from the mean was compared to one constructed from the median, starting with a few blocks of data and progressively including the higher variance blocks. The set of blocks for which the mean-based model best agrees with the median-based model was the set used to construct spectra.

The process was applied to each microphone time series individually. Only blocks considered clean for every microphone channel were used to construct the CSM. If fewer than 300 blocks were considered clean for every microphone, the CSM construction procedure reverted to using all 920 of the blocks, and the CSM was flagged for further review, as too little data may remain to construct a meaningful CSM. When only microphone auto spectra were considered, each time series was treated independently and at minimum the 100 lowest-variance blocks of data were retained.

7.3 Post-Test Data Corrections

The following corrections are commonly applied to the data in the first stage of analysis.

7.3.1 Background Subtraction

Background subtraction is a simple data correction, which has been used repeatedly in previous NASA Langley aeroacoustic experiments (Humphreys, Brooks, Hunter, & Meadows, 1998), (Hutcheson & Brooks, 2002), and (Brooks & Humphreys, 2006). Here, auto- and cross-spectra of a facility measurement, without the acoustic source of interest, were subtracted from auto- and cross-spectra of a facility measurement with the acoustic source of interest. This was done with matched acquisition settings, so both voltage and pressure noise were scaled properly between the two measurements. Subtraction occurs on a power scale (Pa^2 or V^2). The process assumed that there was no correlation between the background noise measurement and the source of interest, and that the statistical nature and level of the background noise remained the same between acquisitions.

7.3.2 Shear Layer Correction

In open-jet test section aeroacoustic wind-tunnel testing, shear layer correction was necessary for analysis of the data. Amiet's shear layer correction method was used for this study (Amiet, 1978). The level corrections provided by this correction technique were generally small for the Mach number range considered by the test. However, the shear layer correction also computed the refraction of an acoustic wave passing through the test section shear layer. This provided a modified acoustic path length, necessary for computing total atmospheric attenuation along the propagation path, as well as a modified wave angle of incidence on the microphones, which was necessary for correcting the scattering of the acoustic wave by the microphone installation. Additionally, the emission coordinates of the wave were determined by the shear layer correction method. Emission coordinates were necessary for using the test data in system noise assessments, and equating the test data to an aircraft in motion. The shear layer correction and all subsequent corrections assumed that the location of the acoustic source of interest in the wind tunnel was well-defined, and that the acoustic source was the dominant observed signal after the application of background subtraction.

7.3.3 Atmospheric Attenuation

For full-scale analysis of an HWB aircraft, model-scale data from this test were desired up to 80 kHz. For source-observer distances on the scale of this test, atmospheric attenuation of the acoustic energy due to molecular relaxation could be significant. For many applications, the lossless acoustic measurement was desired. A model of attenuation as a function of temperature, pressure, humidity, and frequency was available (American National Standards Institute, Inc., 1995). With the acoustic path length provided by the shear layer correction, the total attenuation experienced by the acoustic signal could be calculated, and a correction applied to the level of the data. For the scales of this test, the total acoustic loss at higher frequencies could be upwards of 10 dB, so the correction was significant. This process assumed that the flow in the test section had little additional effect on the atmospheric attenuation aside from modifying the acoustic path length.

7.3.4 Microphone Directivity

Microphones are not ideal signal observers, and their installation has an influence on the recorded acoustic field (Brüel and Kjær, 1982). Much of the installation effect for the array microphones was handled by accounting for the pressure doubling on the array face. However, the tower and truss microphones had a free-field installation, and thus required the application of correction curves provided by the microphone manufacturer. For high frequencies, an additional, analytic directivity correction was applied to the array microphones, and is described elsewhere (Bahr, Brooks, Humphreys, Spalt, & Stead, 2014).

7.4 Data Results and Analyses

This report does not attempt to present the HWB data reduction or analysis. Test data analyses have been published separately by the principal investigators and researchers in the following papers:

1. Hutcheson, F. V., Brooks, T. F., Burley, C. L., Bahr, C. J., Stead, D. J., and Pope, D. S. (2014). Shielding of Turbomachinery Broadband Noise from a Hybrid Wing Body Aircraft Configuration, AIAA-2014-2624. *20th AIAA/CEAS Aeroacoustics Conference*, Atlanta, GA, June 16–20, 2014.
2. Doty, M. J., Brooks, T. F., Burley, C. L., Bahr, C. J., Pope, D. S. (2014). Jet Noise Shielding Provided by a Hybrid Wing Body Aircraft, AIAA-2014-2625. *20th AIAA/CEAS Aeroacoustics Conference*, Atlanta, GA, June 16–20, 2014.
3. Burley, C. L., Brooks, T. F., Hutcheson, F. V., Doty, M. J., Lopes, L. V., and Pope, D. S. (2014). Noise Scaling and Community Noise Metrics for the Hybrid Wing Body Aircraft, AIAA-2014-2626. *20th AIAA/CEAS Aeroacoustics Conference*, Atlanta, GA, June 16–20, 2014.
4. Bahr, C. J., Brooks, T. F., Humphreys, W. M., Spalt, T. B., Stead, D. J. (2014). Acoustics Data Processing and Transient Signal Analysis for the Hybrid Wing Body 14- by 22-Foot Subsonic Wind Tunnel Test, AIAA-2014-2345. *20th AIAA/CEAS Aeroacoustics Conference*, Atlanta, GA, June 16–20, 2014.
5. Spalt, T. B., Brooks, T. F., Bahr, C. J., Plassman, G. E., Becker, L. E., and Stead, D. J. (2014). Calibration of the NASA Langley 14- by 22-Foot Subsonic Tunnel in Acoustic Configuration, AIAA-2014-2344. *20th AIAA/CEAS Aeroacoustics Conference*, Atlanta, GA, June 16–20, 2014.
6. Humphreys, W. M., Brooks, T. F., Bahr, C. J., Spalt, T. B., Bartram, S. M., Culliton, W. G., Becker, L. E. (2014). Development of a Microphone Phased Array Capability for the Langley 14- by 22-Foot

Subsonic Tunnel, AIAA-2014-2343. *20th AIAA/CEAS Aeroacoustics Conference*, Atlanta, GA, June 16–20, 2014.

7. Sutliff, D. L. and Walker, B. E. (2014). Characteristics using an Ultrasonic Configurable Fan Artificial Noise Source to Generate Modes - Experimental Measurements and Analytical Predictions, AIAA-2014-2346. *20th AIAA/CEAS Aeroacoustics Conference*, Atlanta, GA, June 16–20, 2014.

8 Summary

The experimental investigation of a 5.8-percent scale low-noise, reduced fuel burn N2A-EXTE hybrid wing body configuration aircraft was concluded successfully in the NASA Langley 14- by 22-Foot Subsonic Tunnel. This test was in support of the NASA ERA goals of reduced noise, emissions, and fuel burn. The test was a success with regard to the primary purpose, namely that of gathering sufficient noise measurements to define the noise exposure to the community from this low-noise-designed HWB aircraft and comparing this to the current fleet. Also, aeroacoustic data were obtained for the N2A-EXTE that can be used as the basis for reduced noise configurations and noise shielding validation. This testing effort followed an extensive, multi-year effort to develop and install a world-class aeroacoustic test capability in the 14- by 22-Foot Subsonic Tunnel. A summary describing the HWB test preparations and facility upgrades is contained in AIAA-2013-2623 (Heath et al., 2013).

9 References

- American National Standards Institute, Inc. (1995, July 24). *American National Standard Method for Calculation of the Absorption of Sound by the Atmosphere, ANSI S1.26-1995 (ASA 113-1995)*. New York, New York.
- Amiet, R. (1978). Effect of the incident surface pressure field on noise due to turbulent flow past a trailing edge. *J. Sound and Vibration*, 57(2), 305-306.
- Bahr, C. J., Brooks, T. F., Humphreys, W. M., Spalt, T. B., & Stead, D. J. (2014). Acoustics Data Processing and Transient Signal Analysis for the Hybrid Wing Body 14- by 22-foot Subsonic Wind Tunnel Test. AIAA-2014-2345. *20th AIAA/CEAS Aeroacoustics Conference, June 16-20, 2014*. Atlanta, GA.
- Bendat, & Piersol. (2000). *Random Data: Analysis & Measurement Procedures*. Wiley-Interscience.
- Berton, J. J., Envia, E., & Burley, C. (2009). An Analytical Assessment of NASA's N+1 Subsonic Fixed Wing. AIAA-2009-3144. *15th AIAA/CEAS Aeroacoustics Conference (30th AIAA Aeroacoustics Conference)*. Miami, FL.
- Braslow, A. L., & Knox, E. C. (1958). *Simplified Method for Determination of Critical Height of Distributed Roughness Particles for Boundary Layer Transition at Mach Numbers from 0 to 5*. Langley Field, VA: NASA, NACA TN 4363.
- Brooks, T. (2011). Aeroacoustic Scaling Principles and the Hybrid Wing Body Test. *Tuesday Keynote Address, 17th AIAA/CEAS Aeroacoustic Conference, June 6-8, 2011*. Portland, Oregon, USA.
- Brooks, T. F. (2010, July). *NASA LaRC 14x22 Wind Tunnel Survey Test of Microphone Signal Interaction Region with Turbulent Shear Layer*.
- Brooks, T., & Humphreys, W. (2006). A Deconvolution approach for the mapping of Acoustic Sources (DAMAS) Determined from Phased Microphone Arrays. *Journal of Sound and Vibration, Vol. 294*, 856-879.
- Brüel and Kjær. (1982, September). *Condenser Microphones and Microphone Preamplifiers for Acoustic Measurements - Data Handbook*, pg 54. Nærum, Denmark.
- Collier, F. S. (2009). Environmentally Responsible Aviation (ERA) Project,” presentation at the NASA Fundamental Aeronautics Program. *Third Annual Technical Conference September 29-October 1, 2009*. Atlanta, Georgia.
- Doty, M. J., & Haskin, H. H. (2013). Acoustic Characterization of Compact Jet Engine Simulator Units. AIAA-2103-2035. *19th AIAA/CEAS Aeroacoustic Conference, May 27-29, 2013*. Berlin, Germany.
- Doty, M. J., Brooks, T. F., Burley, C. L., Bahr, C. J., & Pope, D. S. (2014). Jet Noise Shielding Provided by a Hybrid Wing Body Aircraft, AIAA-2014-2625. *20th AIAA/CEAS Aeroacoustics Conference, June 16-20, 2014*. Atlanta, GA.
- Gatlin, G. M., Vicroy, D. D., & Carter, M. (2012). Experimental Investigation of the Low-Speed Aerodynamic Characteristics of a 5.8-Percent Scale Hybrid Wing Body Configuration. AIAA-2012-2669. *30th AIAA Applied Aerodynamics Conference, 25 - 28 June 2012*. New Orleans, LA.
- Gentry, G. L., Quinto, P. F., Gatlin, G. M., & Applin, Z. T. (September 1990, September). *The Langley 14 by 22 Foot Subsonic Tunnel: Description, Flow Characteristics, and Guide for Users*.
- Heath, Brooks, Hutcheson, Doty, Haskin, Spalt, Bahr, Burley, Bartram, Humphreys, Lundsford, Popernack, Colbert, Hoad, Becker, Stead, Yeh, & Kutcha. (2013). Hybrid Wing Body Aircraft Acoustic Test Preparations and Facility Upgrades. AIAA-2013-2623. *28th AIAA Aerodynamic Measurement Technology, Ground Testing, and Flight Testing Conference*. San Diego, California, June 24-27, 2013.
- Humphreys, Brooks, Hunter, & Meadows. (1998). Design and Use of Microphone Directional Arrays for Aeroacoustic Measurements. AIAA-98-0471. *36th Aerospace Sciences Meeting & Exhibit, January 12-15, 1998*. Reno, NV.
- Humphreys, W. M. (2010, July). *NASA Langley 14- by 22-foot Subsonic Tunnel Ceiling Flow Risk Reduction Test Plan*. NASA.

- Hutcheson, F. V., & Brooks, T. F. (2002). Measurement of Trailing Edge Noise Using Directional Array and Coherent Output Power Methods. AIAA-2002-2472. *8th AIAA/CEAS Aeroacoustics Conference & Exhibit, June 17-19, 2002*. Breckenridge, Colorado.
- Kawai, R. (2011). *Acoustic Prediction Methodology and Test Validation for an Efficient Low-Noise Hybrid Wing Body Transport*. Final Report for NASA Contract NNL07AA54C.
- Lytle, J. (2000). The Numerical Propulsion System Simulation: An Overview. *NASA TM 209915*.
- McCullers, L. (2008, April). *FLOPS Weight Module Documentation, Wate.doc, FLOPS Users Manual*. NASA.
- Noise Standards: Aircraft Type and Airworthiness Certification. Title 14, Chapter I, Parts 36 and 91. (2003, July 15). Code of Federal Regulations (C.F.R.).
- Spalt, T. B., Brooks, T. F., Bahr, C. J., Plassman, G. E., Becker, L. E., & Stead, D. J. (2014). Calibration of the LaRC's 14- by 22-Foot Subsonic Wind Tunnel in Acoustic Configuration. AIAA-2014-2346. *20th AIAA/CEAS Aeroacoustic Conference, June 16-20, 2014*. Atlanta, GA.

10 Appendices

The HWB Test Data Report contains the following supporting appendices.

Appendix A: HWB Model Flight Condition Settings

Appendix B: Tunnel DAS Data Listing

Appendix C: Acoustic DAS Data Listing

Appendix A: HWB Model Flight Condition Settings

The trim conditions of the HWB during the aeroacoustic test program were set to match the flight conditions that meet the approach, lateral and flyover noise certification requirements specified by the Stage 4 noise certification requirements (Noise Standards: Aircraft Type and Airworthiness Certification, Title 14, Chapter I, Parts 36 and 91, 2003). The flight conditions define the aircraft configuration (landing gear position, control surface settings, etc.), vehicle operating condition (angle-of-attack, velocity, etc.) and flight trajectory. The flight conditions were determined using the FLIGHT Optimization System (FLOPS) (McCullers, 2008) with measured input of the HWB low speed aerodynamic characteristics. The measured low speed aerodynamic characteristics were obtained during the HWB aerodynamic test program (Gatlin, Vicroy, & Carter, 2012) and were defined in terms of the lift, drag and moment as a function of vehicle configuration and angle-of-attack. The FLOPS analysis code used this input to determine viable trim conditions for the certification flight profiles. Since the low speed aerodynamic characteristics were not obtained at full-scale Reynolds numbers, a correction was determined considering the data published for a BWB 450 that was tested in the National Transonic Facility (NTF). The difference in Re number between full-scale and model scale was accounted for by reducing the model-scale drag by 10 counts.

Table A.1 indicates the lift coefficient determined by FLOPS for each of the 4 flight conditions: Approach condition 1 (A1), approach condition 2 (A2), take-off condition (TO) and cut-back condition (CB). The lift coefficient determined by FLOPS was then used to find test points with the aerodynamic test database of the N2A-EXTE that either matched or bracketed the FLOPS lift coefficient. Linear interpolation was used because no exact matches were found. Once the bracketed test points were found for each of the conditions shown in Table A.1, all other parameters associated with those test points were available for interpolation, including the associated chordwise pressure distributions for the 7 spanwise locations shown in Figure A. 1 - Figure A. 3. The BL values shown in Figure A. 1 to Figure A. 3 indicate the spanwise location from the centerline of the vehicle in inches. The nominal span of the model was 74.12 inches for the purposes of computing the nondimensional spanwise locations. The spanwise locations are shown at the top of Figure A. 4. Figure A. 4 also shows example chordwise pressure distributions obtained during the aerodynamic test at 5 selected angles of attack. The actual measured aerodynamic data were obtained at every degree, ranging from 6 to 14 degrees and every 2 degrees outside that range from -12 to 36 degrees.

Figure A. 5 shows examples of the chordwise pressure distributions at the 90.6% spanwise location for the TO configuration. The target lift coefficient for the HWB for the TO condition is 0.565. The aerodynamic database does not contain measurements that exactly match that lift coefficient (Cl) but at a lift coefficient that is slightly greater (Cl=0.5919, AOA=12 deg) and one that is slightly lower (Cl=0.4902, AOA=10 deg). Linearly interpolating between these data, the upper and lower chordwise pressure distribution for the target Cl=0.565 is obtained and shown in Figure A. 5. Since the chordwise pressure distributions are nearly the same, they all fall within a line width of each other, and hence cannot be clearly discerned on the plot. Similar results were found for the other flight conditions. The interpolated pressure distributions or target pressure distributions for each of the flight conditions of interest were made available during the aeroacoustic test. The target chordwise pressure distributions for each of these conditions are shown as solid symbols in Figure A. 6 to Figure A. 9.

The target pressure distributions from the aerodynamic test were displayed in real time during the test and were compared with the measured aeroacoustic pressure distributions. The measured pressure data are shown in Figure A. 6 to Figure A. 9 along with the target pressures, shown as the hollow symbols. The geometric angle-of-attack of the HWB was adjusted until the pressure distributions for the outer four span locations were best matched simultaneously. For this matching processing more weight was put on the distributions at 30.5%, 51.0% and 90.6%, since those measurements were minimally influenced by any flow from the large aeroacoustic test stand. The distribution at 13.4%, particularly in the leading edge region, is influenced by flow from the test stand. At that spanwise station, only the region aft of the quarter chord is used in the matching process. The geometric angle-of-attack for which the pressure distributions matched the target distributions is given in the last column of Table A.1. The differences between the flight vehicle AOA and the geometric AOA were primarily due to the influence of the wind tunnel “wall” interference effect and the flow distortion from the test stand.

Table A.1 Flight Condition and equivalent AOA setting used in aeroacoustic wind tunnel test.			
Condition	Flight Lift Coefficient from FLOPS analysis	Flight Vehicle AOA (deg) from FLOPS analysis	Aeroacoustic test AOA(deg) required to match flight lift coefficient
A1	0.6574	12.1	13.10
A2	0.526	13.9	15.50
TO	0.565	11.9	13.25
CB	0.601	12.7	14.50

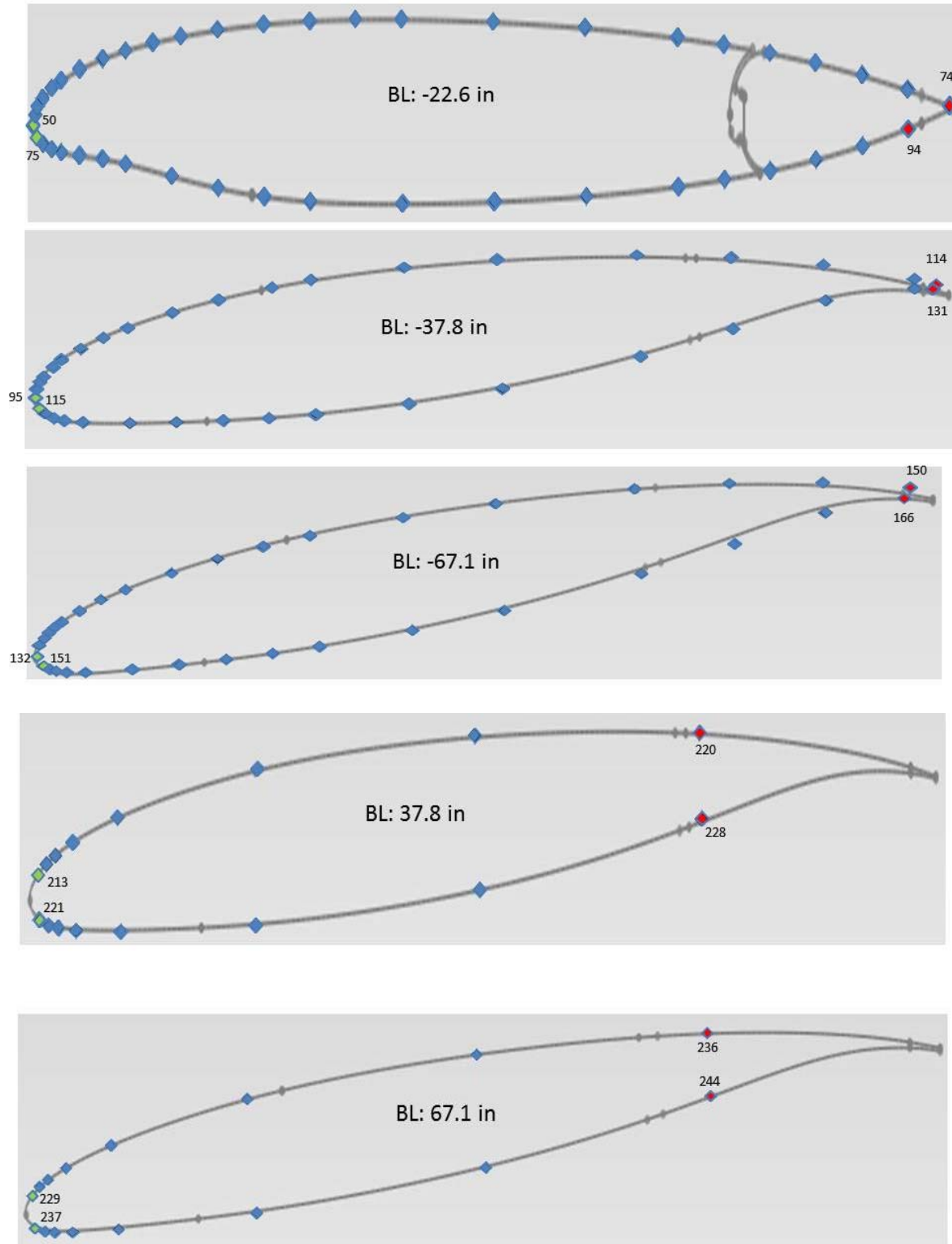


Figure A. 1. Pressure tap locations for span sections on the starboard and port sides, with non-drooped leading edge configuration.

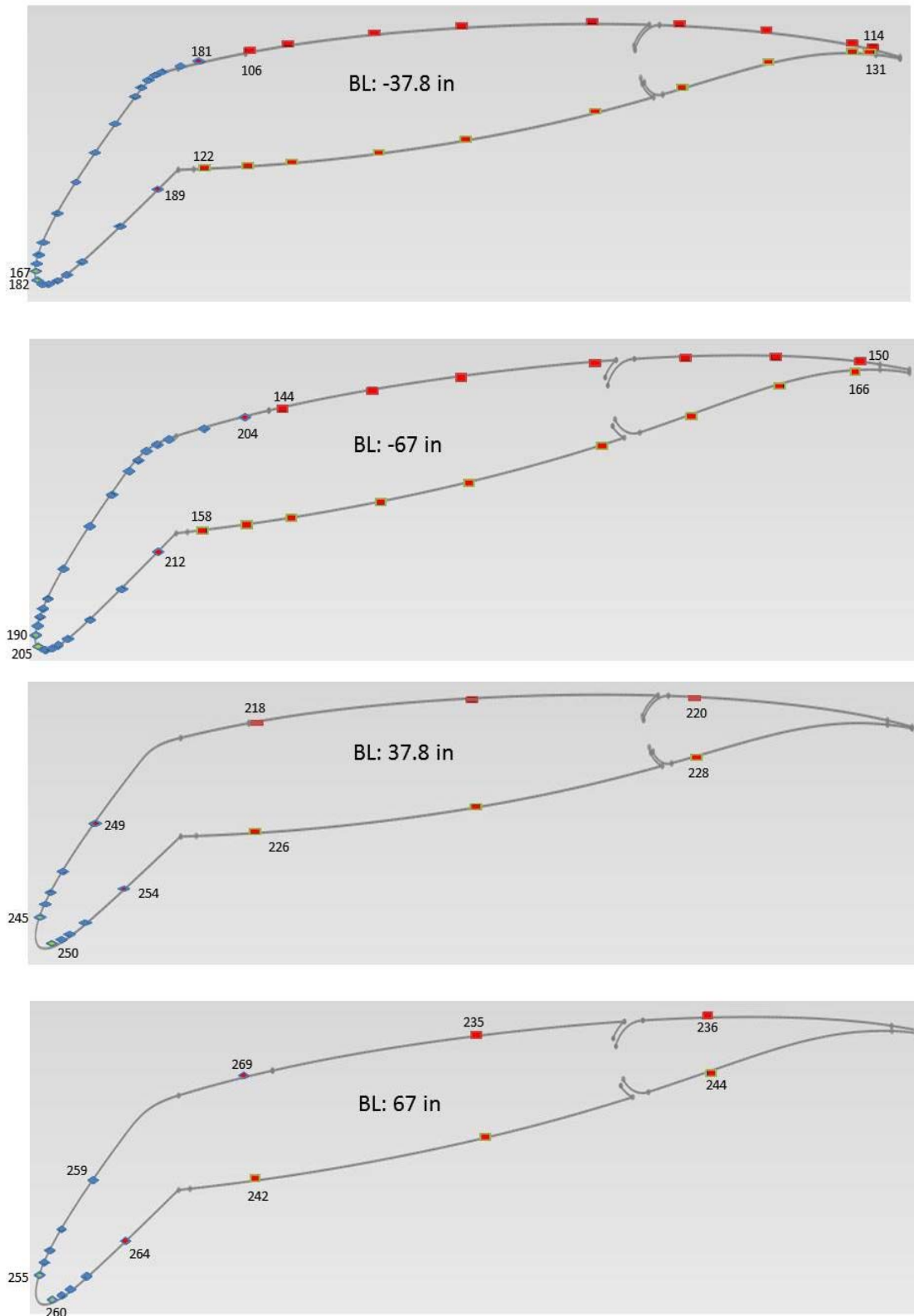


Figure A. 2. Pressure tap locations for span sections on the starboard and port sides with drooped leading edge configuration.

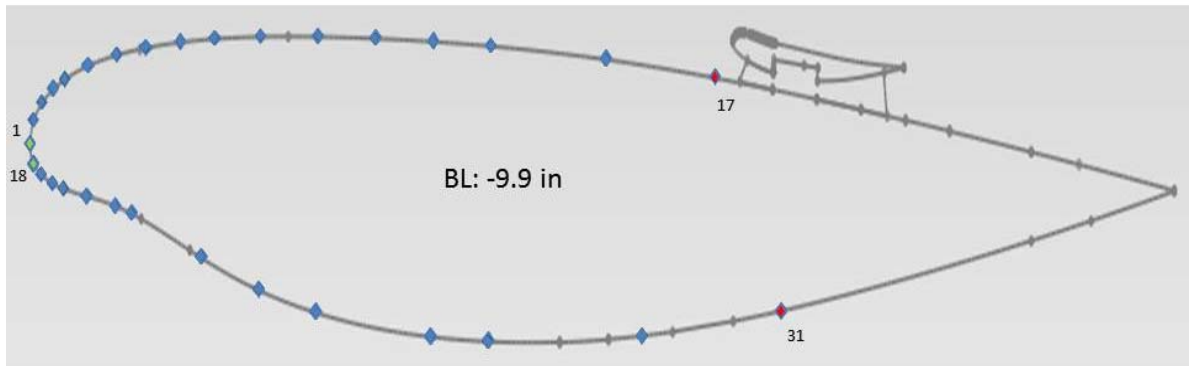
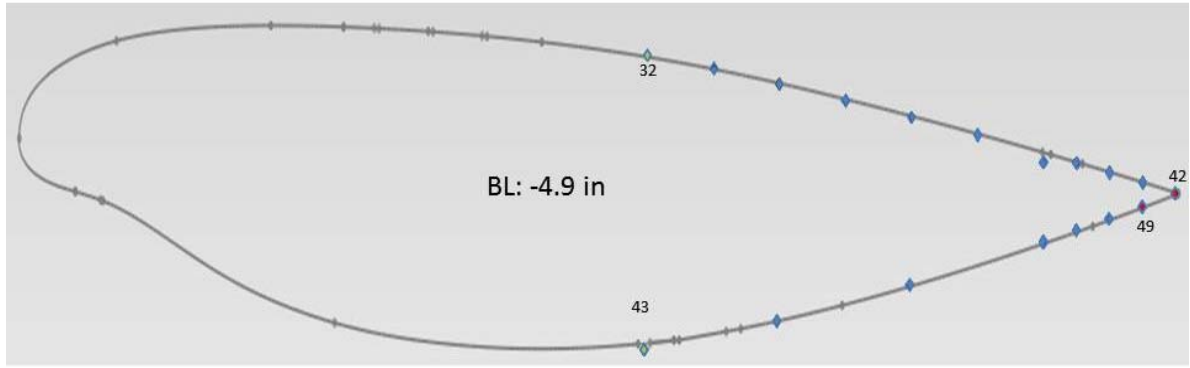


Figure A. 3. Pressure tap locations on the airframe center body for 2 port side spanwise sections.

α , deg

- 0°
- 4°
- ◇ 8°
- △ 12°
- ▽ 16°

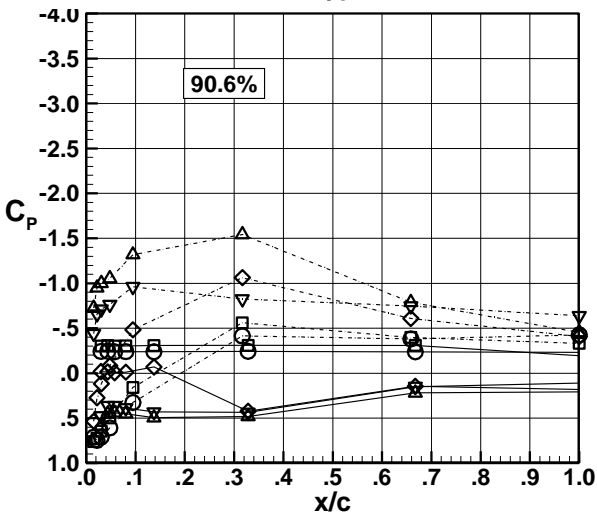
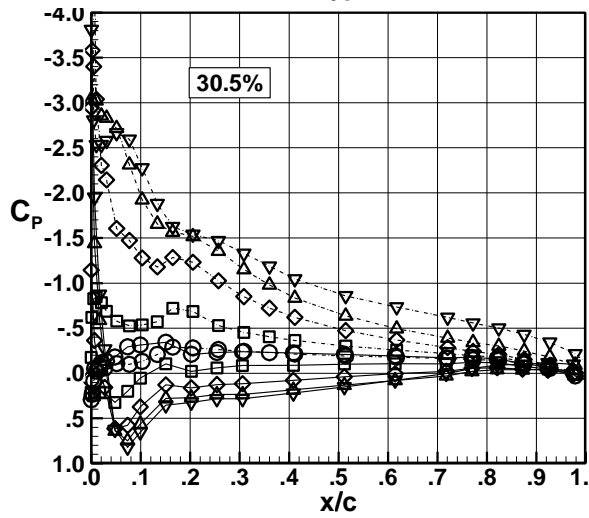
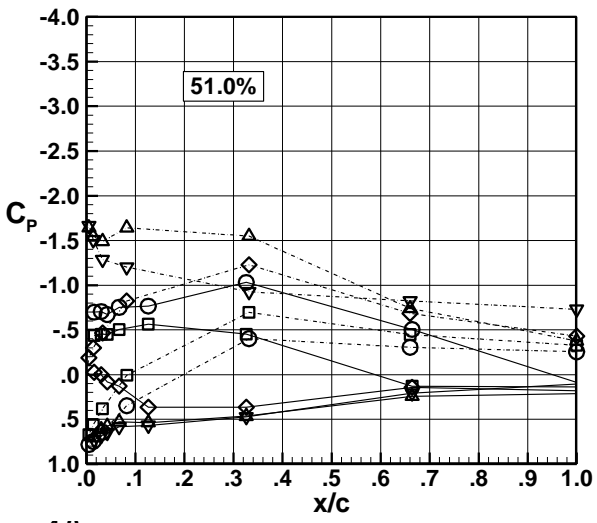
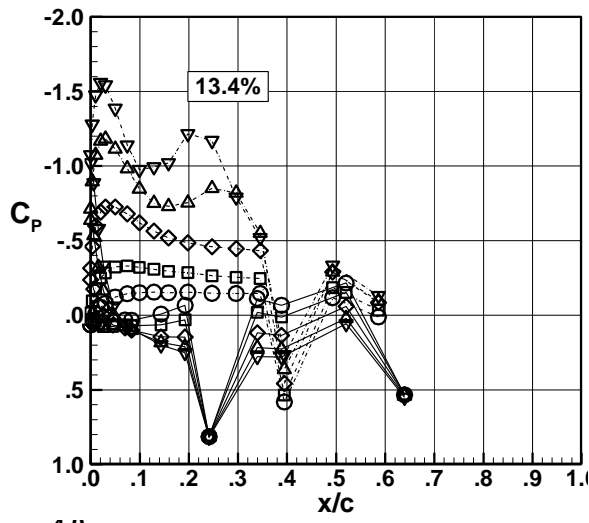
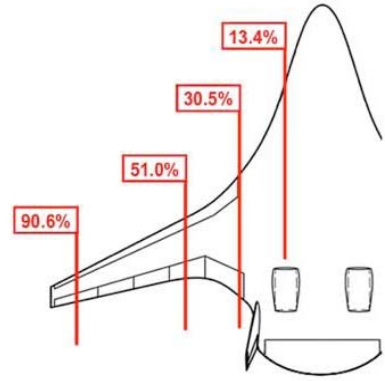


Figure A. 4 Chordwise pressure coefficients obtained for 5 angles-of-attack for 4 spanwise locations.

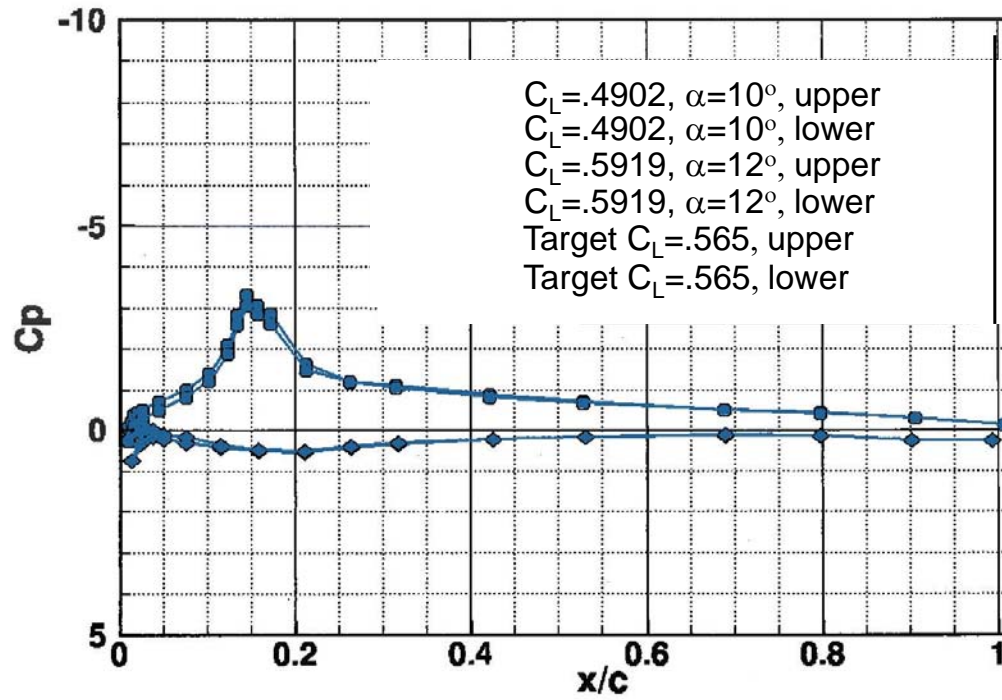
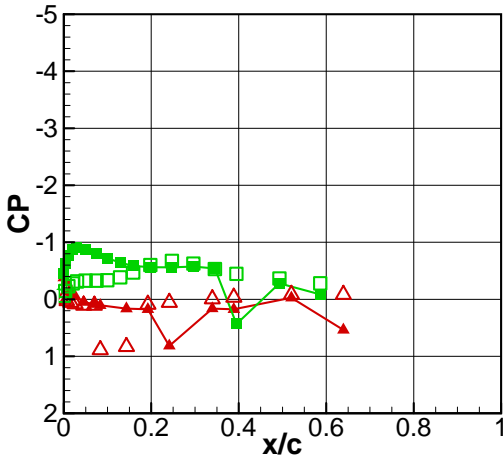
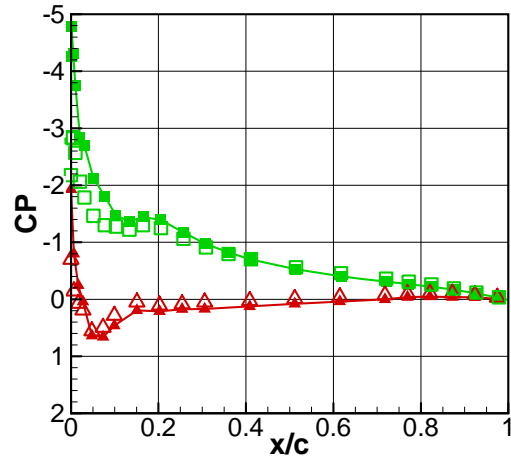


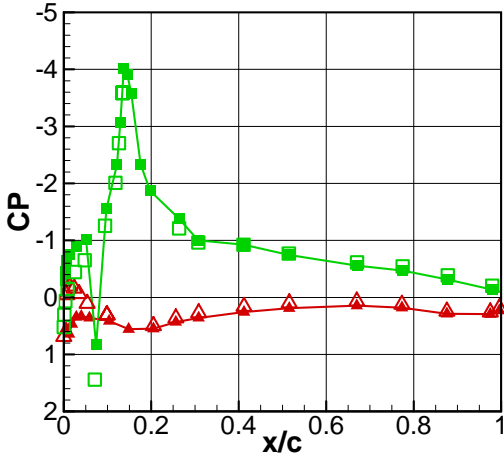
Figure A. 5. Measured upper and lower chordwise pressure distributions at lift coefficients of 0.4902 and 0.5919 and upper and lower chordwise pressure distribution interpolated to target lift coefficient of 0.565. Takeoff (sideline) condition.



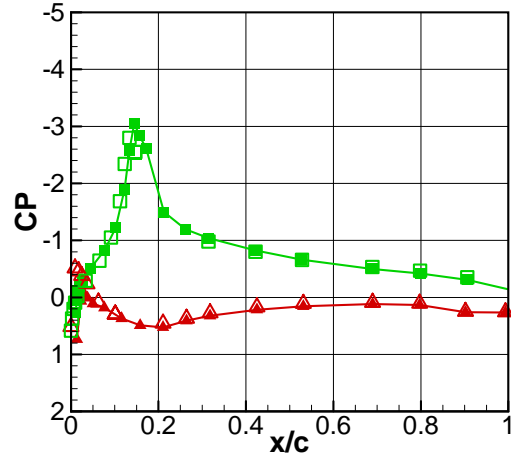
a) spanwise: 13.4%



b) spanwise: 30.5%

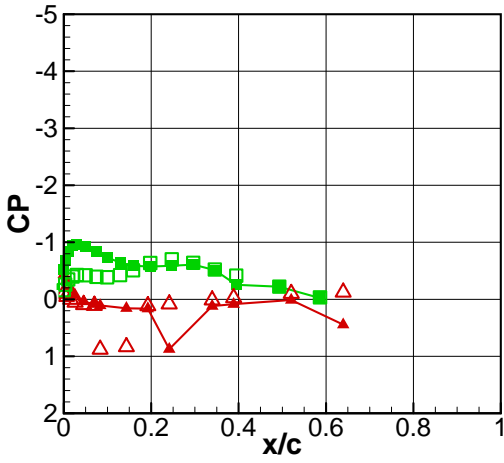


c) spanwise: 51.0%

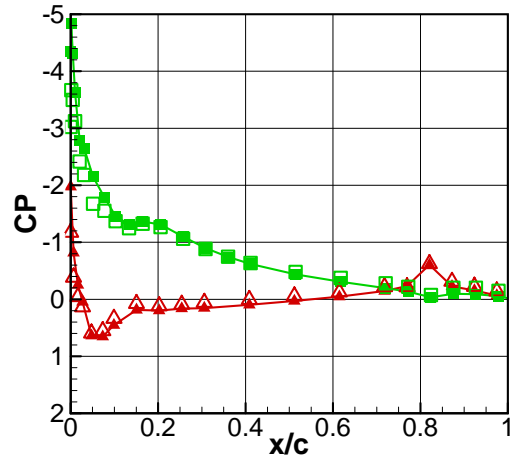


d) spanwise: 90.6%

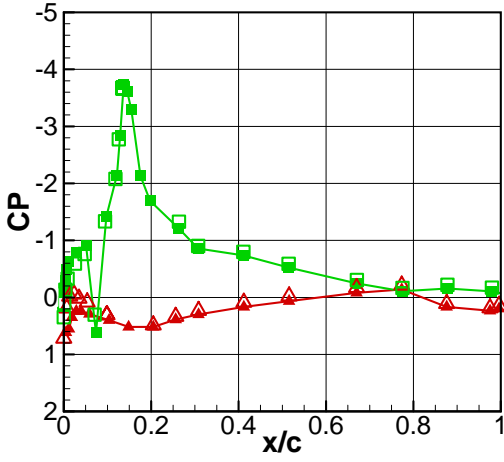
Figure A. 6. Upper (green) and lower (red) chordwise pressure distributions for the A1 condition. Closed symbols represent target data from the aerodynamic test. Open symbols represent measured aeroacoustic data.



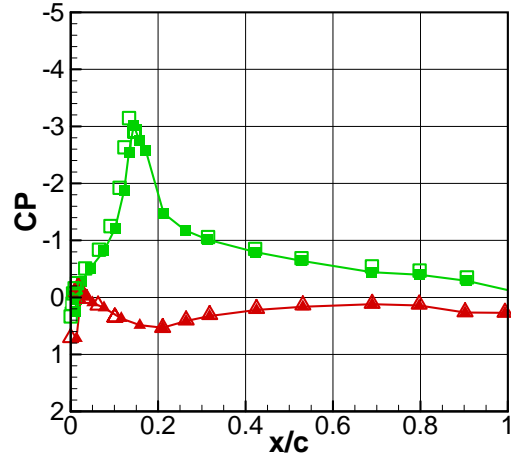
a) spanwise: 13.4%



b) spanwise: 30.5%

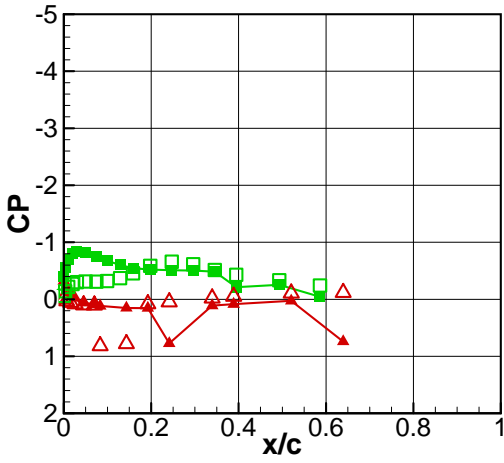


c) spanwise: 51.0%

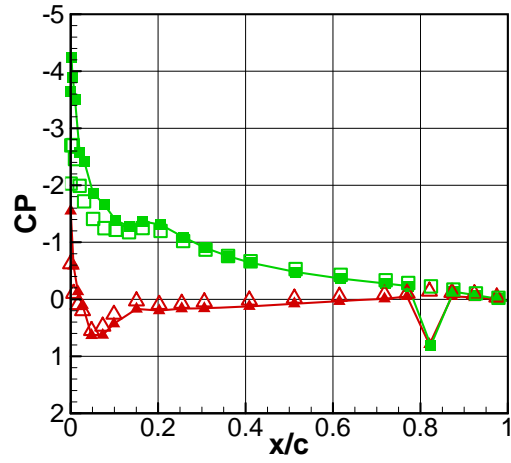


d) spanwise: 90.6%

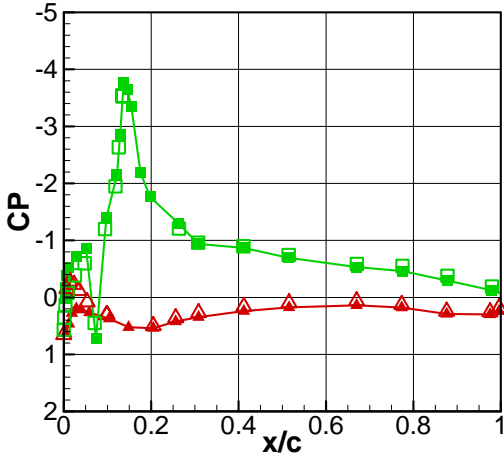
Figure A. 7. Upper (green) and lower (red) chordwise pressure distributions for the A2 condition. Closed symbols represent target data from the aerodynamic test. Open symbols represent measured aeroacoustic data.



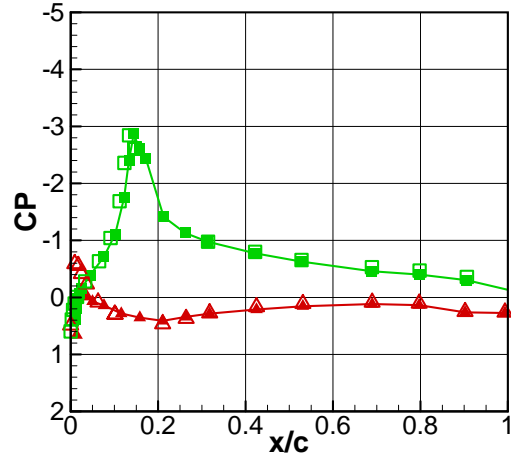
a) spanwise: 13.4%



b) spanwise: 30.5%



c) spanwise: 51.0%



d) spanwise: 90.6%

Figure A. 8. Interpolated upper (green) and lower (red) chordwise pressure distributions for the TO condition. Closed symbols represent target data from the aerodynamic test. Open symbols represent measured aeroacoustic data.

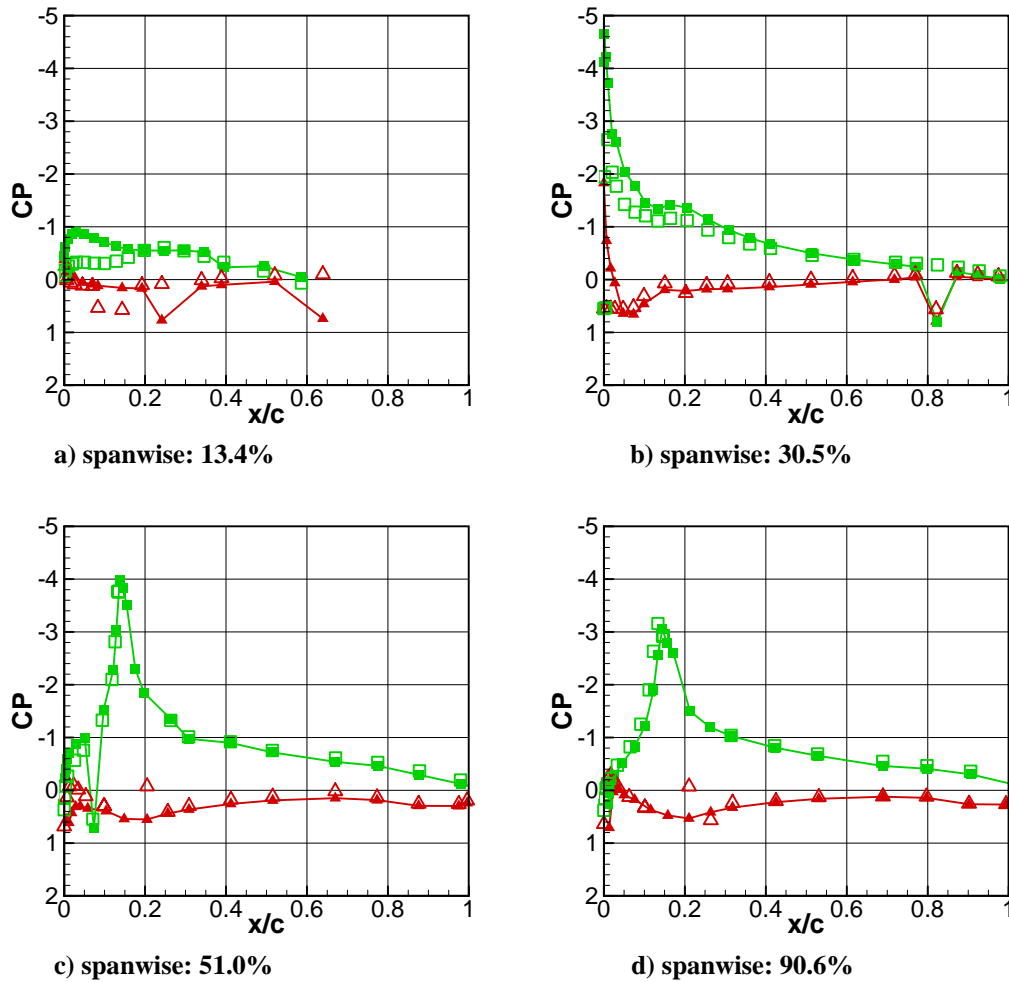


Figure A. 9. Interpolated upper (green) and lower (red) chordwise pressure distributions for the CB condition. Closed symbols represent target data from the aerodynamic test. Open symbols represent measured aeroacoustic data.

References:

- Gatlin, G. M., Vicroy, D. D., & Carter, M. (2012). Experimental Investigation of the Low-Speed Aerodynamic Characteristics of a 5.8-Percent Scale Hybrid Wing Body Configuration. AIAA-2012-2669. *30th AIAA Applied Aerodynamics Conference, 25 - 28 June 2012*. New Orleans, LA.
- McCullers, L. (2008, April). *FLOPS Weight Module Documentation, Wate.doc, FLOPS Users Manual*. NASA.
- Noise Standards: Aircraft Type and Airworthiness Certification. Title 14, Chapter I, Parts 36 and 91. (2003, July 15). Code of Federal Regulations (C.F.R.).

Appendix B: Tunnel DAS Data Listing

The DAS data listings are included below. They consist of Tunnel Parameter Calculations, Model Temperatures, Model Rotations, CJES Parameters, BENS Parameters, Raw Tunnel DAS data available, and HWB Model Pressure Tap data.

TUNNEL PARAMETER CALCULATIONS		
DPI	lbs/sqft	MEASURED INDICATED DIFFERENCE BETWEEN TOTAL AND STATIC PRESSURE
DPINF	lbs/sqft	DYNAMIC PRESSURE UNCORRECTED FOR COMPRESSIBILITY
MACH		FREE STREAM MACH NUMBER
MACHU		UNCORRECTED FREE STREAM MACH NUMBER
MU	lbs/sec	ABSOLUTE VISCOSITY OF AIR CORRECTED FOR TEMPERATURE
PSTAT	lbs/sqft	TEST SECTION STATIC PRESSURE CORRECTED FOR BLOCKAGE
PSTATU	lbs/sqft	TEST SECTION STATIC PRESSURE UNCORRECTED FOR BLOCKAGE
PV	lbs/sqft	VAPOR PRESSURE CALCULATED FROM DEW POINT
Q	lbs/sqft	TUNNEL DYNAMIC PRESSURE CORRECTED FOR BLOCKAGE
QU	lbs/sqft	TUNNEL DYNAMIC PRESSURE CORRECTED FOR COMPRESSIBILITY
RHO	slugs/cuft	AIR DENSITY
RHOU	slugs/cuft	UNCORRECTED AIR DENSITY
RN/FT	1/feet	CALCULATED TEST SECTION REYNOLDS NUMBER
RN/FTU	1/feet	UNCORRECTED CALCULATED TEST SECTION REYNOLDS NUMBER
TR	degR	AMBIENT TEMPERATURE
VEL	ft/sec	TEST SECTION FREE STREAM VELOCITY
VELU	ft/sec	UNCORRECTED TEST SECTION FREE STREAM VELOCITY
MODEL TEMPERATURES		
T1	degF	MODEL TEMPERATURE, ELEVON 1
T2	degF	MODEL TEMPERATURE, UPPER BODY LEFT SIDE
T3	degF	MODEL TEMPERATURE, UPPER BODY CENTERLINE
T4	degF	MODEL TEMPERATURE, UPPER BODY RIGHT SIDE
MODEL ROTATIONS		
ALPHA	deg	ANGLE OF ATTACK WITH NO JET BOUNDARY CORRECTIONS
BETA	deg	CALCULATED ANGLE OF SIDESLIP
MODROL	deg	MODEL ROLL ANGLE

CJES 1 PARAMETERS (CJES 1 represents the port side engine of the HWB)		
E1COPSUP	psiA	CJES 1 CORE STATIC PRESSURE, UPSTREAM
E1CODP	psi	CJES 1 DELTA PRESSURE ACROSS CORE FLOW CONDITIONER (E1COPSUP - E1COPSAV)
E1COPTAV	psiA	CJES 1 CORE TOTAL PRESSURE AVERAGED
E1COPSAV	psiA	CJES 1 CORE STATIC PRESSURE AVERAGED
E1COTTAV	degF	CJES 1 CORE TOTAL TEMPERATURE AVERAGED
E1CONPR		CJES 1 CORE NOZZLE PRESSURE RATIO (E1COPTAV / PSTAT)
E1CONTR		CJES 1 CORE NOZZLE TEMPERATURE RATIO (E1COTTAV / TA)
E1FNPSUP	psiA	CJES 1 FAN STATIC PRESSURE, UPSTREAM
E1FNNDP	psi	CJES 1 DELTA PRESSURE ACROSS FAN FLOW CONDITIONER (E1FNPSUP - E1FNPSAV)
E1FNPTAV	psiA	CJES 1 FAN TOTAL PRESSURE AVERAGED
E1FNPSAV	psiA	CJES 1 FAN STATIC PRESSURE AVERAGED
E1FNTTAV	degF	CJES 1 FAN TOTAL TEMPERATURE AVERAGED
E1FNNPR		CJES 1 FAN NOZZLE PRESSURE RATIO (E1FNPTAV / PSTAT)
E1FNNTR		CJES 1 FAN NOZZLE TEMPERATURE RATIO (E1FNTTAV / TA)
E1PTCL	psiA	CJES 1 CORE PRESSURE CENTERLINE
E1PTR1C1	psiA	CJES 1 CORE PRESSURE RAKE 1 PROBE 1
E1PTR1C2	psiA	CJES 1 CORE PRESSURE RAKE 1 PROBE 2
E1PTR1C3	psiA	CJES 1 CORE PRESSURE RAKE 1 PROBE 3
E1PTR1C4	psiA	CJES 1 CORE PRESSURE RAKE 1 PROBE 4
E1PTR2C1	psiA	CJES 1 CORE PRESSURE RAKE 2 PROBE 1
E1PTR2C2	psiA	CJES 1 CORE PRESSURE RAKE 2 PROBE 2
E1PTR2C3	psiA	CJES 1 CORE PRESSURE RAKE 2 PROBE 3
E1PTR2C4	psiA	CJES 1 CORE PRESSURE RAKE 2 PROBE 4
E1PSR1C	psiA	CJES 1 CORE STATIC PRESSURE RAKE 1
E1PSR2C	psiA	CJES 1 CORE STATIC PRESSURE RAKE 2
E1PTR1F1	psiA	CJES 1 FAN PRESSURE RAKE 1 PROBE 1
E1PTR1F2	psiA	CJES 1 FAN PRESSURE RAKE 1 PROBE 2
E1PTR1F3	psiA	CJES 1 FAN PRESSURE RAKE 1 PROBE 3
E1PTR1F4	psiA	CJES 1 FAN PRESSURE RAKE 1 PROBE 4
E1PTR1F5	psiA	CJES 1 FAN PRESSURE RAKE 1 PROBE 5
E1PTR2F1	psiA	CJES 1 FAN PRESSURE RAKE 2 PROBE 1
E1PTR2F2	psiA	CJES 1 FAN PRESSURE RAKE 2 PROBE 2
E1PTR2F3	psiA	CJES 1 FAN PRESSURE RAKE 2 PROBE 3
E1PTR2F4	psiA	CJES 1 FAN PRESSURE RAKE 2 PROBE 4
E1PTR2F5	psiA	CJES 1 FAN PRESSURE RAKE 2 PROBE 5
E1PSR1F	psiA	CJES 1 FAN STATIC PRESSURE RAKE 1

E1PSR2F	psiA	CJES 1 FAN STATIC PRESSURE RAKE 2
E1TTR1C1	degF	CJES 1 CORE TEMPERATURE RAKE 1 PROBE 1
E1TTR1C2	degF	CJES 1 CORE TEMPERATURE RAKE 1 PROBE 2
E1TTR1C3	degF	CJES 1 CORE TEMPERATURE RAKE 1 PROBE 3
E1TTR1C4	degF	CJES 1 CORE TEMPERATURE RAKE 1 PROBE 4
E1TTR2C1	degF	CJES 1 CORE TEMPERATURE RAKE 2 PROBE 1
E1TTR2C2	degF	CJES 1 CORE TEMPERATURE RAKE 2 PROBE 2
E1TTR2C3	degF	CJES 1 CORE TEMPERATURE RAKE 2 PROBE 3
E1TTR2C4	degF	CJES 1 CORE TEMPERATURE RAKE 2 PROBE 4
E1TTR1F1	degF	CJES 1 FAN TEMPERATURE RAKE 1 PROBE 1
E1TTR1F2	degF	CJES 1 FAN TEMPERATURE RAKE 1 PROBE 2
E1TTR1F3	degF	CJES 1 FAN TEMPERATURE RAKE 1 PROBE 3
E1TTR1F4	degF	CJES 1 FAN TEMPERATURE RAKE 1 PROBE 4
E1TTR1F5	degF	CJES 1 FAN TEMPERATURE RAKE 1 PROBE 5
E1TTR2F1	degF	CJES 1 FAN TEMPERATURE RAKE 2 PROBE 1
E1TTR2F2	degF	CJES 1 FAN TEMPERATURE RAKE 2 PROBE 2
E1TTR2F3	degF	CJES 1 FAN TEMPERATURE RAKE 2 PROBE 3
E1TTR2F4	degF	CJES 1 FAN TEMPERATURE RAKE 2 PROBE 4
E1TTR2F5	degF	CJES 1 FAN TEMPERATURE RAKE 2 PROBE 5
E1SUPFLO	lb/sec	CJES 1 PROPANE SUPPLY FLOW RATE
E1SUPPS	psi	CJES 1 PROPANE SUPPLY PRESSURE
E1SUPTT	degF	CJES 1 PROPANE SUPPLY TEMPERATURE
E1COFLO	lb/sec	CJES 1 CORE AIR SUPPLY FLOW RATE
E1COPUP	psi	CJES 1 CORE AIR SUPPLY UPSTREAM PRESSURE
E1COTUP	degF	CJES 1 CORE AIR SUPPLY UPSTREAM TEMPERATURE
E1COPDN	psi	CJES 1 CORE AIR SUPPLY DOWNSTREAM PRESSURE
E1COTDN	degF	CJES 1 CORE AIR SUPPLY DOWNSTREAM TEMPERATURE
E1FNFLO	lb/sec	CJES 1 FAN AIR SUPPLY FLOW RATE
E1FNPUP	psi	CJES 1 FAN AIR SUPPLY UPSTREAM PRESSURE
E1FNTUP	degF	CJES 1 FAN AIR SUPPLY UPSTREAM TEMPERATURE
E1FNPDN	psi	CJES 1 FAN AIR SUPPLY DOWNSTREAM PRESSURE
E1FNTDN	degF	CJES 1 FAN AIR SUPPLY DOWNSTREAM TEMPERATURE
CJES 2 PARAMETERS (CJES 2 represents the starboard side engine of the HWB)		
E2COPSUP	psiA	CJES 2 CORE STATIC PRESSURE, UPSTREAM
E2CODP	psi	CJES 2 DELTA PRESSURE ACROSS CORE FLOW CONDITIONER (E2COPSUP - E2COPSAV)

E2COPTAV	psiA	CJES 2 CORE TOTAL PRESSURE AVERAGED
E2COPSAV	psiA	CJES 2 CORE STATIC PRESSURE AVERAGED
E2COTTAV	degF	CJES 2 CORE TOTAL TEMPERATURE AVERAGED
E2CONPR		CJES 2 CORE NOZZLE PRESSURE RATIO (E2COPTAV / PSTAT)
E2CONTR		CJES 2 CORE NOZZLE TEMPERATURE RATIO (E2COTTAV / TA)
E2FNPSUP	psiA	CJES 2 FAN STATIC PRESSURE, UPSTREAM
E2FNPD	psi	CJES 2 DELTA PRESSURE ACROSS FAN FLOW CONDITIONER (E2FNPSUP - E2FNPSAV)
E2FNPTAV	psiA	CJES 2 FAN TOTAL PRESSURE AVERAGED
E2FNPSAV	psiA	CJES 2 FAN STATIC PRESSURE AVERAGED
E2FNTTAV	degF	CJES 2 FAN TOTAL TEMPERATURE AVERAGED
E2FNNPR		CJES 2 FAN NOZZLE PRESSURE RATIO (E2FNPTAV / PSTAT)
E2FNNTR		CJES 2 FAN NOZZLE TEMPERATURE RATIO (E2FNTTAV / TA)
E2PTCL	psiA	CJES 2 CORE PRESSURE CENTERLINE
E2PTR1C1	psiA	CJES 2 CORE PRESSURE RAKE 1 PROBE 1
E2PTR1C2	psiA	CJES 2 CORE PRESSURE RAKE 1 PROBE 2
E2PTR1C3	psiA	CJES 2 CORE PRESSURE RAKE 1 PROBE 3
E2PTR1C4	psiA	CJES 2 CORE PRESSURE RAKE 1 PROBE 4
E2PTR2C1	psiA	CJES 2 CORE PRESSURE RAKE 2 PROBE 1
E2PTR2C2	psiA	CJES 2 CORE PRESSURE RAKE 2 PROBE 2
E2PTR2C3	psiA	CJES 2 CORE PRESSURE RAKE 2 PROBE 3
E2PTR2C4	psiA	CJES 2 CORE PRESSURE RAKE 2 PROBE 4
E2PSR1C	psiA	CJES 2 CORE STATIC PRESSURE RAKE 1
E2PSR2C	psiA	CJES 2 CORE STATIC PRESSURE RAKE 2
E2PTR1F1	psiA	CJES 2 FAN PRESSURE RAKE 1 PROBE 1
E2PTR1F2	psiA	CJES 2 FAN PRESSURE RAKE 1 PROBE 2
E2PTR1F3	psiA	CJES 2 FAN PRESSURE RAKE 1 PROBE 3
E2PTR1F4	psiA	CJES 2 FAN PRESSURE RAKE 1 PROBE 4
E2PTR1F5	psiA	CJES 2 FAN PRESSURE RAKE 1 PROBE 5
E2PTR2F1	psiA	CJES 2 FAN PRESSURE RAKE 2 PROBE 1
E2PTR2F2	psiA	CJES 2 FAN PRESSURE RAKE 2 PROBE 2
E2PTR2F3	psiA	CJES 2 FAN PRESSURE RAKE 2 PROBE 3
E2PTR2F4	psiA	CJES 2 FAN PRESSURE RAKE 2 PROBE 4
E2PTR2F5	psiA	CJES 2 FAN PRESSURE RAKE 2 PROBE 5
E2PSR1F	psiA	CJES 2 FAN STATIC PRESSURE RAKE 1
E2PSR2F	psiA	CJES 2 FAN STATIC PRESSURE RAKE 2
E2TTR1C1	degF	CJES 2 CORE TEMPERATURE RAKE 1 PROBE 1

E2TTR1C2	degF	CJES 2 CORE TEMPERATURE RAKE 1 PROBE 2
E2TTR1C3	degF	CJES 2 CORE TEMPERATURE RAKE 1 PROBE 3
E2TTR1C4	degF	CJES 2 CORE TEMPERATURE RAKE 1 PROBE 4
E2TTR2C1	degF	CJES 2 CORE TEMPERATURE RAKE 2 PROBE 1
E2TTR2C2	degF	CJES 2 CORE TEMPERATURE RAKE 2 PROBE 2
E2TTR2C3	degF	CJES 2 CORE TEMPERATURE RAKE 2 PROBE 3
E2TTR2C4	degF	CJES 2 CORE TEMPERATURE RAKE 2 PROBE 4
E2TTR1F1	degF	CJES 2 FAN TEMPERATURE RAKE 1 PROBE 1
E2TTR1F2	degF	CJES 2 FAN TEMPERATURE RAKE 1 PROBE 2
E2TTR1F3	degF	CJES 2 FAN TEMPERATURE RAKE 1 PROBE 3
E2TTR1F4	degF	CJES 2 FAN TEMPERATURE RAKE 1 PROBE 4
E2TTR1F5	degF	CJES 2 FAN TEMPERATURE RAKE 1 PROBE 5
E2TTR2F1	degF	CJES 2 FAN TEMPERATURE RAKE 2 PROBE 1
E2TTR2F2	degF	CJES 2 FAN TEMPERATURE RAKE 2 PROBE 2
E2TTR2F3	degF	CJES 2 FAN TEMPERATURE RAKE 2 PROBE 3
E2TTR2F4	degF	CJES 2 FAN TEMPERATURE RAKE 2 PROBE 4
E2TTR2F5	degF	CJES 2 FAN TEMPERATURE RAKE 2 PROBE 5
E2SUPFLO	lb/sec	CJES 2 PROPANE SUPPLY FLOW RATE
E2SUPPS	psi	CJES 2 PROPANE SUPPLY PRESSURE
E2SUPTT	degF	CJES 2 PROPANE SUPPLY TEMPERATURE
E2COFLO	lb/sec	CJES 2 CORE AIR SUPPLY FLOW RATE
E2COPUP	psi	CJES 2 CORE AIR SUPPLY UPSTREAM PRESSURE
E2COTUP	degF	CJES 2 CORE AIR SUPPLY UPSTREAM TEMPERATURE
E2COPDN	psi	CJES 2 CORE AIR SUPPLY DOWNSTREAM PRESSURE
E2COTDN	degF	CJES 2 CORE AIR SUPPLY DOWNSTREAM TEMPERATURE
E2FNFLO	lb/sec	CJES 2 FAN AIR SUPPLY FLOW RATE
E2FNUP	psi	CJES 2 FAN AIR SUPPLY UPSTREAM PRESSURE
E2FNTUP	degF	CJES 2 FAN AIR SUPPLY UPSTREAM TEMPERATURE
E2FNPDN	psi	CJES 2 FAN AIR SUPPLY DOWNSTREAM PRESSURE
E2FNTDN	degF	CJES 2 FAN AIR SUPPLY DOWNSTREAM TEMPERATURE

BENS 1 PARAMETERS		
B1FLOHZ	Hz	BENS 1 FLOW METER FREQUENCY
B1FLOPS	psi	BENS 1 FLOW METER STATIC PRESSURE

B1FLOTT	degF	BENS 1 FLOW METER TEMPERATURE
B1DEN	lb/cuft	BENS 1 FLOW DENSITY
B1FLO	lb/sec	BENS 1 MASS FLOW
BENS 2 PARAMETERS		
B2FLOHZ	Hz	BENS 2 FLOW METER FREQUENCY
B2FLOPS	psi	BENS 2 FLOW METER STATIC PRESSURE
B2FLOTT	degF	BENS 2 FLOW METER TEMPERATURE
B2DEN	lb/cuft	BENS 2 FLOW DENSITY
B2FLO	lb/sec	BENS 2 MASS FLOW

NAME	UNIT	DESCRIPTION
TEST		
RUN		
POINT		
ID		DATA TYPE IDENTIFIER, 0 = Windoff Zero, 1 = Weight Tare, 2 = Wind On Data, 5 = Balance Span ,6 = Transducer Ca
YEAR		
MONTH		
DAY		
HOUR		
MINUTE		
SECOND		
PA	psf	AMBIENT PRESSURE
PTOT	psf	SETTLING CHAMBER TOTAL PRESSURE
DPIHS	psf	DIFFERENTIAL PRESSURE OF SIDEWALL STATIC PRESSURE IN THE ENTRANCE CONE REFERENCED TO PTOT
DPCEIL	psf	DIFFERENTIAL PRESSURE OF CEILING PITOT-STATIC PROBE
DPAT	psf	DELTA PRESSURE BETWEEN PTOT AND PA
DPRT	psf	DELTA PRESSURE BETWEEN WALL REFERENCE AND TOTAL PRESSURE
DPI3	psf	DELTA PRESSURE BETWEEN TUNNEL TOTAL AND WALL STATIC ORIFICE
DPS2	psf	DELTA PRESSURE BETWEEN TUNNEL STATIC AND WALL STATIC ORIFICE
TA	degF	ENTRANCE CONE AMBIENT TEMPERATURE
TDEW	degF	DEW POINT TEMPERATURE
TAIR	degF	OUTSIDE AMBIENT TEMPERATURE
ELEV	in	MAST HEIGHT
HGT	in	MODEL HEIGHT ABOVE THE FLOOR
YAW	deg	YAW TABLE POSITION
PITCHM	deg	MAST PITCH ANGLE
QCODE		DYNAMIC PRESSURE COMPUTATION CODE, 2 = CTS, BLRS Off, 3 = CTS, BLRS On, 4 = OTS, BLRS Off, 5 = OTS, BLRS O
SCODE		MODEL SUPPORT OR STING CODE, 0 = Model Height Not Calculated, 1 = Sting Mount (Cart 1 & Cart 7), 2 = Alpha Beta Sting (Obsolete), 3 = Post Mount (Cart 2)
WCODE		TEST SECTION CONFIGURATION CODE FOR WALL CORRECTIONS, 0 = No Wall Correction, 1 = CTS Wall Corrections (Table Lookup), 2 = OTS Wall Corrections (Table Lookup), 3 = Buoyancy & Jet Boundary Corrections
RLENGTH	in	HORIZONTAL DISTANCE FROM MODEL REFERENCE TO CENTER OF MAST
VLENGTH	in	VERTICAL DISTANCE FROM MODEL REFERENCE TO TOP OF MAST
SAREA1	sqft	MODEL REFERENCE WING AREA

BSPAN1	in	MODEL REFERENCE WING SPAN
CHORD1	in	MODEL REFERENCE CHORD LENGTH
LAMBDA	deg	WING SWEEP ANGLE
SIGMA		WING SPAN TO TUNNEL WIDTH RATIO
WINGAR		WING ASPECT RATIO
WINGLOAD		WING LOADING
WINGBLOK		MODEL BLOCKAGE DUE TO WING
BODYBLOK		MODEL BLOCKAGE DUE TO BODY
JBCORR1		JET BOUNDARY FACTOR FOR DRAG COEFFICIENT, NOT USED
JBCORR2		ANGLE OF ATTACK CORRECTION FACTOR
JBCORR3		PITCHING MOMENT CORRECTION FACTOR
CHANxxxx	mv	RAW VOLTAGE FOR A SPECIFIED CHANNEL, xxxx = CHANNEL NUMBER
ESP Info		
ESPxyy	psi or psf	ESP PRESSURE ON A SPECIFIC MODULE AND PORT (xx = MODULE NUMBER, yy = PORT NUMBER)
CPPxyy		PRESSURE COEFFICIENT ON A SPECIFIC MODULE AND PORT (xx = MODULE NUMBER, yy = PORT NUMBER)
Wall Pressure Info		
WSPxyy	psf	WALL PRESSURE ON A SPECIFIC MODULE AND PORT (xx = MODULE NUMBER, yy = PORT NUMBER)
WPPxyy		WALL PRESSURE COEFFICIENT ON A SPECIFIC MODULE AND PORT (xx = MODULE NUMBER, yy = PORT NUMBER)
ESPTMP50	degF	WALL MODULE 50 TEMPERATURE
ESPTMP51	degF	WALL MODULE 51 TEMPERATURE
ESPTMP52	degF	WALL MODULE 52 TEMPERATURE

HWB Model Pressure Taps

The orifice description and variable/coefficient names listed for the pressure taps are correct as seen in the table below for all of the data runs. However, the variable indices are not listed in the table below. To locate the exact variable index corresponding to the pressure tap coefficient name, it is necessary to search the ascii files listed for each run, for example *r011.ascii*. The variable indices are different for the following segmented groups of run numbers: Runs 11-20 contain 1254 indices; runs 21-251 contain 1942 indices; runs 252-287 contain 1899 indices; and runs 288-297 contain 1192 indices.

Name	Unit	Description	Coefficient Name
LW13B003	psfA	Orifice 18	L13B003C
LW13B01	psfA	Orifice 19	LW13B01C
LW13B02	psfA	Orifice 20	LW13B02C
LW13B03	psfA	Orifice 21	LW13B03C
LW13B05	psfA	Orifice 22	LW13B05C
LW13B07	psfA	Orifice 23	LW13B07C
LW13B089	psfA	Orifice 24	L13B089C
LW13B15	psfA	Orifice 25	LW13B15C
LW13B20	psfA	Orifice 26	LW13B20C
LW13B25	psfA	Orifice 27	LW13B25C
LW13B35	psfA	Orifice 28	LW13B35C
LW13B40	psfA	Orifice 29	LW13B40C
LW13B53	psfA	Orifice 30	LW13B53C
LW13B65	psfA	Orifice 31	LW13B65C
LW13LE	psfA	Orifice 1	LW13LEC

Name	Unit	Description	Coefficient Name
LW13T003	psfA	Orifice 2	L13T003C
LW13T01	psfA	Orifice 3	LW13T01C
LW13T02	psfA	Orifice 4	LW13T02C
LW13T03	psfA	Orifice 5	LW13T03C
LW13T05	psfA	Orifice 6	LW13T05C
LW13T07	psfA	Orifice 7	LW13T07C
LW13T10	psfA	Orifice 8	LW13T10C
LW13T13	psfA	Orifice 9	LW13T13C
LW13T16	psfA	Orifice 10	LW13T16C
LW13T20	psfA	Orifice 11	LW13T20C
LW13T25	psfA	Orifice 12	LW13T25C
LW13T30	psfA	Orifice 13	LW13T30C
LW13T35	psfA	Orifice 14	LW13T35C
LW13T40	psfA	Orifice 15	LW13T40C
LW13T50	psfA	Orifice 16	LW13T50C
LW13T59	psfA	Orifice 17	LW13T59C
LW30B003	psfA	Orifice 75	L30B003C
LW30B01	psfA	Orifice 76	LW30B01C
LW30B02	psfA	Orifice 77	LW30B02C
LW30B03	psfA	Orifice 78	LW30B03C
LW30B05	psfA	Orifice 79	LW30B05C
LW30B07	psfA	Orifice 80	LW30B07C
LW30B10	psfA	Orifice 81	LW30B10C
LW30B15	psfA	Orifice 82	LW30B15C
LW30B20	psfA	Orifice 83	LW30B20C
LW30B25	psfA	Orifice 84	LW30B25C
LW30B30	psfA	Orifice 85	LW30B30C
LW30B40	psfA	Orifice 86	LW30B40C
LW30B50	psfA	Orifice 87	LW30B50C
LW30B60	psfA	Orifice 88	LW30B60C
LW30B70	psfA	Orifice 89	LW30B70C
LW30B75	psfA	Orifice 90	LW30B75C
LW30B80	psfA	Orifice 91	LW30B80C
LW30B85	psfA	Orifice 92	LW30B85C
LW30B90	psfA	Orifice 93	LW30B90C
LW30B95	psfA	Orifice 94	LW30B95C
LW30LE	psfA	Orifice 50	LW30LEC
LW30T001	psfA	Orifice 51	L30T001C
LW30T005	psfA	Orifice 52	L30T005C
LW30T01	psfA	Orifice 53	LW30T01C
LW30T02	psfA	Orifice 54	LW30T02C
LW30T03	psfA	Orifice 55	LW30T03C
LW30T05	psfA	Orifice 56	LW30T05C
LW30T07	psfA	Orifice 57	LW30T07C
LW30T10	psfA	Orifice 58	LW30T10C
LW30T13	psfA	Orifice 59	LW30T13C
LW30T16	psfA	Orifice 60	LW30T16C
LW30T20	psfA	Orifice 61	LW30T20C
LW30T25	psfA	Orifice 62	LW30T25C
LW30T30	psfA	Orifice 63	LW30T30C
LW30T35	psfA	Orifice 64	LW30T35C
LW30T40	psfA	Orifice 65	LW30T40C
LW30T50	psfA	Orifice 66	LW30T50C
LW30T60	psfA	Orifice 67	LW30T60C
LW30T70	psfA	Orifice 68	LW30T70C
LW30T75	psfA	Orifice 69	LW30T75C
LW30T80	psfA	Orifice 70	LW30T80C

Name	Unit	Description	Coefficient Name
LW30T85	psfA	Orifice 71	LW30T85C
LW30T90	psfA	Orifice 72	LW30T90C
LW30T95	psfA	Orifice 73	LW30T95C
LW30T99	psfA	Orifice 74	LW30T99C
LW51B20	psfA	Orifice 122	LW51B20C
LW51B25	psfA	Orifice 123	LW51B25C
LW51B30	psfA	Orifice 124	LW51B30C
LW51B40	psfA	Orifice 125	LW51B40C
LW51B50	psfA	Orifice 126	LW51B50C
LW51B65	psfA	Orifice 127	LW51B65C
LW51B75	psfA	Orifice 128	LW51B75C
LW51B85	psfA	Orifice 129	LW51B85C
LW51B94	psfA	Orifice 130	LW51B94C
LW51B96	psfA	Orifice 131	LW51B96C
LW51T25	psfA	Orifice 106	LW51T25C
LW51T30	psfA	Orifice 107	LW51T30C
LW51T40	psfA	Orifice 108	LW51T40C
LW51T50	psfA	Orifice 109	LW51T50C
LW51T65	psfA	Orifice 110	LW51T65C
LW51T75	psfA	Orifice 111	LW51T75C
LW51T85	psfA	Orifice 112	LW51T85C
LW51T94	psfA	Orifice 113	LW51T94C
LW51T96	psfA	Orifice 114	LW51T96C
LW6B60	psfA	Orifice 43	LW6B60C
LW6B70	psfA	Orifice 44	LW6B70C
LW6B80	psfA	Orifice 45	LW6B80C
LW6B90	psfA	Orifice 46	LW6B90C
LW6B92	psfA	Orifice 47	LW6B92C
LW6B95	psfA	Orifice 48	LW6B95C
LW6B97	psfA	Orifice 49	LW6B97C
LW6T60	psfA	Orifice 32	LW6T60C
LW6T65	psfA	Orifice 33	LW6T65C
LW6T70	psfA	Orifice 34	LW6T70C
LW6T75	psfA	Orifice 35	LW6T75C
LW6T80	psfA	Orifice 36	LW6T80C
LW6T85	psfA	Orifice 37	LW6T85C
LW6T90	psfA	Orifice 38	LW6T90C
LW6T92	psfA	Orifice 39	LW6T92C
LW6T95	psfA	Orifice 40	LW6T95C
LW6T97	psfA	Orifice 41	LW6T97C
LW6TE	psfA	Orifice 42	LW6TEC
LW90B20	psfA	Orifice 158	LW90B20C
LW90B25	psfA	Orifice 159	LW90B25C
LW90B30	psfA	Orifice 160	LW90B30C
LW90B40	psfA	Orifice 161	LW90B40C
LW90B50	psfA	Orifice 162	LW90B50C
LW90B65	psfA	Orifice 163	LW90B65C
LW90B75	psfA	Orifice 164	LW90B75C
LW90B85	psfA	Orifice 165	LW90B85C
LW90B92	psfA	Orifice 166	LW90B92C
LW90T30	psfA	Orifice 144	LW90T30C
LW90T40	psfA	Orifice 145	LW90T40C
LW90T50	psfA	Orifice 146	LW90T50C
LW90T65	psfA	Orifice 147	LW90T65C
LW90T75	psfA	Orifice 148	LW90T75C
LW90T85	psfA	Orifice 149	LW90T85C
LW90T93	psfA	Orifice 150	LW90T93C

Name	Unit	Description	Coefficient Name
RW51B25	psfA	Orifice 226	RW51B25C
RW51B50	psfA	Orifice 227	RW51B50C
RW51B75	psfA	Orifice 228	RW51B75C
RW51T25	psfA	Orifice 218	RW51T25C
RW51T50	psfA	Orifice 219	RW51T50C
RW51T75	psfA	Orifice 220	RW51T75C
RW90B125	psfA	Orifice 242	R90B125C
RW90B50	psfA	Orifice 243	RW90B50C
RW90B75	psfA	Orifice 244	RW90B75C
RW90T50	psfA	Orifice 235	RW90T50C
RW90T75	psfA	Orifice 236	RW90T75C
Engine 2 Pressure			
RN000	psfA	Orifice 265	RN000C
RN090	psfA	Orifice 266	RN090C
RN180	psfA	Orifice 267	RN180C
RN270	psfA	Orifice 268	RN270C
Cruise Leading Edge			
LW51B004	psfA	Orifice 115	L51B004C
LW51B01	psfA	Orifice 116	LW51B01C
LW51B02	psfA	Orifice 117	LW51B02C
LW51B03	psfA	Orifice 118	LW51B03C
LW51B05	psfA	Orifice 119	LW51B05C
LW51B10	psfA	Orifice 120	LW51B10C
LW51B15	psfA	Orifice 121	LW51B15C
LW51LE	psfA	Orifice 95	LW51LEC
LW51T001	psfA	Orifice 96	L51T001C
LW51T005	psfA	Orifice 97	L51T005C
LW51T01	psfA	Orifice 98	LW51T01C
LW51T02	psfA	Orifice 99	LW51T02C
LW51T03	psfA	Orifice 100	LW51T03C
LW51T05	psfA	Orifice 101	LW51T05C
LW51T07	psfA	Orifice 102	LW51T07C
LW51T10	psfA	Orifice 103	LW51T10C
LW51T15	psfA	Orifice 104	LW51T15C
LW51T20	psfA	Orifice 105	LW51T20C
LW90B005	psfA	Orifice 151	L90B005C
LW90B011	psfA	Orifice 152	L90B011C
LW90B018	psfA	Orifice 153	L90B018C
LW90B03	psfA	Orifice 154	LW90B03C
LW90B05	psfA	Orifice 155	LW90B05C
LW90B10	psfA	Orifice 156	LW90B10C
LW90B15	psfA	Orifice 157	LW90B15C
LW90LE	psfA	Orifice 132	LW90LEC
LW90T003	psfA	Orifice 133	L90T003C
LW90T008	psfA	Orifice 134	L90T008C
LW90T01	psfA	Orifice 135	LW90T01C
LW90T02	psfA	Orifice 136	LW90T02C
LW90T03	psfA	Orifice 137	LW90T03C
LW90T05	psfA	Orifice 138	LW90T05C
LW90T07	psfA	Orifice 139	LW90T07C
LW90T10	psfA	Orifice 140	LW90T10C
LW90T15	psfA	Orifice 141	LW90T15C
LW90T20	psfA	Orifice 142	LW90T20C
LW90T25	psfA	Orifice 143	LW90T25C
RW51B01	psfA	Orifice 221	RW51B01C
RW51B02	psfA	Orifice 222	RW51B02C
RW51B03	psfA	Orifice 223	RW51B03C

Name	Unit	Description	Coefficient Name
RW51B05	psfA	Orifice 224	RW51B05C
RW51B10	psfA	Orifice 225	RW51B10C
RW51T01	psfA	Orifice 213	RW51T01C
RW51T02	psfA	Orifice 214	RW51T02C
RW51T03	psfA	Orifice 215	RW51T03C
RW51T05	psfA	Orifice 216	RW51T05C
RW51T10	psfA	Orifice 217	RW51T10C
RW90B01	psfA	Orifice 237	RW90B01C
RW90B02	psfA	Orifice 238	RW90B02C
RW90B03	psfA	Orifice 239	RW90B03C
RW90B05	psfA	Orifice 240	RW90B05C
RW90B10	psfA	Orifice 241	RW90B10C
RW90T01	psfA	Orifice 229	RW90T01C
RW90T02	psfA	Orifice 230	RW90T02C
RW90T03	psfA	Orifice 231	RW90T03C
RW90T05	psfA	Orifice 232	RW90T05C
RW90T10	psfA	Orifice 233	RW90T10C
RW90T25	psfA	Orifice 234	RW90T25C
Drooped Leading Edge			
LD51B003	psfA	Orifice 182	L51B003C
LD51B009	psfA	Orifice 183	L51B009C
LD51B01	psfA	Orifice 184	LD51B01C
LD51B02	psfA	Orifice 185	LD51B02C
LD51B03	psfA	Orifice 186	LD51B03C
LD51B05	psfA	Orifice 187	LD51B05C
LD51B10	psfA	Orifice 188	LD51B10C
LD51T001	psfA	Orifice 167	L51T001C
LD51T003	psfA	Orifice 168	L51T003C
LD51T005	psfA	Orifice 169	L51T005C
LD51T01	psfA	Orifice 170	LD51T01C
LD51T02	psfA	Orifice 171	LD51T02C
LD51T05	psfA	Orifice 172	LD51T05C
LD51T07	psfA	Orifice 173	LD51T07C
LD51T09	psfA	Orifice 174	LD51T09C
LD51T12	psfA	Orifice 175	LD51T12C
LD51T131	psfA	Orifice 176	L51T131C
LD51T139	psfA	Orifice 177	L51T139C
LD90B009	psfA	Orifice 205	L90B009C
LD90B01	psfA	Orifice 206	LD90B01C
LD90B02	psfA	Orifice 207	LD90B02C
LD90B03	psfA	Orifice 208	LD90B03C
LD90B04	psfA	Orifice 209	LD90B04C
LD90B06	psfA	Orifice 210	LD90B06C
LD90B10	psfA	Orifice 211	LD90B10C
LD90T008	psfA	Orifice 190	L90T008C
LD90T01	psfA	Orifice 191	LD90T01C
LD90T014	psfA	Orifice 192	L90T014C
LD90T018	psfA	Orifice 193	L90T018C
LD90T02	psfA	Orifice 194	LD90T02C
LD90T04	psfA	Orifice 195	LD90T04C
LD90T07	psfA	Orifice 196	LD90T07C
LD90T10	psfA	Orifice 197	LD90T10C
LD90T12	psfA	Orifice 198	LD90T12C
LD90T13	psfA	Orifice 199	LD90T13C
LD90T14	psfA	Orifice 200	LD90T14C
LD90T15	psfA	Orifice 201	LD90T15C
RD51B01	psfA	Orifice 250	RD51B01C

Name	Unit	Description	Coefficient Name
RD51B02	psfA	Orifice 251	RD51B02C
RD51B03	psfA	Orifice 252	RD51B03C
RD51B05	psfA	Orifice 253	RD51B05C
RD51B10	psfA	Orifice 254	RD51B10C
RD51T005	psfA	Orifice 245	R51T005C
RD51T011	psfA	Orifice 246	R51T011C
RD51T018	psfA	Orifice 247	R51T018C
RD51T03	psfA	Orifice 248	RD51T03C
RD51T07	psfA	Orifice 249	RD51T07C
RD90B02	psfA	Orifice 260	RD90B02C
RD90B03	psfA	Orifice 261	RD90B03C
RD90B04	psfA	Orifice 262	RD90B04C
RD90B06	psfA	Orifice 263	RD90B06C
RD90B10	psfA	Orifice 264	RD90B10C
RD90T011	psfA	Orifice 255	R90T011C
RD90T017	psfA	Orifice 256	R90T017C
RD90T02	psfA	Orifice 257	RD90T02C
RD90T03	psfA	Orifice 258	RD90T03C
RD90T07	psfA	Orifice 259	RD90T07C
RD90T25	psfA	Orifice 269	RD90T25C
Pressure taps for orifices 178-181, 189, 202-204 and 212 at the droop leading edge transitions of section BL:-37.8 and BL:-67 are not included in this list.			

Appendix C: Acoustic DAS Data Listing

This appendix contains a complete listing of the acoustic data acquisition system. However, the reader should be cautioned that while this appendix contains the initial channel assignments and descriptions of the Acoustic DAS data, it may not contain all data updates pertaining to individual microphone replacements, etc. Run-to-run changes are contained in the CSV Sensor Information stored with the test data.

HWB 14x22 Channel Assignments 1-148 (w/o BENS)							
Note: Channel assignments are nominal. See CSV sensor information stored with the HWB data for run-to-run variations.							
6 December 2012							
DAQ Chan#	Sensor	PF28k Unit#	PF28k Chan#	NI Client#	NI-6120 Chan#	Location	Classification
1/4" Array Mics							
1	M1	1	1	1	1	Array Mic 1	analog in
2	M2	1	2	1	2	Array Mic 2	analog in
3	M3	1	3	1	3	Array Mic 3	analog in
4	M4	1	4	1	4	Array Mic 4	analog in
5	M5	1	5	1	5	Array Mic 5	analog in
6	M6	1	6	1	6	Array Mic 6	analog in
7	M7	1	7	1	7	Array Mic 7	analog in
8	M8	1	8	1	8	Array Mic 8	analog in
9	M9	1	9	1	9	Array Mic 9	analog in
10	M10	1	10	1	10	Array Mic 10	analog in
11	M11	1	11	1	11	Array Mic 11	analog in
12	M12	1	12	1	12	Array Mic 12	analog in
13	M13	1	13	1	13	Array Mic 13	analog in
14	M14	1	14	1	14	Array Mic 14	analog in
15	M15	1	15	1	15	Array Mic 15	analog in
16	M16	1	128/127	1	16	Array Mic 16	analog in
17	M17	1	17	1	17	Array Mic 17	analog in
18	M18	1	18	1	18	Array Mic 18	analog in
19	M19	1	19	1	19	Array Mic 19	analog in
20	M20	1	20	1	20	Array Mic 20	analog in
21	M21	1	21	1	21	Array Mic 21	analog in
22	M22	1	22	1	22	Array Mic 22	analog in
23	M23	1	23	1	23	Array Mic 23	analog in
24	M24	1	24	1	24	Array Mic 24	analog in
25	M25	1	25	1	25	Array Mic 25	analog in
26	M26	1	26	1	26	Array Mic 26	analog in

27	M27	1	27	1	27	Array Mic 27	analog in
28	M28	1	28	1	28	Array Mic 28	analog in
29	M29	1	29	1	29	Array Mic 29	analog in
30	M30	1	30	1	30	Array Mic 30	analog in
31	M31	1	31	1	31	Array Mic 31	analog in
32	M32	1	32	1	32	Array Mic 32	analog in
33	M33	1	33	1	33	Array Mic 33	analog in
34	M34	1	34	1	34	Array Mic 34	analog in
35	M35	1	35	1	35	Array Mic 35	analog in
36	M36	1	36	1	36	Array Mic 36	analog in
37	M37	1	37	1	37	Array Mic 37	analog in
38	M38	1	38	1	38	Array Mic 38	analog in
39	M39	1	39	1	39	Array Mic 39	analog in
40	M40	1	40	1	40	Array Mic 40	analog in
41	M41	1	41	1	41	Array Mic 41	analog in
42	M42	1	42	1	42	Array Mic 42	analog in
43	M43	1	43	1	43	Array Mic 43	analog in
44	M44	1	44	1	44	Array Mic 44	analog in
45	M45	1	45	1	45	Array Mic 45	analog in
46	M46	1	46	1	46	Array Mic 46	analog in
47	M47	1	47	1	47	Array Mic 47	analog in
48	M48	1	48	1	48	Array Mic 48	analog in
49	M49	1	49	1	49	Array Mic 49	analog in
50	M50	1	50	1	50	Array Mic 50	analog in
51	M51	1	51	1	51	Array Mic 51	analog in
52	M52	1	52	1	52	Array Mic 52	analog in
53	M53	1	53	1	53	Array Mic 53	analog in
54	M54	1	54	1	54	Array Mic 54	analog in
55	M55	1	55	1	55	Array Mic 55	analog in
56	M56	1	56	1	56	Array Mic 56	analog in
57	M57	1	57	1	57	Array Mic 57	analog in
58	M58	1	58	1	58	Array Mic 58	analog in
59	M59	1	59	1	59	Array Mic 59	analog in
60	M60	1	60	1	60	Array Mic 60	analog in
61	M61	1	61	1	61	Array Mic 61	analog in
62	M62	1	62	1	62	Array Mic 62	analog in
63	M63	1	63	1	63	Array Mic 63	analog in
127	M64	1	64	2	127	Array Mic 64	analog in
65	M65	1	65	2	65	Array Mic 65	analog in
66	M66	1	66	2	66	Array Mic 66	analog in
67	M67	1	67	2	67	Array Mic 67	analog in

68	M68	1	68	2	68	Array Mic 68	analog in
69	M69	1	69	2	69	Array Mic 69	analog in
70	M70	1	70	2	70	Array Mic 70	analog in
71	M71	1	71	2	71	Array Mic 71	analog in
72	M72	1	72	2	72	Array Mic 72	analog in
73	M73	1	73	2	73	Array Mic 73	analog in
74	M74	1	74	2	74	Array Mic 74	analog in
75	M75	1	75	2	75	Array Mic 75	analog in
76	M76	1	76	2	76	Array Mic 76	analog in
77	M77	1	77	2	77	Array Mic 77	analog in
78	M78	1	78	2	78	Array Mic 78	analog in
79	M79	1	79	2	79	Array Mic 79	analog in
80	M80	1	80	2	80	Array Mic 80	analog in
81	M81	1	81	2	81	Array Mic 81	analog in
82	M82	1	82	2	82	Array Mic 82	analog in
83	M83	1	83	2	83	Array Mic 83	analog in
84	M84	1	84	2	84	Array Mic 84	analog in
85	M85	1	85	2	85	Array Mic 85	analog in
86	M86	1	86	2	86	Array Mic 86	analog in
87	M87	1	87	2	87	Array Mic 87	analog in
88	M88	1	88	2	88	Array Mic 88	analog in
89	M89	1	89	2	89	Array Mic 89	analog in
90	M90	1	90	2	90	Array Mic 90	analog in
91	M91	1	91	2	91	Array Mic 91	analog in
92	M92	1	92	2	92	Array Mic 92	analog in
93	M93	1	93	2	93	Array Mic 93	analog in
94	M94	1	94	2	94	Array Mic 94	analog in
95	M85	1	95	2	95	Array Mic 95	analog in
96	M86	1	96	2	96	Array Mic 96	analog in
97	M97	1	97	2	97	Array Mic 97	analog in
1/8" Tower & Truss Mics		Start from North Side Tower (closer to cntrl rm) : Bottom to top ->South Side Bottom to top->Over to truss#1					
98	M98	1	98	2	98	NST Mic 1 (bottom of NS twr)	analog in
99	M99	1	99	2	99	NST Mic 2	analog in
100	M100	1	100	2	100	NST Mic 3	analog in
101	M101	1	101	2	101	NST Mic 4	analog in
102	M102	1	102	2	102	NST Mic 5	analog in
103	M103	1	103	2	103	NST Mic 6	analog in
104	M104	1	104	2	104	NST Mic 7	analog in
105	M105	1	105	2	105	NST Mic 8	analog in

106	M106	1	106	2	106	Truss Mic 1 (closest to CR)	analog in
107	M107	1	107	2	107	Truss Mic 2	analog in
108	M108	1	108	2	108	Truss Mic 3	analog in
109	M109	1	109	2	109	Truss Mic 4	analog in
110	M110	1	110	2	110	Truss Mic 5	analog in
111	M111	1	111	2	111	Truss Mic 6	analog in
112	M112	1	112	2	112	Truss Mic 7	analog in
113	M113	1	113	2	113	Truss Mic 8	analog in
114	M114	1	114	2	114	Truss Mic 9	analog in
115	M115	1	115	2	115	Truss Mic 10	analog in
116	M116	1	116	2	116	Truss Mic 11	analog in
117	M117	1	117	2	117	Truss Mic 12	analog in
118	M118	1	118	2	118	Truss Mic 13	analog in
119	M119	1	119/128	2	119	SST Mic 1 (bottom of SS twr)	analog in
120	M120	1	120	2	120	SST Mic 2	analog in
121	M121	1	121	2	121	SST Mic 3	analog in
122	M122	1	122	2	122	SST Mic 4	analog in
123	M123	1	123	2	123	SST Mic 5	analog in
124	M124	1	124	2	124	SST Mic 6	analog in
125	M125	1	125	2	125	SST Mic 7	analog in
126	M126	1	126	2	126	SST Mic 8	analog in
Array Accelerometers							
129	A1	2	none	3	none	Mic Array	analog in
130	A2	2	none	3	none	Mic Array	analog in
131	A3	2	none	3	none	Mic Array	analog in
132	A4	2	none	3	none	Mic Array	analog in
133	A5	2	none	3	none	Mic Array	analog in
134	A6	2	none	3	none	Mic Array	analog in
135	A7	2	none	3	none	Mic Array	analog in
136	A8	2	none	3	none	Mic Array	analog in
137	A9	2	none	3	none	Mic Array	analog in
DAQ Analog Driver Outputs							
138	AO1	none	none	3	none	Model Pt. Source Speaker 1	analog out:port-acq
139	AO2	none	none	3	none	Model Pt. Source Speaker 2	analog out:port-acq
140	AO3	none	none	3	none	Model Pt. Source Speaker 3	analog out:port-acq

141	AO4	none	none	3	none	Model Pt. Source Speaker 4	analog out:port-acq
142	AO5	none	none	3	none	Model Pt. Source Speaker 5	analog out:port-acq
143	AO6	none	none	3	none	Model Pt. Source Speaker 6	analog out:port-acq
144	AO7	none	none	3	none	Mic Array Cal Speaker South A1	analog out 1033 S5:ao1 (A1)
145	AO8	none	none	3	none	Mic Array Cal Speaker Throat A2	analog out 1033 S5:ao0 (A2)
146	AO9	none	none	3	none	Mic Array Cal Speaker North A3	analog out 1033 S6:ao0 (A3)
147	AO10	none	none	3	none	Injection Cal Source	analog out 1033 S6:ao1
DAQ Synchronization Signals							
64	C1-IRIGB	none	none	1	64	rack	analog in
128	C2-IRIGB	none	none	2	128	rack	analog in
148	C3-IRIGB	none	none	3	148	rack	analog in
DAQ Re-Assigned Signals 12/20/12							
16	M16	1	128/127	1	16	Note: <ul style="list-style-type: none"> • M16: filter channel 16 went bad (gain) so M16 was reassigned to filter channel 128 (first) then to channel 127. • M64: moved to DAQ (digitizer) channel 127 so that the IRIG-B signal could occupy this slot. Each digitizer unit (there were 3) used the last channel as the IRIG signal input. • M119: filter channel 119 went bad (gain) so M119 was reassigned to filter channel 128. 	
127	M64	1	64	1	127		
119	M119	1	128	2	119		

HWB 14x22 Channel Assignments 1-188 (with BENS)							
6 December 2012							
DAQ Chan#	Sensor	PF28k Unit#	PF28k Chan#	NI Client#	NI-6120 Chan#	Location	Classification
1/4" Array Mics							
1	M1	1	1	1	1	Array Mic 1	analog in
2	M2	1	2	1	2	Array Mic 2	analog in
3	M3	1	3	1	3	Array Mic 3	analog in
4	M4	1	4	1	4	Array Mic 4	analog in
5	M5	1	5	1	5	Array Mic 5	analog in
6	M6	1	6	1	6	Array Mic 6	analog in
7	M7	1	7	1	7	Array Mic 7	analog in
8	M8	1	8	1	8	Array Mic 8	analog in
9	M9	1	9	1	9	Array Mic 9	analog in
10	M10	1	10	1	10	Array Mic 10	analog in
11	M11	1	11	1	11	Array Mic 11	analog in
12	M12	1	12	1	12	Array Mic 12	analog in
13	M13	1	13	1	13	Array Mic 13	analog in
14	M14	1	14	1	14	Array Mic 14	analog in
15	M15	1	15	1	15	Array Mic 15	analog in
16	M16	1	128/127	1	16	Array Mic 16	analog in
17	M17	1	17	1	17	Array Mic 17	analog in
18	M18	1	18	1	18	Array Mic 18	analog in
19	M19	1	19	1	19	Array Mic 19	analog in
20	M20	1	20	1	20	Array Mic 20	analog in
21	M21	1	21	1	21	Array Mic 21	analog in
22	M22	1	22	1	22	Array Mic 22	analog in
23	M23	1	23	1	23	Array Mic 23	analog in
24	M24	1	24	1	24	Array Mic 24	analog in
25	M25	1	25	1	25	Array Mic 25	analog in
26	M26	1	26	1	26	Array Mic 26	analog in
27	M27	1	27	1	27	Array Mic 27	analog in
28	M28	1	28	1	28	Array Mic 28	analog in
29	M29	1	29	1	29	Array Mic 29	analog in
30	M30	1	30	1	30	Array Mic 30	analog in
31	M31	1	31	1	31	Array Mic 31	analog in
32	M32	1	32	1	32	Array Mic 32	analog in
33	M33	1	33	1	33	Array Mic 33	analog in
34	M34	1	34	1	34	Array Mic 34	analog in

35	M35	1	35	1	35	Array Mic 35	analog in
36	M36	1	36	1	36	Array Mic 36	analog in
37	M37	1	37	1	37	Array Mic 37	analog in
38	M38	1	38	1	38	Array Mic 38	analog in
39	M39	1	39	1	39	Array Mic 39	analog in
40	M40	1	40	1	40	Array Mic 40	analog in
41	M41	1	41	1	41	Array Mic 41	analog in
42	M42	1	42	1	42	Array Mic 42	analog in
43	M43	1	43	1	43	Array Mic 43	analog in
44	M44	1	44	1	44	Array Mic 44	analog in
45	M45	1	45	1	45	Array Mic 45	analog in
46	M46	1	46	1	46	Array Mic 46	analog in
47	M47	1	47	1	47	Array Mic 47	analog in
48	M48	1	48	1	48	Array Mic 48	analog in
49	M49	1	49	1	49	Array Mic 49	analog in
50	M50	1	50	1	50	Array Mic 50	analog in
51	M51	1	51	1	51	Array Mic 51	analog in
52	M52	1	52	1	52	Array Mic 52	analog in
53	M53	1	53	1	53	Array Mic 53	analog in
54	M54	1	54	1	54	Array Mic 54	analog in
55	M55	1	55	1	55	Array Mic 55	analog in
56	M56	1	56	1	56	Array Mic 56	analog in
57	M57	1	57	1	57	Array Mic 57	analog in
58	M58	1	58	1	58	Array Mic 58	analog in
59	M59	1	59	1	59	Array Mic 59	analog in
60	M60	1	60	1	60	Array Mic 10	analog in
61	M61	1	61	1	61	Array Mic 61	analog in
62	M62	1	62	1	62	Array Mic 62	analog in
63	M63	1	63	1	63	Array Mic 63	analog in
127	M64	1	64	2	127	Array Mic 64	analog in
65	M65	1	65	2	65	Array Mic 65	analog in
66	M66	1	66	2	66	Array Mic 66	analog in
67	M67	1	67	2	67	Array Mic 67	analog in
68	M68	1	68	2	68	Array Mic 68	analog in
69	M69	1	69	2	69	Array Mic 69	analog in
70	M70	1	70	2	70	Array Mic 70	analog in
71	M71	1	71	2	71	Array Mic 71	analog in
72	M72	1	72	2	72	Array Mic 72	analog in
73	M73	1	73	2	73	Array Mic 73	analog in
74	M74	1	74	2	74	Array Mic 74	analog in
75	M75	1	75	2	75	Array Mic 75	analog in

76	M76	1	76	2	76	Array Mic 76	analog in
77	M77	1	77	2	77	Array Mic 77	analog in
78	M78	1	78	2	78	Array Mic 78	analog in
79	M79	1	79	2	79	Array Mic 79	analog in
80	M80	1	80	2	80	Array Mic 80	analog in
81	M81	1	81	2	81	Array Mic 81	analog in
82	M82	1	82	2	82	Array Mic 82	analog in
83	M83	1	83	2	83	Array Mic 83	analog in
84	M84	1	84	2	84	Array Mic 84	analog in
85	M85	1	85	2	85	Array Mic 85	analog in
86	M86	1	86	2	86	Array Mic 86	analog in
87	M87	1	87	2	87	Array Mic 87	analog in
88	M88	1	88	2	88	Array Mic 88	analog in
89	M89	1	89	2	89	Array Mic 89	analog in
90	M90	1	90	2	90	Array Mic 90	analog in
91	M91	1	91	2	91	Array Mic 91	analog in
92	M92	1	92	2	92	Array Mic 92	analog in
93	M93	1	93	2	93	Array Mic 93	analog in
94	M94	1	94	2	94	Array Mic 94	analog in
95	M85	1	95	2	95	Array Mic 95	analog in
96	M86	1	96	2	96	Array Mic 96	analog in
97	M97	1	97	2	97	Array Mic 97	analog in
1/8" Tower & Truss Mics		Start from North Side Tower (closer to cntrl rm) : Bottom to top ->South Side Bottom to top->Over to truss#1					
98	M98	1	98	2	98	NST Mic 1 (bottom of NS twr)	analog in
99	M99	1	99	2	99	NST Mic 2	analog in
100	M100	1	100	2	100	NST Mic 3	analog in
101	M101	1	101	2	101	NST Mic 4	analog in
102	M102	1	102	2	102	NST Mic 5	analog in
103	M103	1	103	2	103	NST Mic 6	analog in
104	M104	1	104	2	104	NST Mic 7	analog in
105	M105	1	105	2	105	NST Mic 8	analog in
106	M106	1	106	2	106	Truss Mic 1 (closest to CR)	analog in
107	M107	1	107	2	107	Truss Mic 2	analog in
108	M108	1	108	2	108	Truss Mic 3	analog in
109	M109	1	109	2	109	Truss Mic 4	analog in
110	M110	1	110	2	110	Truss Mic 5	analog in
111	M111	1	111	2	111	Truss Mic 6	analog in
112	M112	1	112	2	112	Truss Mic 7	analog in

113	M113	1	113	2	113	Truss Mic 8	analog in
114	M114	1	114	2	114	Truss Mic 9	analog in
115	M115	1	115	2	115	Truss Mic 10	analog in
116	M116	1	116	2	116	Truss Mic 11	analog in
117	M117	1	117	2	117	Truss Mic 12	analog in
118	M118	1	118	2	118	Truss Mic 13	analog in
119	M119	1	119/128	2	119	SST Mic 1 (bottom of SS twr)	analog in
120	M120	1	120	2	120	SST Mic 2	analog in
121	M121	1	121	2	121	SST Mic 3	analog in
122	M122	1	122	2	122	SST Mic 4	analog in
123	M123	1	123	2	123	SST Mic 5	analog in
124	M124	1	124	2	124	SST Mic 6	analog in
125	M125	1	125	2	125	SST Mic 7	analog in
126	M126	1	126	2	126	SST Mic 8	analog in
BENS Kulites							
129	K1	2	129	3	129	BENS	analog in
130	K2	2	130	3	130	BENS	analog in
131	K3	2	131	3	131	BENS	analog in
132	K4	2	132	3	132	BENS	analog in
133	K5	2	133	3	133	BENS	analog in
134	K6	2	134	3	134	BENS	analog in
135	K7	2	135	3	135	BENS	analog in
136	K8	2	136	3	136	BENS	analog in
137	K9	2	137	3	137	BENS	analog in
138	K10	2	138	3	138	BENS	analog in
139	K11	2	139	3	139	BENS	analog in
140	K12	2	140	3	140	BENS	analog in
141	K13	2	141	3	141	BENS	analog in
142	K14	2	142	3	142	BENS	analog in
143	K15	2	143	3	143	BENS	analog in
144	K16	2	144	3	144	BENS	analog in
145	K17	2	145	3	145	BENS	analog in
146	K18	2	146	3	146	BENS	analog in
147	K19	2	147	3	147	BENS	analog in
148	K20	2	148	3	148	BENS	analog in
148	K21	2	149	3	149	BENS	analog in
150	K22	2	150	3	150	BENS	analog in
151	K23	2	151	3	151	BENS	analog in

152	K24	2	152	3	152	BENS	analog in
153	K25	2	153	3	153	BENS	analog in
154	K26	2	154	3	154	BENS	analog in
155	K27	2	155	3	155	BENS	analog in
156	K28	2	156	3	156	BENS	analog in
157	K29	2	157	3	157	BENS	analog in
158	K30	2	158	3	158	BENS	analog in
159	K31	2	159	3	159	BENS	analog in
160	K32	2	160	3	160	BENS	analog in
161	K33	2	161	3	161	BENS	analog in
162	K34	2	162	3	162	BENS	analog in
163	K35	2	163	3	163	BENS	analog in
164	K36	2	164	3	164	BENS	analog in
165	K37	2	165	3	165	BENS	analog in
166	K38	2	166	3	166	BENS	analog in
167	K39	2	167	3	167	BENS	analog in
168	K40	2	168	3	168	BENS	analog in
Array Accelerometers							
169	A1	2	169	3	none	Mic Array	analog in
170	A2	2	170	3	none	Mic Array	analog in
171	A3	2	171	3	none	Mic Array	analog in
172	A4	2	172	3	none	Mic Array	analog in
173	A5	2	173	3	none	Mic Array	analog in
174	A6	2	174	3	none	Mic Array	analog in
175	A7	2	175	3	none	Mic Array	analog in
176	A8	2	176	3	none	Mic Array	analog in
177	A9	2	177	3	none	Mic Array	analog in
DAQ Analog Driver Outputs							
178	AO1	none	none	3	none	Model Pt. Source Speaker 1	analog out:port-acq
179	AO2	none	none	3	none	Model Pt. Source Speaker 2	analog out:port-acq
180	AO3	none	none	3	none	Model Pt. Source Speaker 3	analog out:port-acq
181	AO4	none	none	3	none	Model Pt. Source Speaker 4	analog out:port-acq
182	AO5	none	none	3	none	Model Pt. Source Speaker 5	analog out:port-acq
183	AO6	none	none	3	none	Model Pt. Source Speaker 6	analog out:port-acq
184	AO7	none	none	3	none	Mic Array Cal Speaker South A1	analog out S5:ao1
185	AO8	none	none	3	none	Mic Array Cal Speaker Throat A2	analog out S5:ao0

186	AO9	none	none	3	none	Mic Array Cal Speaker North A3	analog out S6:ao0
187	AO10	none	none	3	none	Injection Cal Source	analog out S6:ao1
DAQ Synchronization Signals							
64	C1- IRIGB	none	none	1	64	rack	analog in
128	C2- IRIGB	none	none	2	128	rack	analog in
188	C3- IRIGB	none	none	3	188	rack	analog in
DAQ Re-Assigned Signals 12/20/12							
16	M16	1	128/127	1	16	Note: <ul style="list-style-type: none"> M16: filter channel 16 went bad (gain) so M16 was reassigned to filter channel 128 (first) then to channel 127. M64: moved to DAQ (digitizer) channel 127 so that the IRIG-B signal could occupy this slot. Each digitizer unit (there were 3) used the last channel as the IRIG signal input. M119: filter channel 119 went bad (gain) so M119 was reassigned to filter channel 128. 	
127	M64	1	64	1	127		
119	M119	1	128	2	119		

REPORT DOCUMENTATION PAGE			Form Approved OMB No. 0704-0188		
<p>The public reporting burden for this collection of information is estimated to average 1 hour per response, including the time for reviewing instructions, searching existing data sources, gathering and maintaining the data needed, and completing and reviewing the collection of information. Send comments regarding this burden estimate or any other aspect of this collection of information, including suggestions for reducing this burden, to Department of Defense, Washington Headquarters Services, Directorate for Information Operations and Reports (0704-0188), 1215 Jefferson Davis Highway, Suite 1204, Arlington, VA 22202-4302. Respondents should be aware that notwithstanding any other provision of law, no person shall be subject to any penalty for failing to comply with a collection of information if it does not display a currently valid OMB control number.</p> <p>PLEASE DO NOT RETURN YOUR FORM TO THE ABOVE ADDRESS.</p>					
1. REPORT DATE (DD-MM-YYYY) 01-04-2016		2. REPORT TYPE Technical Memorandum		3. DATES COVERED (From - To)	
4. TITLE AND SUBTITLE NASA Hybrid Wing Body Aircraft Aeroacoustic Test Documentation Report			5a. CONTRACT NUMBER		
			5b. GRANT NUMBER		
			5c. PROGRAM ELEMENT NUMBER		
			5d. PROJECT NUMBER		
6. AUTHOR(S) Heath, Stephanie L.; Brooks, Thomas F.; Hutcheson, Florence V.; Doty, Michael J.; Bahr, Christopher J.; Hoad, Danny; Becker, Lawrence; Humphreys, William M.; Burley, Casey L.; Stead, Daniel; Pope, Dennis, S.; Spalt, Taylor B.; Kuchta, Dennis H.; Plassman, Gerald E.; Moen, Jaye A.			5e. TASK NUMBER		
			5f. WORK UNIT NUMBER 699959.02.07.07.01		
			8. PERFORMING ORGANIZATION REPORT NUMBER L-20425		
7. PERFORMING ORGANIZATION NAME(S) AND ADDRESS(ES) NASA Langley Research Center Hampton, VA 23681-2199			8. PERFORMING ORGANIZATION REPORT NUMBER		
9. SPONSORING/MONITORING AGENCY NAME(S) AND ADDRESS(ES) National Aeronautics and Space Administration Washington, DC 20546-0001			10. SPONSOR/MONITOR'S ACRONYM(S) NASA		
			11. SPONSOR/MONITOR'S REPORT NUMBER(S) NASA-TM-2016-219185		
12. DISTRIBUTION/AVAILABILITY STATEMENT Unclassified - Unlimited Subject Category 71 Availability: NASA STI Program (757) 864-9658					
13. SUPPLEMENTARY NOTES					
14. ABSTRACT This report summarizes results of the Hybrid Wing Body (HWB) N2A-EXTE Model aeroacoustic test. The N2A-EXTE model was tested in the NASA Langley 14-by 22-Foot Subsonic Tunnel (14x22 Tunnel) from September 12,2012 until January 28, 2013 and was designated as test T598.This document contains the following main sections: Section 1 – Introduction, Section 2 – Main Personnel, Section 3 – Test Equipment, Section 4 – Data Acquisition Systems, Section 5 – Instrumentation and Calibration, Section 6 –Test Matrix, Section 7 – Data Processing, and Section 8 – Summary. Due to the amount of material to be documented, this HWB test documentation report does not cover analysis of acquired data, which is to be presented separately by the principal investigators. Also, no attempt was made to include preliminary risk reduction tests (such as Broadband Engine Noise Simulator and Compact Jet Engine Simulator characterization tests, shielding measurement technique studies, and speaker calibration method studies), which were performed in support of this HWB test. Separate reports containing these preliminary Tests are referenced where applicable.					
15. SUBJECT TERMS Aeroacoustics; Aircraft; Body wing; Hybrid					
16. SECURITY CLASSIFICATION OF:			17. LIMITATION OF ABSTRACT	18. NUMBER OF PAGES	19a. NAME OF RESPONSIBLE PERSON
a. REPORT	b. ABSTRACT	c. THIS PAGE			STI Help Desk (email: help@sti.nasa.gov)
U	U	U	UU	85	19b. TELEPHONE NUMBER (Include area code) (757) 864-9658